UNIVERSITY OF CAPE TOWN

DEPARTMENT OF MECHANICAL ENGINEERING

A STUDY OF PROJECTILE MOTION ON IMPACT WITH THIN ALUMINIUM PLATES

A Thesis submitted to the Department of Mechanical Engineering for the degree of Master of Science in Engineering

by

G.C. Pearson, B.Sc.(Eng).

March, 1975

ACKNOWLEDGEMENTS

This research project was carried out in the Department of Mechanical Engineering, University of Cape Town, under the supervision of Dr. W.P. Boyle and Professor R.K. Dutkiewicz whose guidance and encouragement throughout the project is gratefully acknowledged.

The author also wishes to thank Mr. T. Miles, Mr. R.M. Stegen and Mr. B. Payne for their helpful advice.

Finally a word of thanks to Mr. W.K. Bettesworth and his workshop staff for their assistance with the construction of the apparatus, and to Mrs. L.E. Edwards who patiently typed the script.

ABSTRACT

A new technique has been developed to examine projectile motion on impact with thin aluminium plates.

A brief review of the field of penetration is given to show where the need for the present research arises. This is followed by an examination of alternative methods which could be used to determine penetration behaviour of projectiles and a discussion of their respective merits.

Any impact phenomenon of elastic bodies is accompanied by inherent vibrations. Because of the greater sensitivity of the method used by the author over previous methods, vibrations set up in the projectiles sensing mechanism played a very significant role in the penetration process. To take account of the vibration phenomenon, recourse was made to Masket's ((1) 1949) work which enables the motion of the centre of mass of the projectile to be determined from a knowledge of the motion of any point on the projectile.

The new technique has many advantages over previous methods, the main one being the simultaneous production of deceleration-time data as the projectile penetrates the target material. Although the data must still be processed to remove superimposed vibrations, it does not have to undergo the drastic smoothing process of double differentiation used in previous methods. Because of this, the overall characteristic shape of the deceleration-time plot is preserved.

Frontispiece: The experimental Rig designed and built specifically to investigate projectile impact phenomena.

TABLE OF CONTENTS

(Table of Contents, Cont.) Page No.

NOMENCLATURE FOR CHAPTERS I TO VI

F	-	Force
K	-	Constant
V	-	Instantaneous Projectile Velocity.
V_o	-	Approach Velocity on Impact.
E	-	Energy
T	-	Target Plate Thickness
R	-	Projectile Radius
Y	-	Target Yield Strength
t	-	Time
R_1	-	Maximum radius of deformation
ΔV	-	Velocity drop.
d	-	Projectile diameter
L_1	-	Fragment length
P_o	-	Static punching force
B	-	Magnetic field strength
ℓ	-	Active length of conductor cutting magnetic field.
A	-	Area
E_{in}	-	Input voltage
E_{out}	-	Output voltage
V_{min}	-	Minimum velocity to penetrate.
c_p	-	Acoustic velocity in projectile.
c_s	-	Acoustic velocity in target.
x	-	Penetration distance in axial direction.
L	-	Length of projectile head.
M	-	Mass of projectile
α	-	Semi cone angle of projectile head.
φ	-	Magnetic flux
μ	-	Permeability
ρ_p	-	Projectile density
ρ_s	-	Target material density
η	-	Function of shear stress (assumed constant).
Ψ	-	$(\rho_p c_p + \rho_s c_s)/\rho_p \rho_s c_p c_s$
σ_r	-	Radial stress
σ_θ	-	Circumferential stress

Nomenclature for Appendix C/ .....

NOMENCLATURE FOR APPENDIX C

λ	-	Complex variable
u	-	displacement relative to lab. co-ordinates.
x	-	position measured from projectile tail.
c	-	local acoustic velocity
t	-	time
V_o	-	initial velocity
F(t)	-	retarding force function
U	-	Laplace transgorm of u
E	-	Young's modulus
A	-	Cross sectional area of projectile
ℓ	-	effective length of projectile
d	-	distance of sensor from projectile tail
$\tilde{X}$	-	dummy variable representing displacement, velocity or deceleration.
U^*	-	dummy variable
t', T	-	integral limits in time

CHAPTER I

1.1 General Review On the Field of Penetration

Penetration may be defined as the entrance of a projectile into a target without completing its passage through the target, whereas perforation implies the complete piercing of the target by the projectile. The penetration of projectiles into metallic and non-metallic targets has long been of interest to ordnance engineers, however, because of its military connection, little published material is available on this topic. More recently, interest in this field has arisen due to the need for information concerning:

(i) The dynamic properties of materials at high strain rates Wingrove,(2, 1972);*

(ii) The containment of fragments resulting from the failure of high speed rotating machinery; e.g. turbine blades Brown (3,1964);

(iii) The micro-meteoroidal damage of space vehicles Huth (4, 1956);

The earliest examination of penetration was probably carried out by the German scientist Euler (5, 1745), who provided experimentally determined values of the (assumed constant) resisting force of elm wood and earth; i.e.

$$F = K_1 \quad \ldots\ldots\ldots\ldots\ldots\ldots\ldots\ldots\ldots\ldots\ldots\ldots\ldots\ldots \quad (1.1)$$

Poncelet (6,1829) subsequently included a further term proportional to the square of the velocity, arguing that the constant term represents the force required to overcome the cohesion of the target material, whilst the second term represents the force required to move the material from the path of the projectile. Thus two coefficients were required to be determined experimentally, the coefficients varying with the target material, projectile shape and angle of impact.

$$F = K_1 + K_2 V_o^2 \quad \ldots\ldots\ldots\ldots\ldots\ldots\ldots\ldots\ldots\ldots\ldots\ldots\ldots \quad (1.2)$$

Work carried out on a wide variety of target materials and analysed on this basis, was discussed by Bashforth (7,1873)

Limited information concerning the resistance of armour plate to penetration by a high speed projectile was published in 1937 in the Encyclopaedia Britannica, where the following unreferenced expression relating the kinetic energy, bullet radius and plate thickness was

* (Reference No; Date of Publication.)

provided/2.....

provided:

$$E = KT^{n}R^{3-n} \quad \ldots\ldots\ldots\ldots\ldots\ldots\ldots\ldots\ldots\ldots \quad (1.3)$$

where $\frac{4}{3} < n < 2$

It will be noticed that for a given target plate and projectile, expression 1.3 gives the energy required for the condition of containment. This has been the trend in analytical studies on penetration as their purpose has been to select shielding materials to stop a certain size of projectile.

Bethe (8, 1941) developed a theoretical model for the penetration of armour plate by a high speed projectile, in which the progressive expansion of a hole in a plate was considered. It was assumed that the final radius of the hole, i.e. the projectile radius, was large compared with the plate thickness, and that the plate was of infinite lateral extent with progressive thickening occurring at the edge of the hole. The stress perpendicular to the plate was assumed zero while in the plane of the plate a stress distribution such that $\sigma_{\theta} - \sigma_{r} = Y$ was assumed. Using the above together with elastic equilibrium conditions, Bethe was able to determine the total energy expended in expanding the hole to radius R, i.e.:

$$E = 2\pi R^{2}\ TY \quad \ldots\ldots\ldots\ldots\ldots\ldots\ldots\ldots\ldots\ldots \quad (1.4)$$

From the above it can be seen that the refinement of Bethe's analysis has brought about the inclusion of Y, the target material yield strength, into the energy relationship. An extension of Bethe's work was carried out by Taylor (9, 1948) who realised that the mass of the target material offered inertial resistance to a penetrating projectile. His expression was of the form

where $\gamma = K\rho V_{o}^{2}$

$$E = \gamma R^{2}\,TY \quad \ldots\ldots\ldots\ldots\ldots\ldots\ldots\ldots\ldots\ldots \quad (1.5)$$

At about the same time as Bethe and Taylor were deriving purely theoretical relationships, the technology of high speed photography had reached the stage where a projectile's motion could be photographed as the latter penetrated a target. To obtain displacement-time data a framing rate of 10^{6} frames/second or equivalent streak record is required. This was first achieved by Masket(1, 1948), who, using a streak photographic method was able to derive the shape of the force-time curve for a projectile penetration as well as detect vibrations in the tail of the projectile, relative to its centre of mass.

Masket's/3.....

Masket's data was the first to show the shape of the impulse and he attempted to describe the shape of the latter with the following expression:

$$F = Kt^2e^{-\beta t} \quad \ldots\ldots\ldots\ldots\ldots\ldots\ldots\ldots\ldots\ldots \quad (1.6)$$

where the constants β and K were adjusted to fit the experimental data.

Bluhm (10, 1956) following on from Masket's work tried to determine penetration forces using a different approach. He mounted his projectile rigidly, strain gaugedit, and fired targets at it. Although there is some doubt as to the applicability of his results to the normal penetration process, he demonstrated clearly how the nose and tail of the projectile vibrated around its centre of mass, and that the vibrating mode of the projectile could play a considerable role in the penetration process, especially with regard to tensile failure in projectiles after penetration. Bluhm used the same analytical approach as Masket solving the plane wave equations for strain rather than stress. He also used an equation of the form of 1.6 to describe his result, but neither he, nor Masket, attempted to use their data to develop a theory of penetration.

Thompson (11, 1955) made a quasi dynamic analysis of the penetration process, considering the projectile energy to be dissipated in plastic deformation of the target, and obtained expressions relating the energy of containment to the projectile length, radius, impact velocity, and the target plate's density, thickness and yield stress. The analysis was done for conical and ogival projectiles.

$$E = \pi R^2 T[Y/2 + \rho_s(V_o R/L)^2] \quad \ldots\ldots\ldots\ldots\ldots\ldots\ldots \quad (1.7(\text{conical}))$$

$$E = \pi R^2 T[Y/2 + \rho_s(V_o R/L)^2(3\pi^2/16)] \ldots\ldots\ldots\ldots\ldots\ldots \quad (1.8(\text{ogival}))$$

Brown (3, 1964) developed a model similar to Thompson's for determining the minimum plate thickness necessary to contain a high speed projectile based on the assumption that the projectile's kinetic energy is distributed between the plastic deformation of the plate, the shearing of a disc from the plate, and the kinetic energy of the deformed area of the disc and the plate. In the following equation the term V_1 is an assumed constant velocity of penetration - an unrealistic but simplifying assumption:

E = /4.....

$$E = [\pi TYR_1^2/2]/[1 - 2\pi TR_1^2\rho_s/M(V_1/V_o)^2(1 - (R_1/L)^2] \quad ....(1.9)$$

In the energy balance analyses of Brown (3), Thompson (11), Taylor (9) and Bethe (8), no allowance was made for the effects of wave propagation, crack formation, friction, adiabatic heating and strain rate. Zaid and Paul (12, 1957) considering that the penetration effects propagate at a finite rate, proposed a zone of action within which the significant effects are confined. By using the principle of conservation of momentum, the instantaneous velocity of the projectile was described in terms of a quantity known as the effective mass of the target plate, thus enabling the determination of acceleration, penetration and resisting force. The analysis initially for conical projectiles was subsequently extended to cover truncated conical and ogival heads. The expression they developed was for the extreme case of perforation when the impinging projectile suffers only a slight loss of velocity. In expression 1.10, ΔV is the velocity loss and α is the half cone angle of the projectile:

$$\Delta V = \frac{\pi\rho_s TR^2V_o \sin\alpha}{m} \quad ..... (1.10)$$

and $$F = 2\pi\rho TV_o^2 x \tan^2\alpha \sin\alpha \quad ..... (1.11)$$

Using stress wave mechanics and assuming a constant average dynamic shear strength for the target material Recht and Ipson (13, 1963) obtained a rather more complex expression for the minimum velocity to perforate.

$$V_{min} = 4\Omega T^2\psi\eta/Ld[1 + (L+\Omega T)/\Omega T \quad 1 + d/4\rho_s T\eta\psi^2 \quad ^{\frac{1}{2}}] \quad ... (1.12)$$

Much work has been done in the field of thin plate penetration and perforation by Goldsmith (et al) (14, 15, 1971). In experimental work with Calder and Finnegan strain gauges bonded to both sides of the target plate beyond the permanently deformed region were used to provide records of the stress waves propagated during the penetration process, thus enabling an assessment of the relative magnitude of dishing and punching in the deformation pattern. It was found that dishing observed in thin targets

at low/5...

at low velocities disappeared at higher velocities as the perforation mechanism changes from bending to punching. Goldsmith's work in the field of penetration has been merely to test present theories experimentally. No new theories have been presented.

Some of the most recent experimental studies have been done by Wingrove (2, 1972), where interest in the field of penetration came about through work on dynamic stress-strain determination. Using an electrical method to measure displacement-time histories of projectiles, he was probably the first to use an alternative method to the classical photographic one.

Nishiwaki (16, 1951) developed a theoretical analysis to enable an evaluation of the drop in velocity a projectile suffers when penetrating an aluminium plate. His analysis was based on Stutterlin's (26) method of determining frictional resistance of a projectile in the bore of a gun. Using the static punching force Po to represent the material aspect of penetration and the term $\rho V_o^2 \sin^2 \alpha$ for inertia effects, the primary expression for a penetration becomes:

$$F = \int_{\sigma} [Po + \rho V_o^2 \sin^2 \alpha] \sin \alpha \, d\sigma \quad \ldots\ldots\ldots\ldots\ldots\ldots \quad (1.13)$$

Where $d\sigma$ is the incremental contact area between plate and projectile. Expression 1.13 can be integrated numerically to obtain an expression of force-time, which is similar in form to Masket's (.16) empirical relationship.

Projectile impact studies cover a very large range of impact velocities from 10 m/s to 10^5 m/s. The foregoing literature survey considered impact velocities in the range from 100 m/s to 1 000 m/s as these are the velocities with which the present study is concerned. The higher range of velocity from 10^3 m/s to 10^5 m/s, known as the hypervelocity range, has become of interest recently in the study of micro-meteorite impact with space vehicles. Fig (1.1.) shows where the various authors have contributed to the field.

Fig 1.1/6.....

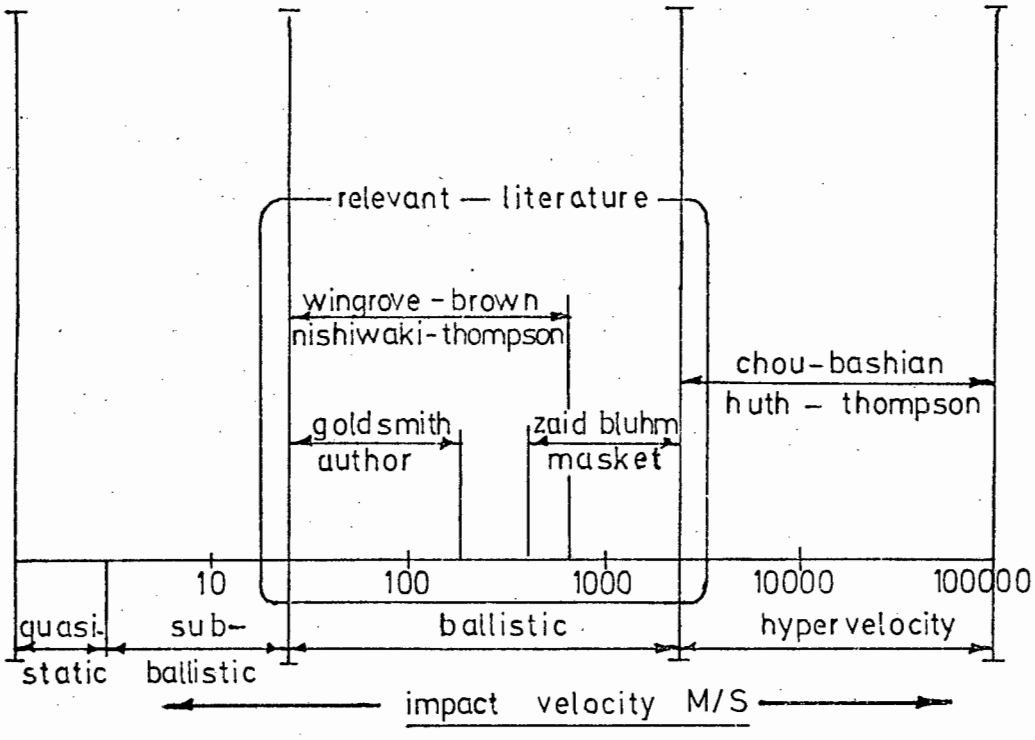

FIG 1.1

Whereas the important parameters in a penetration at ballistic speeds are target density and mechanical strength, (see equations 1.1 to 1.13), the important parameters at hypervelocities are the fluid properties of molten target material, latent heats of fusion and evaporation as well as those of the projectile itself. Thus it can be seen that research in both areas is almost completely unrelated, the ballistic one being an almost pure mechanical problem whereas the hypervelocity problem is one of fluid dynamics and heat flow. This being the case and since the present study is concerned solely with ballistic penetration and perforation, no more will be said about hypervelocity impact. Comprehensive studies have been done by Chou (22) Bashian (23) Thompson (24) and Huth (4) in this field.

1.2 Implications of Penetration Theories

The present study was carried out in the lower ballistic range of impact velocities as shown in Fig. 1.1. The relevant theories are also indicated and the following assumptions are common to these theories:

(i) The projectile radius R $\gg$ T the plate thickness.

(ii) The projectile suffers no permanent deformation.

(iii)/7.....

(iii) Energy associated with cracking of target material is negligibly small.

(iv) Acoustic and heat energy during the impact is negligibly small.

(v) All the projectiles kinetic energy is absorbed by mechanical deformation of the target.

The equations 1.1 to 1.13 have been developed using these assumptions. Although they were derived with different objectives in mind, i.e. to determine the drop in velocity due to a high speed perforation (1.10) or the energy absorbed in a penetration (1.7 and 1.9) it is desirable to judge the expressions using a common criterion.

To do this the deceleration-time predictions of an impact for the various theories are presented in Fig. 1.2. This criterion was chosen since, being a second derivative of the displacement-time history, it provides a very sensitive parameter to compare the various theories. It is also a very relevant parameter since important phenomena such as strain rate and inertia effects are directly related to it.

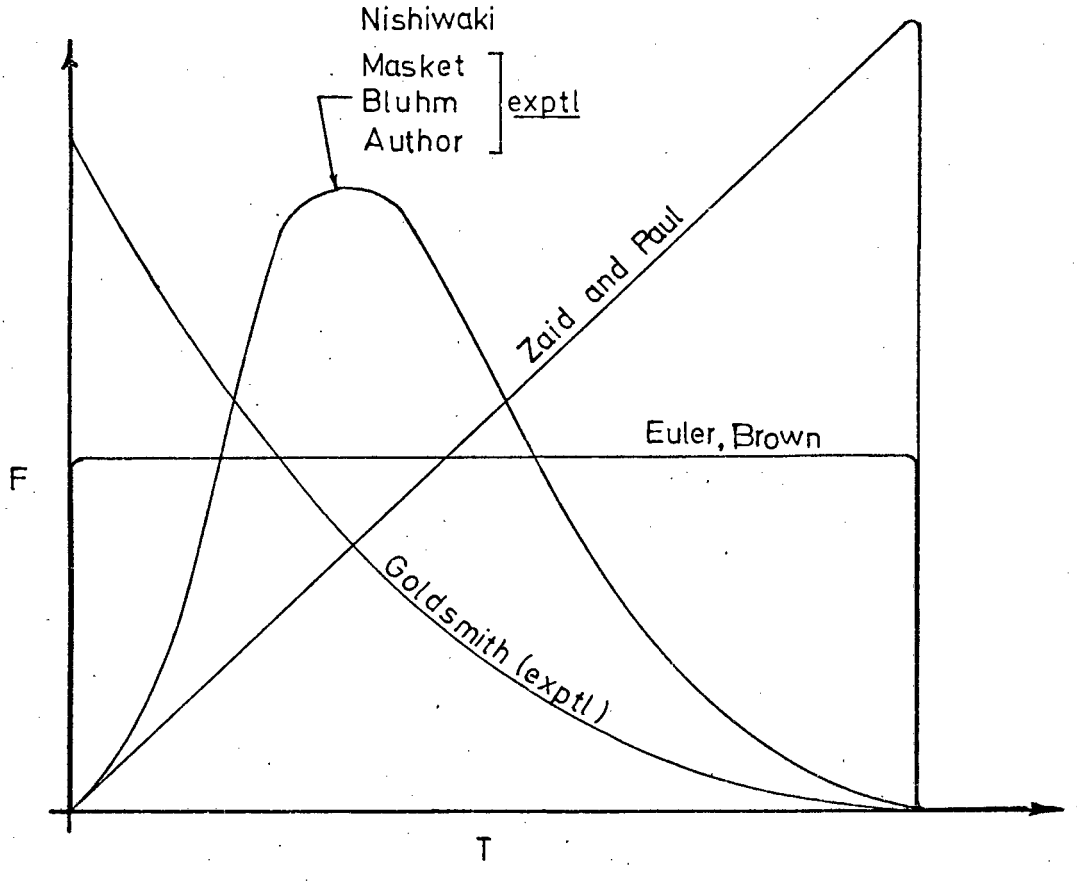

FIG 1.2 IMPULSE SHAPES PREDICTED BY VARIOUS THEORIES

On impact/8.....

On impact, the deceleration of a projectile must start from zero, reach a peak and then return to zero once the projectile has been arrested. This bell-shaped pulse is predicted by equations 1.6 and 1.13 and has been found experimentally by Bluhm, Masket and Wingrove. The present study also provides experimental confirmation of this shape of pulse.

The experimentally derived deceleration-time trace presented by Goldsmith, Liu and Chulay is also shown. The rapid rise in deceleration during the initial stages of the impact cannot be detected with Goldsmith's photographic technique.

The momentum theory of Zaid and Paul predicts a linear increase in deceleration with time, for the duration of the impact. The theories of Brown and Thompson use the concept of an impact occurring at constant velocity, hence the square pulse shape shown.

Figure 1.2 shows clearly the approximate nature of penetration theories to date. Although each has found a degree of success in limited applications, none has been general enough to predict accurately, penetration behaviour over the whole ballistic range.

CHAPTER II

Measurement Techniques

2.1 General

The present research into penetration and perforation of aluminium plates has been carried out in the velocity range from 50 m/s to 100 m/s. In general there are seven basic mechanisms which absorb the kinetic energy of an impinging projectile. They are:

(1) Mechanical strength of the target material.
(2) Density of the target material creating inertial resistance.
(3) Friction between projectile and target.
(4) Crack formation in the target.
(5) Energy dissipated in acoustic waves.
(6) Energy absorbed in a change of state and fluid flow of molten target material.
(7) Energy absorbed by deformation, etc., of the projectile.

Mechanisms 6 and 7 only come into effect at hypervelocities or in the upper ballistic range when the thickness of the target is of the same order as the projectile diameter (4,11).In the present study therefore, these can be neglected.

Using a split Hopkinson bar, Krafft (17, 1955) investigated the frictional effect between target and projectile. A spinning projectile on striking the Hopkinson bar transmitted in addition to an axial pulse, a torsional pulse which was directly proportional to the frictional force between the impacting bodies. His studies were performed in the upper ballistic range and the results were surprising and contradicted theoretical predictions. Only when the target and projectile were very carefully cleaned, permitting welding conditions to exist between the impacting surfaces,could any significant frictional behaviour be detected. Any impurity present was seen to behave as a lubricant between the bodies and reduce the frictional component to a negligibly small force.

Studies performed by Goldsmith and Chulay (18, 1965),using strain gauges mounted on the target,have shown the vibration component of energy to be negligible.

Since the energy associated with crack formation is related to the area of the new surface created by the crack, this component is negligibly small for thin ductile plates which are being used as targets in the

present/10.....

present study. The two remaining parameters are therefore 1 and 2.

To get a clearer understanding of what is involved in the present study, a closer look must be taken at the implications of mechanical strength and inertia effects due to target material. To penetrate or perforate a target, a projectile must push aside the target material. In the case of quasi static punching, the only resistance met by the projectile will be due to the mechanical strength of the material. When a projectile penetrates at speed however, the plate in addition to resisting mechanically, also places considerable mass in the projectile's path, which gives rise to inertial resistance.

To completely describe the interaction of the target and projectile, a complete knowledge of the DISPLACEMENT OF EVERY PARTICLE INVOLVED IN THE COLLISION AS A FUNCTION OF TIME is needed.

2.2 History of Measurement Techniques

The classical approach to the problem has been through high speed photography. Although several photographic studies were carried out in the early 1900's, the method only became of any value after Masket's work in 1946. His experimental layout is shown in Fig 2.1.

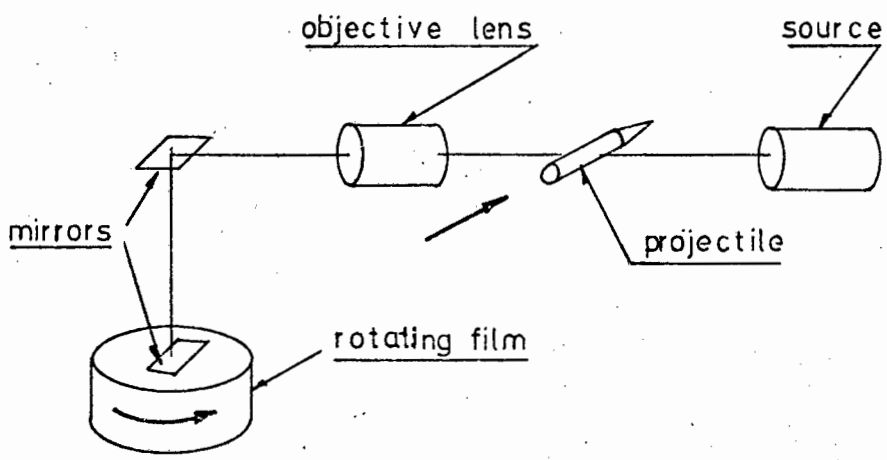

FIG2.1 MASKETS APPARATUS

The apparatus consisted of a 300 mm long piece of film which was rotated in a drum at a peripheral speed of 200 m/s. By means of an optical arrangement, a shadow of the tail of the projectile was made to

fall on/11 .....

fall on the film, recording displacement - time information of the tail. The camera had an equivalent framing rate of 5×10^7 frames/second, an incredibly high speed, even by modern standards. The main limitation of the method was that imposed by the film itself, i.e. resolution limitations due to grain size.

Following on from Masket's work, Bluhm in 1955 tried a completely different approach to the problem of determining stresses in a projectile on impact. To circumvent the problem of trying to collect data from a projectile travelling at high speed, he fixed the latter to a test bench, strain gauged it, and fired targets at it! It is difficult to say just how comparable these results are to the normal penetration process since the projectile was no longer a free body, i.e. its boundary conditions had been changed.

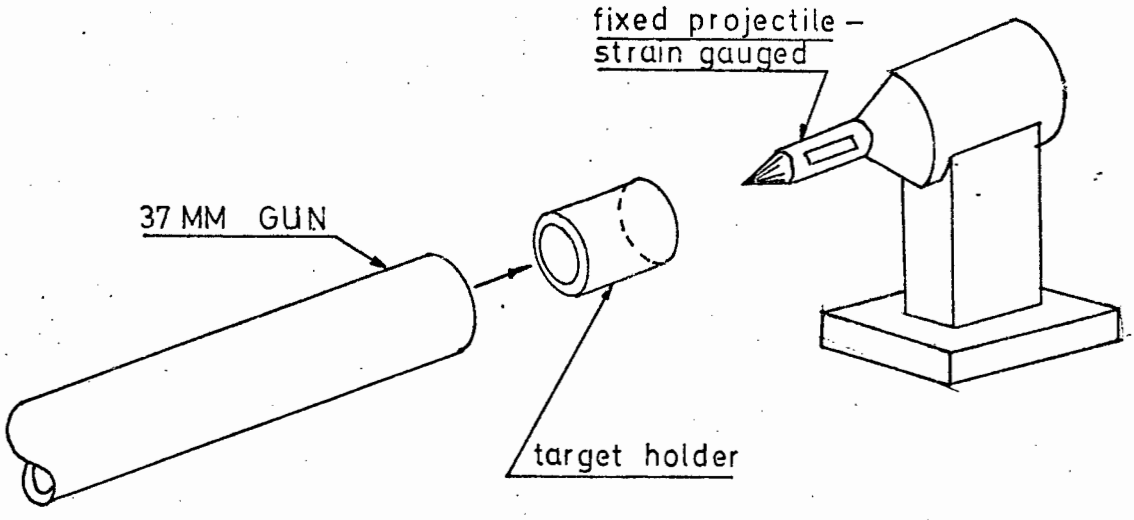

FIG21 BLUHM'S APPARATUS

In 1960 Goldsmith started a research programme into the penetration of thin aluminium plates by projectiles of various shapes. His work with Calder (1970) Finnegan (1971) Lui and Chulay (1965) and Layman (1962) has not produced many changes in the photographic method of Masket. The main improvement over Masket's method has been in the availability of better high speed cameras (Beckman and Witley WB-2 and Bowen RC-4). These

cameras/12.....

cameras have a maximum framing rate of 10^6 frames/second which, although an order slower than Masket's, provide a full field photograph, giving displacement-time information of the plate as well as that of the projectile. Unfortunately, the use of discrete frames as opposed to the continuous streak photograph of Masket, has caused the displacement-time data of Goldsmith (et al) to be far less reliable than Masket's. This is brought out in Fig. 1.2. In Goldsmiths research, the stress has been placed on target response rather than projectile behaviour, although the latter is equally as important, as it is a boundary condition for the penetration process. Fig. 2.3 shows his experimental layout.

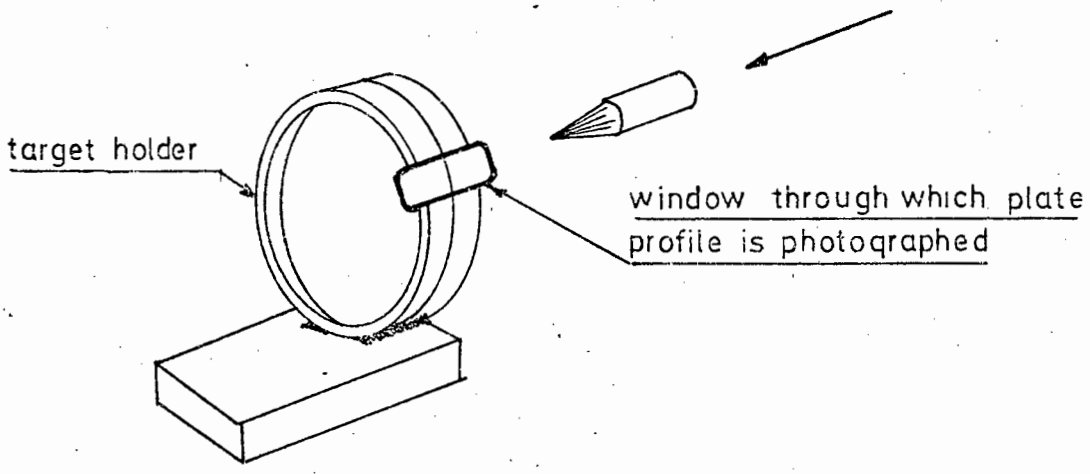

FIG 2.3 GOLDSMITH AND CALDERS APPARATUS

The most recent published experimental study (1972) has used an entirely different approach to the problem of determining displacement-time data of a projectile on impact. The method, due to Wingrove, is an electrical one and is shown in Fig. 2.4. The penetration of the projectile into the target was measured from the movement of the tail end of the projectile through a co-axial capacitor. As the front end of the projectile entered the target, the decrease in capacitance of the co-axial capacitor was recorded as a voltage-time trace on an oscilloscope.

Basically there is no difference between the oscilloscope record obtained by Wingrove and the streak photograph of Masket. The main advantage in Wingrove's method lies in its simplicity and lack of complicated apparatus. It is doubtful though, whether his resolution on a 100 mm oscilloscope storage screen was as good as Masket's record on 300 mm of fine grain film.

Fig 2.4/13.....

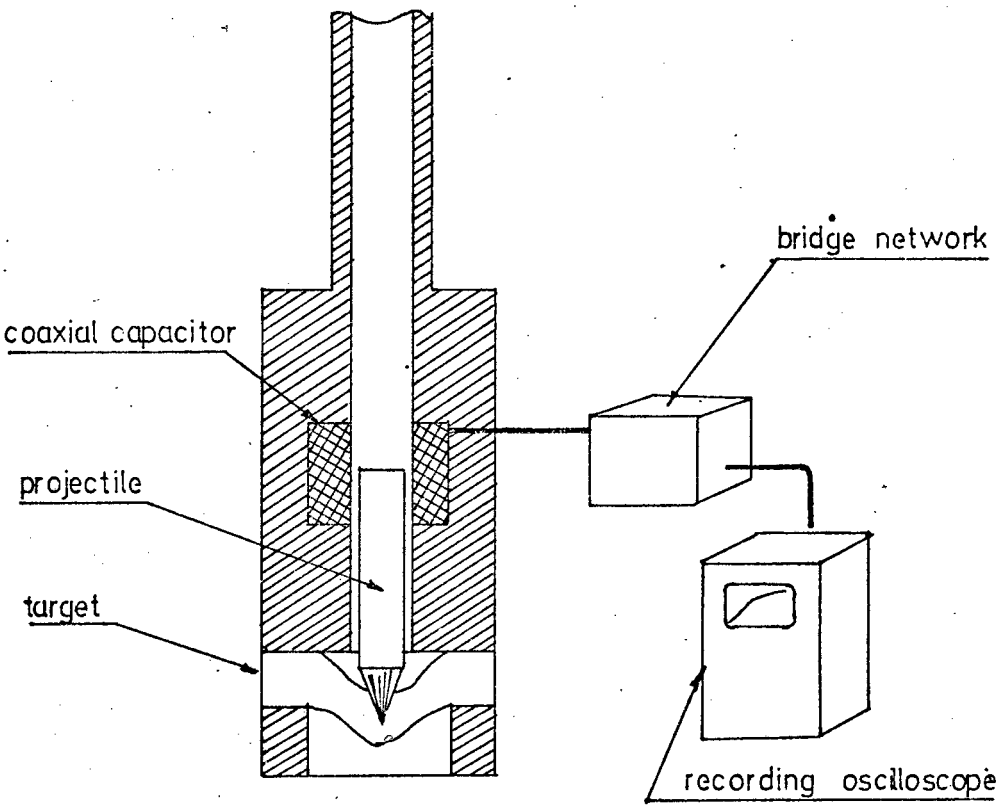

FIG 2.4 WINGROVE'S APPARATUS

2.3 Alternative Measurement Techniques

The following six methods were considered as alternative ways of determining the displacement-time history of an impacting projectile or the first or second derivatives thereof.

2.3.1 Opto-electric Method

By the use of an array of light beams which would be successively uncovered by the tail of the projectile as its head penetrated a target, displacement-time information could be recorded.

The recent advances in fibre optics and in sub-miniature light emitting diodes (L.E.D's) and photo-transistors, makes this method possible. A typical layout is shown in Fig. 2.4. "Motorola Opto-Electronics' manufacture an encapsulated array of L.E.D's and corresponding array of photo-transistors. The centre to centre spacing of the active

elements/14..

elements is only 0,125 mm and the space between elements only 0,0125 mm. This would enable approximately 200 data points to be recorded for an average impact. The output from such a device would be a digital record of the projectile's displacement-time history.

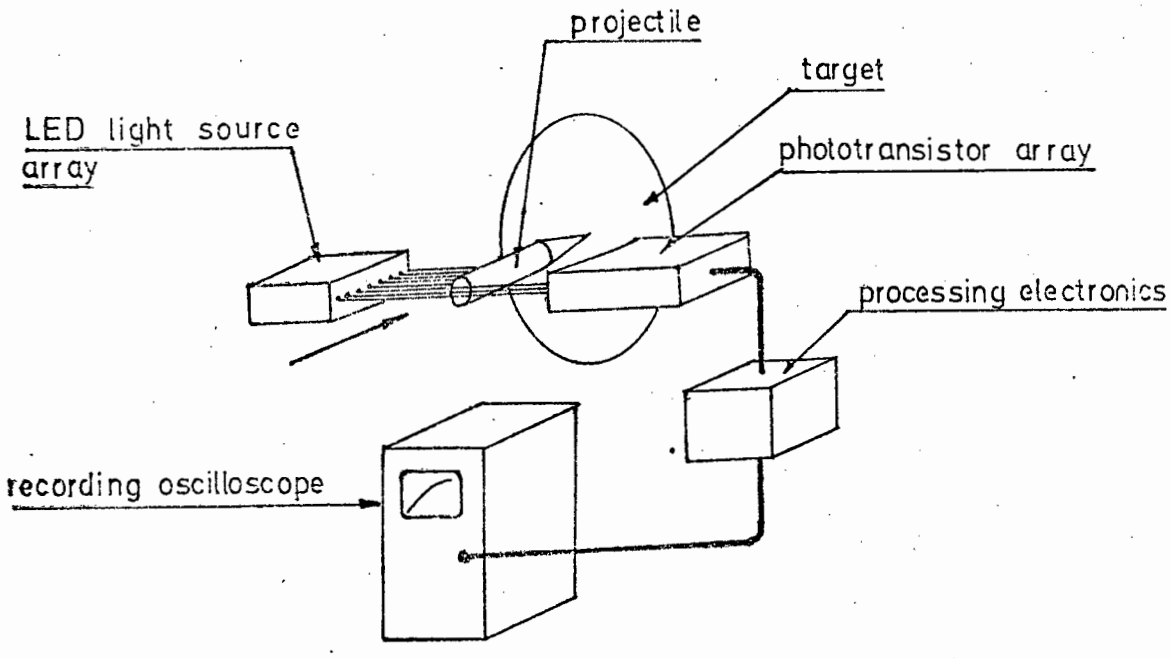

FIG 2.5 OPTO-ELECTRIC METHOD

2.3.2 Inductive or Capacitive Method

This method is the same in principle to Wingrove's method, but was conceived independently. The method was described in section 2.2 and will not be repeated here.

The inductive variation of the method would use a coil of wire to replace the co-axial capacitor. The projectile would thus act as a variable core.

2.3.3. Differential Transformer Method

This method uses the concept of a differential transformer to measure displacement, except that the projectile itself is used as the core of the transformer.

Fig. 2.6/15.....

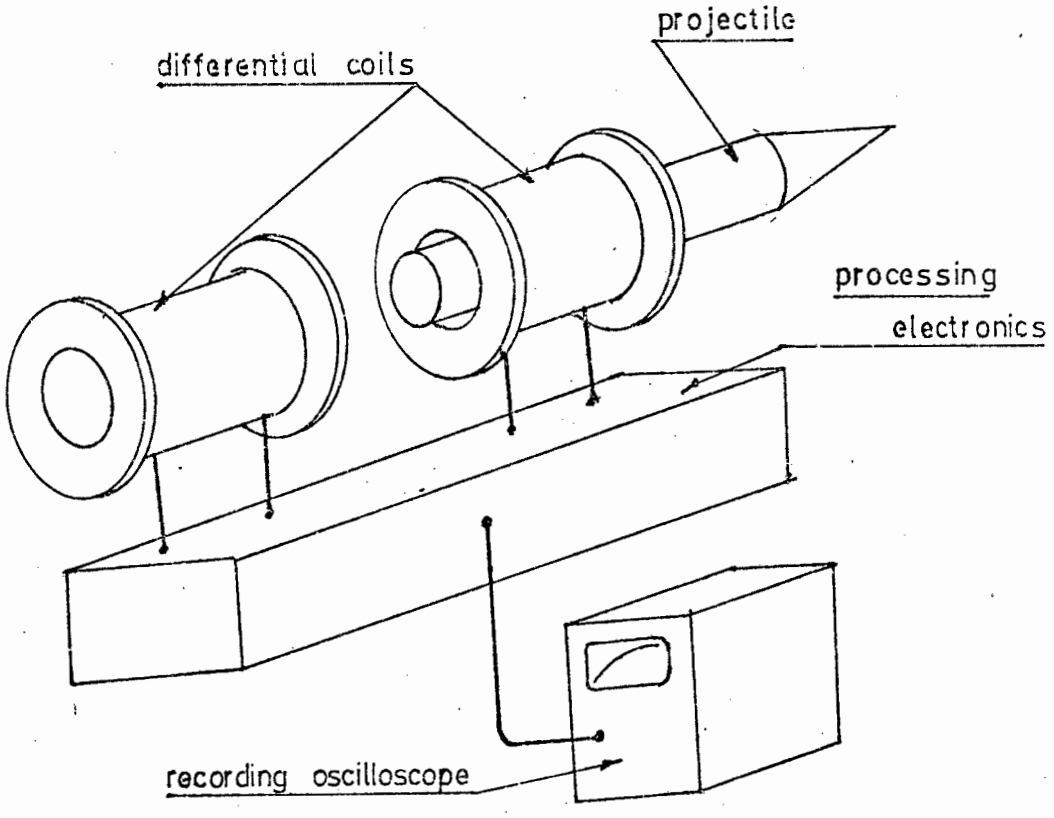

FIG 2.6 DIFF' TRANSFORMER METHOD

2.3.4 Induction By Permanent Magnet

If a permanent magnet were imbedded in a projectile and the latter made to pass through a coil of wire at the instant the projectile struck its target, it would be possible to obtain a velocity-time history of the projectile's penetration, since from Lenz's Law we have:-

$$E = \frac{d\varphi}{dt} \quad \ldots\ldots\ldots\ldots\ldots\ldots\ldots\ldots\ldots\ldots\ldots\ldots\ldots\ldots\ldots\ldots \quad (2.1)$$

and if L is the effective length of the coil of wire, B the magnetic field strength of the magnetic field and V the instantaneous velocity of the projectile, then equation 2.I becomes:-

$$E = BLV \quad \ldots\ldots\ldots\ldots\ldots\ldots\ldots\ldots\ldots\ldots\ldots\ldots\ldots\ldots\ldots\ldots\ldots\ldots\ldots\ldots (2.2)$$

The e.m.f. generated in the coil would therefore be in direct proportion to the projectile's instantaneous velocity.

Fig 2.7/16 .....

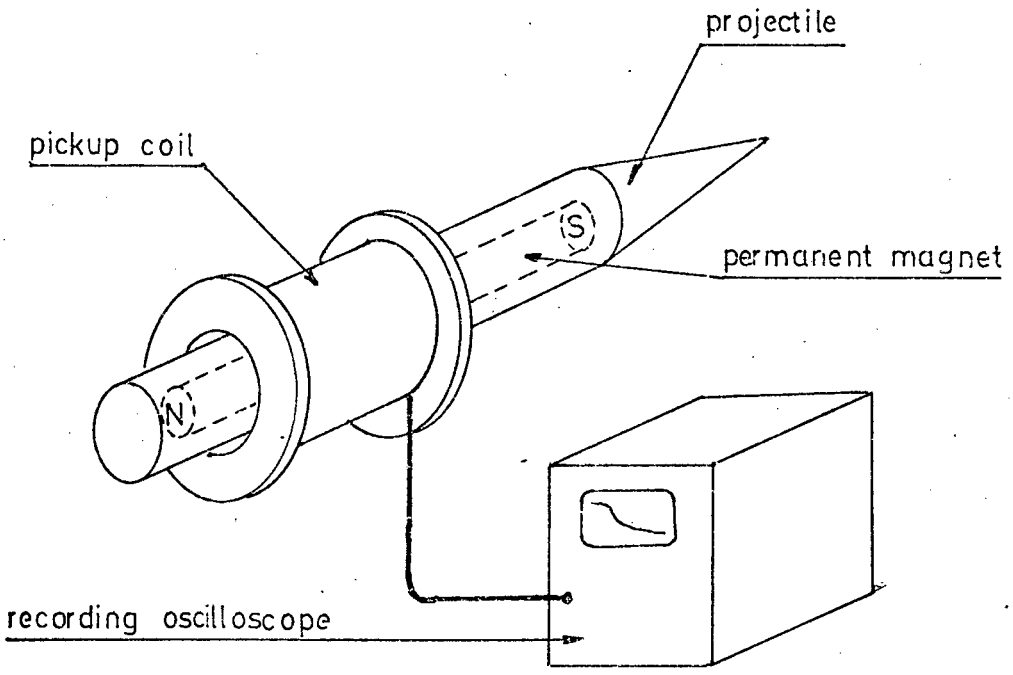

FIG 2.7 PERMANENT MAGNET INDUCTIVE METHOD

The four methods 2.3.1 to 2.3.4 have one characteristic in common and this is that the link between the moving projectile and the stationary detecting equipment is made by means of magnetic or electric fields and light beams. The remaining two methods differ in this respect, requiring a physical electrical contact to be made between the projectile and detecting circuiting.

2.3.5 Accelerometer Method

In this method an accelerometer (strain gauge, or piezoelectric) is directly attached to the projectile. The accelerometer is wired to two insulated commutators which run axially along the sides of the projectile. Just before the projectile impacts the target, the commutators make contact with two brushes, so that when impact occurs the accelerometer is connected into suitable detecting circuitry.

Fig. 2.8/17.....

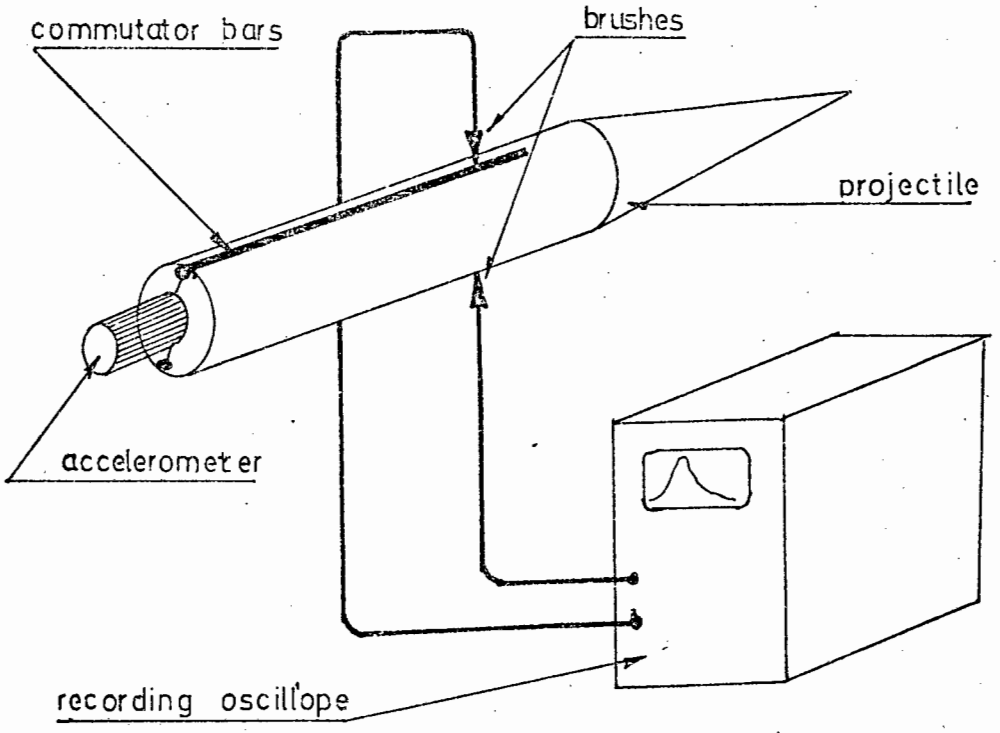

FIG 2.8 ACCELEROMETER METHOD

2.3.6 Velocity Transducer Method

In principle this method is the same as that used in 2.3.4. It differs in that the magnetic field is stationary and the generating coil or conductor is embedded in the projectile. The e.m.f. developed in the conductor is transmitted to the detecting circuitry by means of the commutating arrangement used for method 2.3.5. (see Fig. 2.9).

Fig. 2.9/18.....

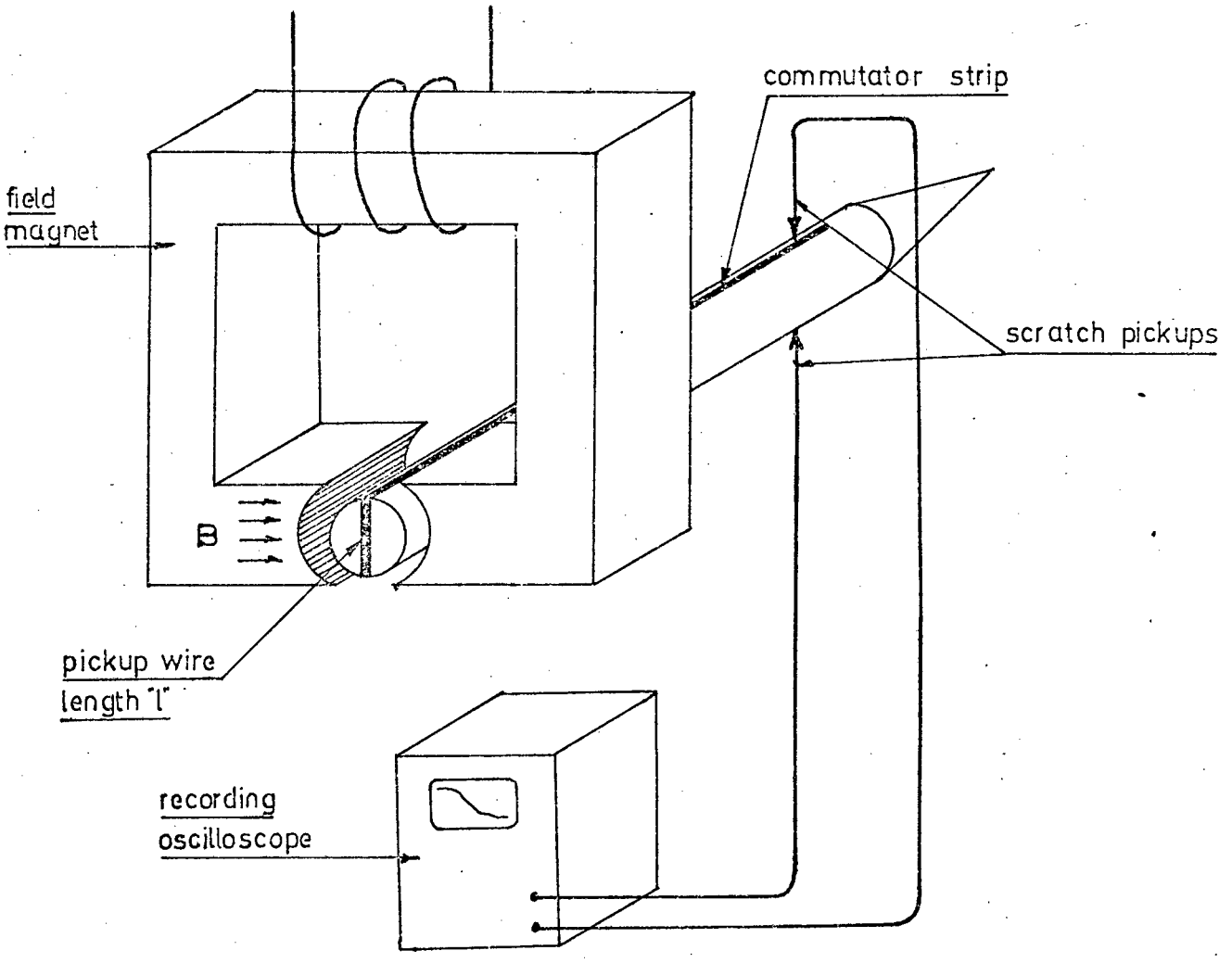

FIG 2.9 VELOCITY TRANSDUCER METHOD

2.4 Choice of Method

Experimenters to date have been concerned with the recording of displacement-time data, either photographically (14, 15, 18) or electrically (2). Since impact generates such effects as inertial resistance and produces high strain rates, the higher derivatives of the displacement-time data play a more significant role in the penetration process. These higher derivatives were obtained in previous studies by numerically differentiating the displacement-time data. This process is very sensitive and unstable and can lead to such erroneous results as those prodeuced by Goldsmith (18) (see Fig 1.2)

Ideally the highest derivative of the displacement-time history should be obtained as primary data and the lower derivatives derived by integration - a process which is both stable and reliable.

Displacement/19.....

	Displacement		Velocity		Acceleration
Normal Photographic Proceedure	x	$\longrightarrow$	$\frac{dx}{dt}$	$\longrightarrow$	$\frac{d^2x}{dt^2}$
Best Approach	$\iint a\,dt$	$\longleftarrow$	$\int a\,dt$	$\longleftarrow$	a
Present Study	$\int v\,dt$	$\longleftarrow$	V	$\longrightarrow$	$\frac{dV}{dr}$

As method 2.3.5 uses an accelerometer, the primary signal it generates is proportional to the deceleration of the projectile on impact. Unfortunately however, the technical difficulties encountered with this method make it impractical. The use of brushes to connect the transducer to the detecting circuitry would not be feasible for either transducer. A piezoelectric transducer requires very good connection to a charge amplifier and in the case of a strain gauge transducer, fluctuations in the contact resistance might swamp the change in resistance of the strain gauge.

Apart from the methods 2.3.4 and 2.3.6, the remaining methods record displacement-time data and have only marginal advantages over previous methods used. The opto electric method for example could record 200 bits of information (as opposed to Goldsmith's 80) in the form of accurate digital signals.

The final choice of method is therefore between the two velocity transducer methods 2.3.4 and 2.3.6. Inherent problems with method 2.3.4 such as loss of magnetism experienced by the permanent magnet on impact and doubtful linearity over the desired range, makes the final choice method 2.3.6.

2.5 Velocity Transducer Method

The velocity transducer consists of an electromagnet to create a uniform magnetic field, a slotted and insulated section of the gun barrel through which the projectile is guided as it cuts the magnetic field, a pair of brushes or "Scratch Pickups" to transmit the generated e.m.f. and a specially constructed projectile which carries the e.m.f. generating conductor and the commutator strips. The separate components are described in detail in Chapter III.

As can be seen from Fig 2.9 a conductor embedded in the projectile is arranged to pass through the uniform magnetic field as the head of the projectile is impacting the target. The e.m.f. generated in the conductor is in direct proportion to its instantaneous velocity and is transmitted to the conditioning circuitry and storage oscilloscope by means of two commutator strips which run axially down the sides of the projectile. These commutator strips make contact with the two "Scratch Pickups"

just/20.....

just before impact occurs and the latter forge grooves in the strips during penetration and thus maintain electrical contact. The generated signal which is proportional to the conductor's instantaneous velocity is connected via the scratch pickups to the conditioning circuitry which electronically differentiates and integrates the signal. The resulting three signals representing displacement, velocity and deceleration of the conductor as a function of time, are fed to a Tektronix storage oscilloscope, where they are recorded simultaneously.

As no material is perfectly rigid, a sensor placed at one location on a projectile can only reveal the motion of that particular location. To determine the overall motion of the projectile, a solution to the Plane Wave Equation must be found and this is carried out in Appendix C and discussed in Chapter 5.

CHAPTER III/21.....

CHAPTER III

The Apparatus

To conduct a study into impact phenomena the following are required:-

(1) A device to launch the projectile at reproducible velocities.

(2) An instrument to measure the muzzle velocities of the launcher.

(3) A means by which the target can be rigidly clamped.

(4) An instrument to measure the desired parameters on impact.

(5) A device to absorb the energy of projectiles perforating the target plate.

In this section only the more relevant aspects of the velocity transducer and associated equipment will be discussed. Further details concerning the Gas Gun and electronic circuitry can be found in Appendix A.

The general layout of the fixed part of the velocity transducer is shown in Fig. 3.1 and Photo 3.1 and 3.2. It consists of a field magnet which produces a uniform magnetic field in the pickup section. The latter also serves to support the commutating brushes or "Scratch Pickups" and the photo-triggering device.

Fig 3.1/22.....

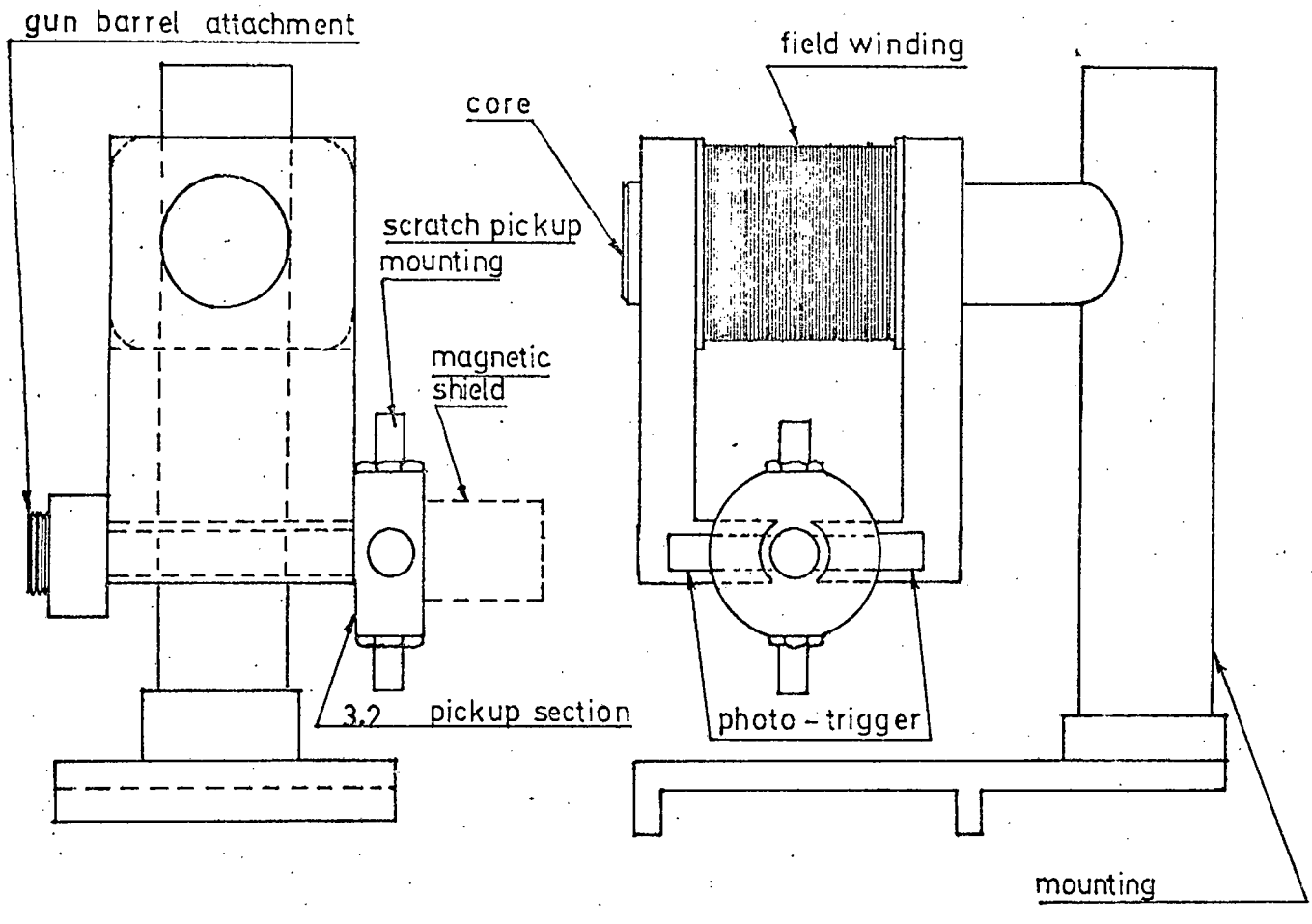

FIG 3.1 GENERAL ASSEMBLY

3.1 Field Magnet And Mounting

An electromagnet of 2 800 turns of 0,1 mm diameter copper wire is used to generate the magnetic field. The latter is conducted via a soft iron core and pole pieces, to produce a uniform field in the pickup section. Using a variable d.c. voltage supply, the magnetic field strength in the air gap can be varied from zero to 1 Wb/m^2.

The electromagnet is mounted using brass and austenitic stainless steel fittings to prevent magnetic leakage to the steel bed of the gun. The clamping arrangement has 3 degrees of freedom to facilitate the alignment of the pickup section and the pole pieces, with the gun barrel.

Photo 3.1/23.....

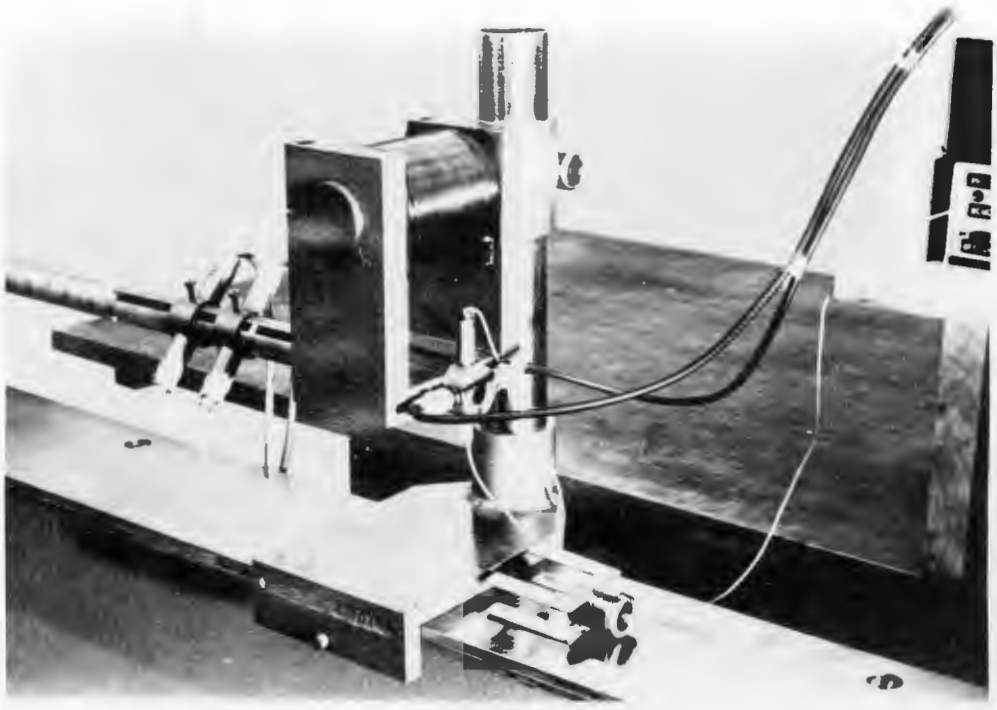

Photo 3.1 Field Magnet and Pickup Section.

Photo 3.2 Approach Velocity Measuring Device Field Magnet and Target Clamping Arrangement. (Note slotted barrel section).

Fig. 3.2/24.....

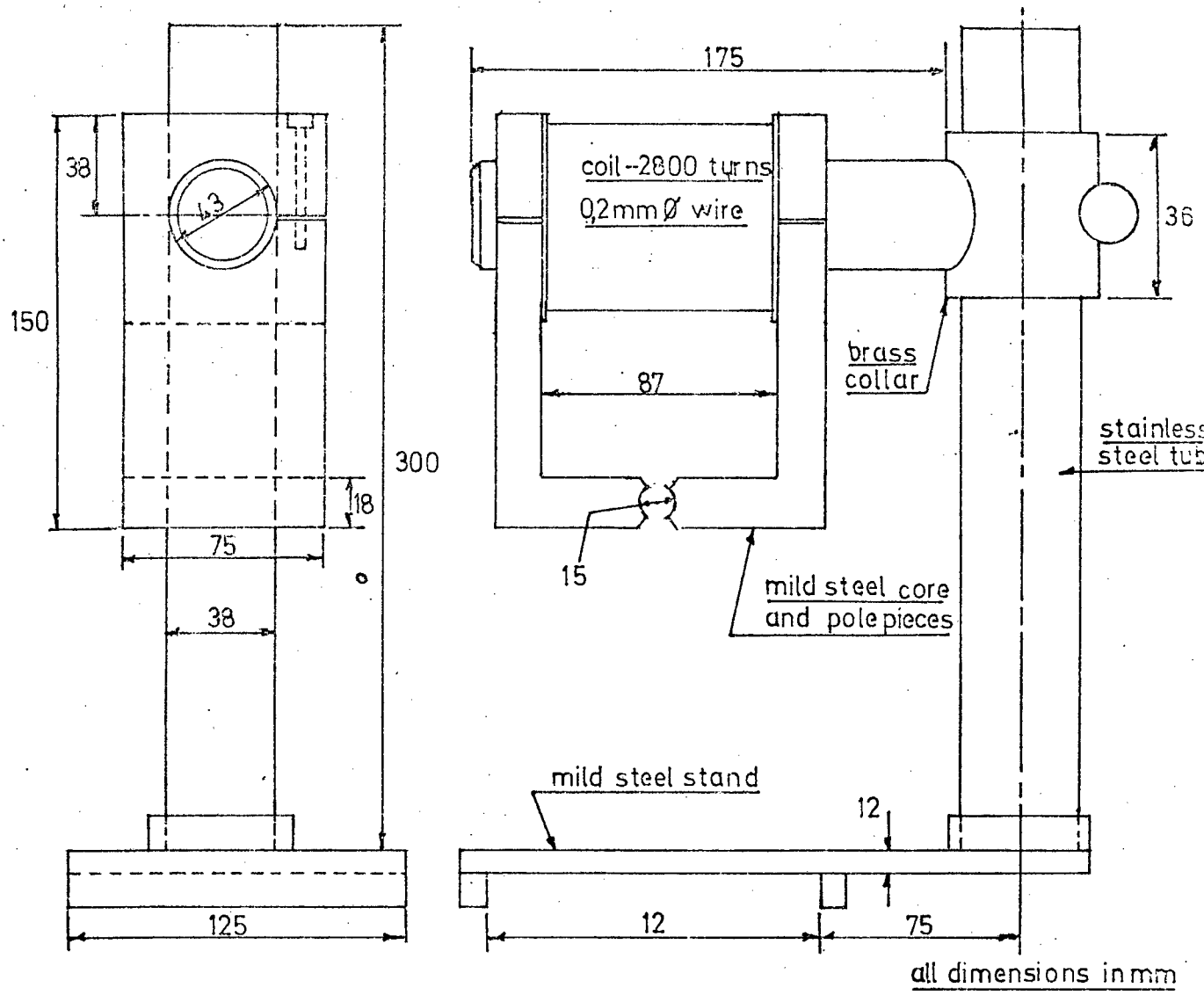

FIG 3.2 FIELD MAGNET AND MOUNTING

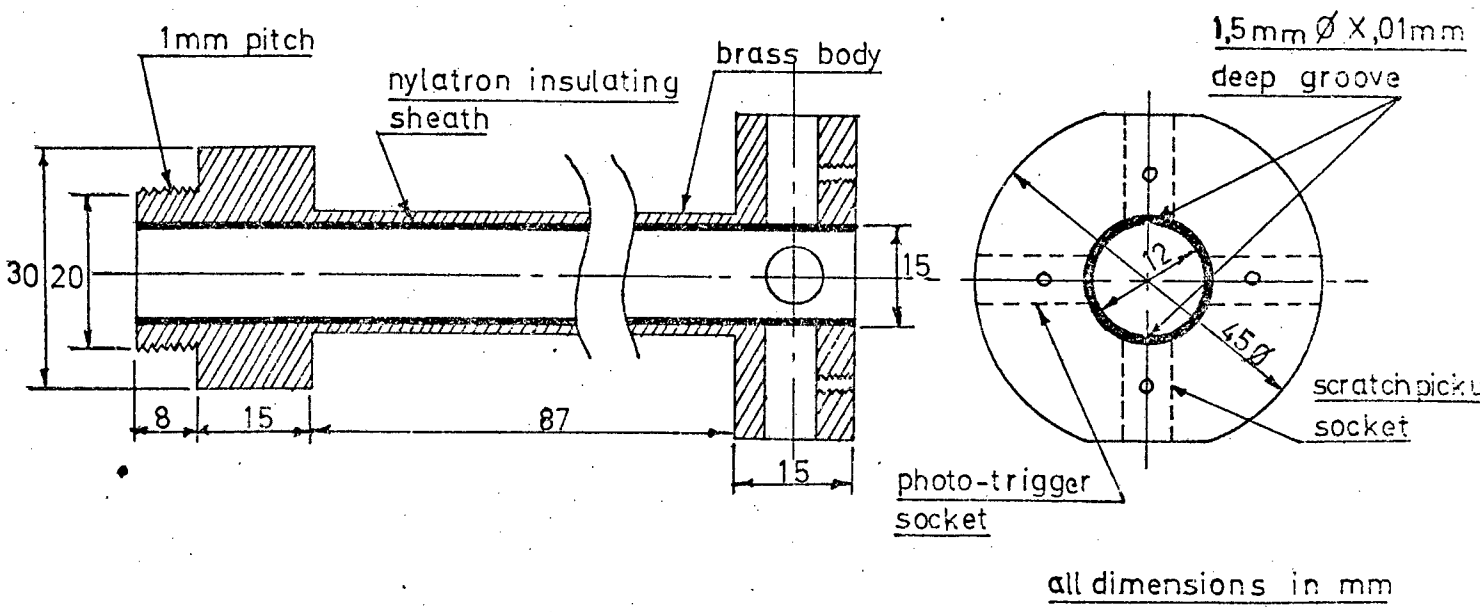

FIG 3.3 PICKUP SECTION

3.2 Pickup Section

The function of this section is to guide the projectile in the correct orientation, through the magnetic field. The walls of the guide-tube are of brass and minimally thick to prevent magnetic field distortion and attenuation. The inner wall of the guide-tube is lined with an insulating plastic (nylatron G.S.) to prevent electrical shorting of the projectile's commutator strips. These strips also act to guide the projectile as they travel along the axial grooves in the barrel and pickup section (see Fig 3.3)

Fig. 3.4 shows the factors which determine the position and size of the various components. The projectile length has been kept to a minimum to keep the sensing conductor as close to the impacting surface as possible.

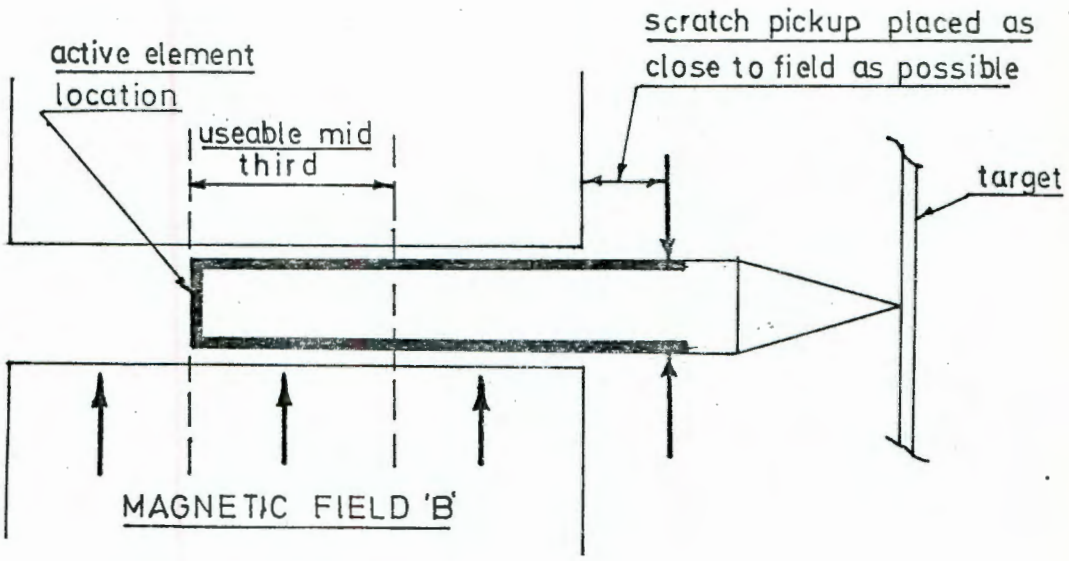

FIG 3.4

The scratch pickups are situated at the target end of the pickup section as close to the magnetic field as possible. Details of their construction are shown in Fig. 3.5. A scratch pickup consists of a 1 mm diameter high-speed steel rod, ground at the contact end to form a wedge-shaped cutting point. The rod is insulated from the brass body of the pickup section and the latter effectively shields the electrical signal from outside electrical noise. Connection to the recording apparatus is made via heavy duty shielded cable.

Initially the cutting point was ground with positive rake so that the passing commutator strips were actually "machined". This arrangement however, did not produce a uniform contact pressure, and the swarf

produced/26.....

produced often shorted out the signal to earth if it came into contact with the brass body of the pickup section. The present "negative rake" configuration gives a good uniform contact pressure and the cutting point tends to forge a groove through the commutator material leaving no swarf. The points hold their edge and are still sharp after more than two hundred shots.

Depth of cut is regulated by means of the adjustment nut shown in Fig. 3.5. This is done by inserting a 12,5 mm plug into the barrel and lowering the scratch pickups until they just make contact with the plug. Since the commutator groove is 0.1 mm deep, when the projectile passes with the pickups adjusted as above, a 0.1 mm deep groove is cut along the commutator strip.

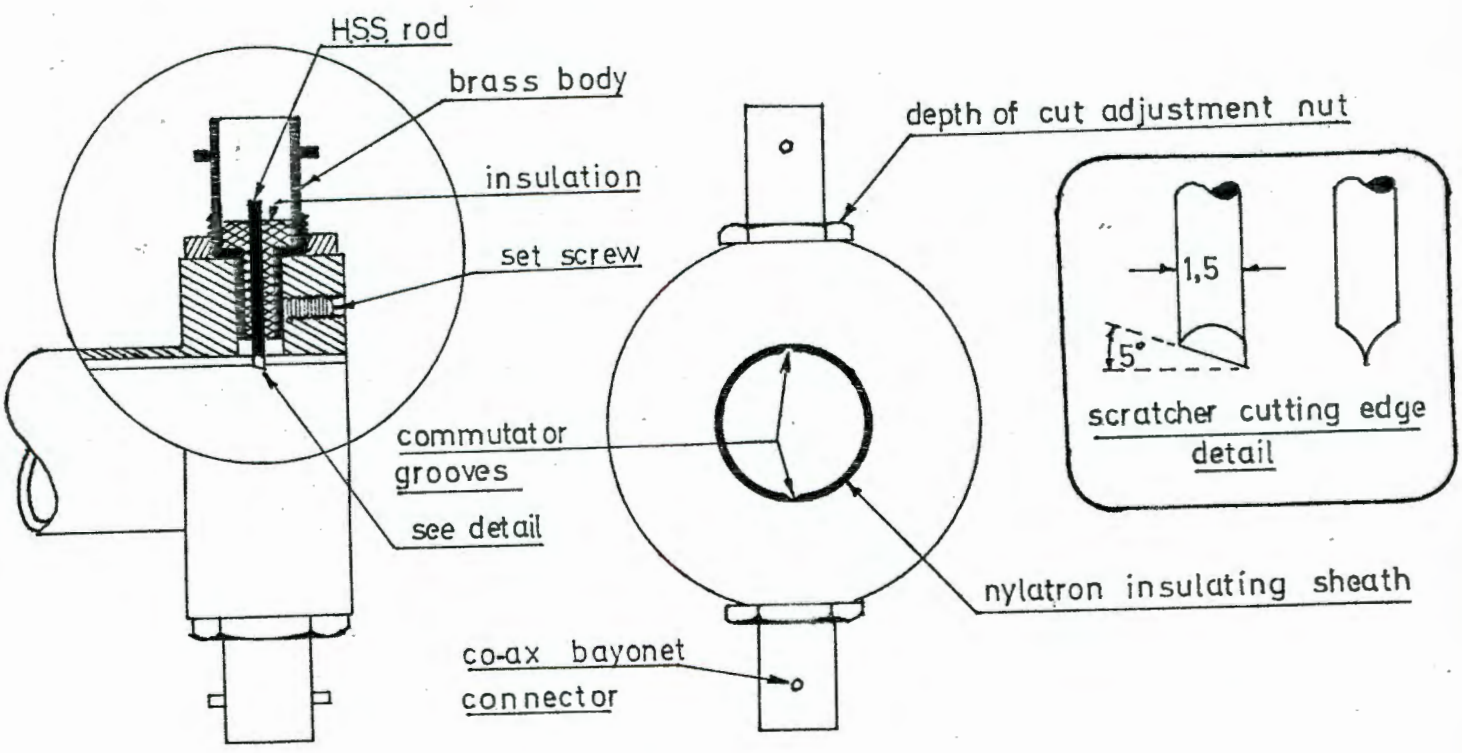

FIG 3.5 SCRATCH PICKUP DETAIL

3.3 Projectile

Two configurations were tried. The first shown in Fig. 3.6 is appealing in its simplicity, but as its output voltage is limited at low velocities, noise associated with the scratch pickups, becomes too significant.

Fig. 3.6/27.....

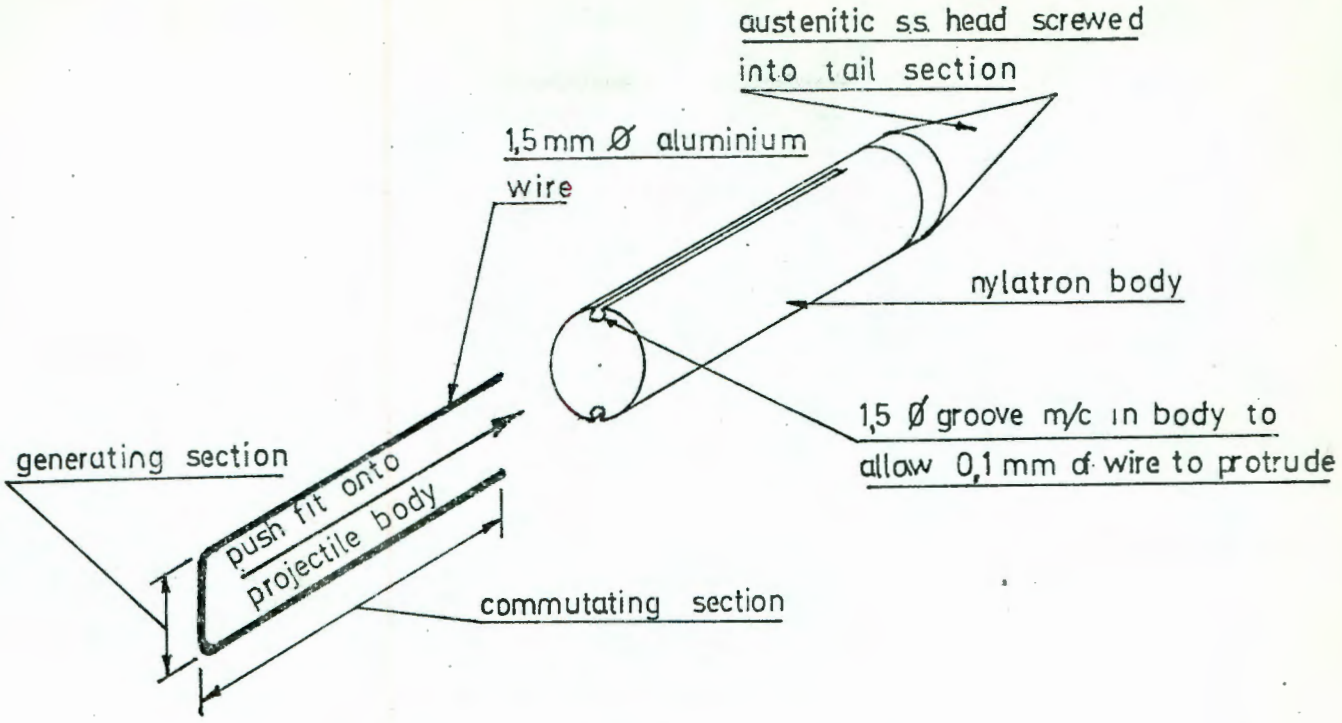

FIG 3.6 PROJECTILE MK I

After experimenting with the Mk I projectile it was realised that a far larger signal/noise ratio is necessary if electronic differentiation is to be attempted. With an upper bound on the magnetic field strength due to saturation of the iron pole pieces, the only alternative was to effectively increase the number of generating conductors and connect them together in series. This was accomplished by winding a coil of wire on the projectile body as shown in Fig 3.7.

Fig. 3.7/28 .....

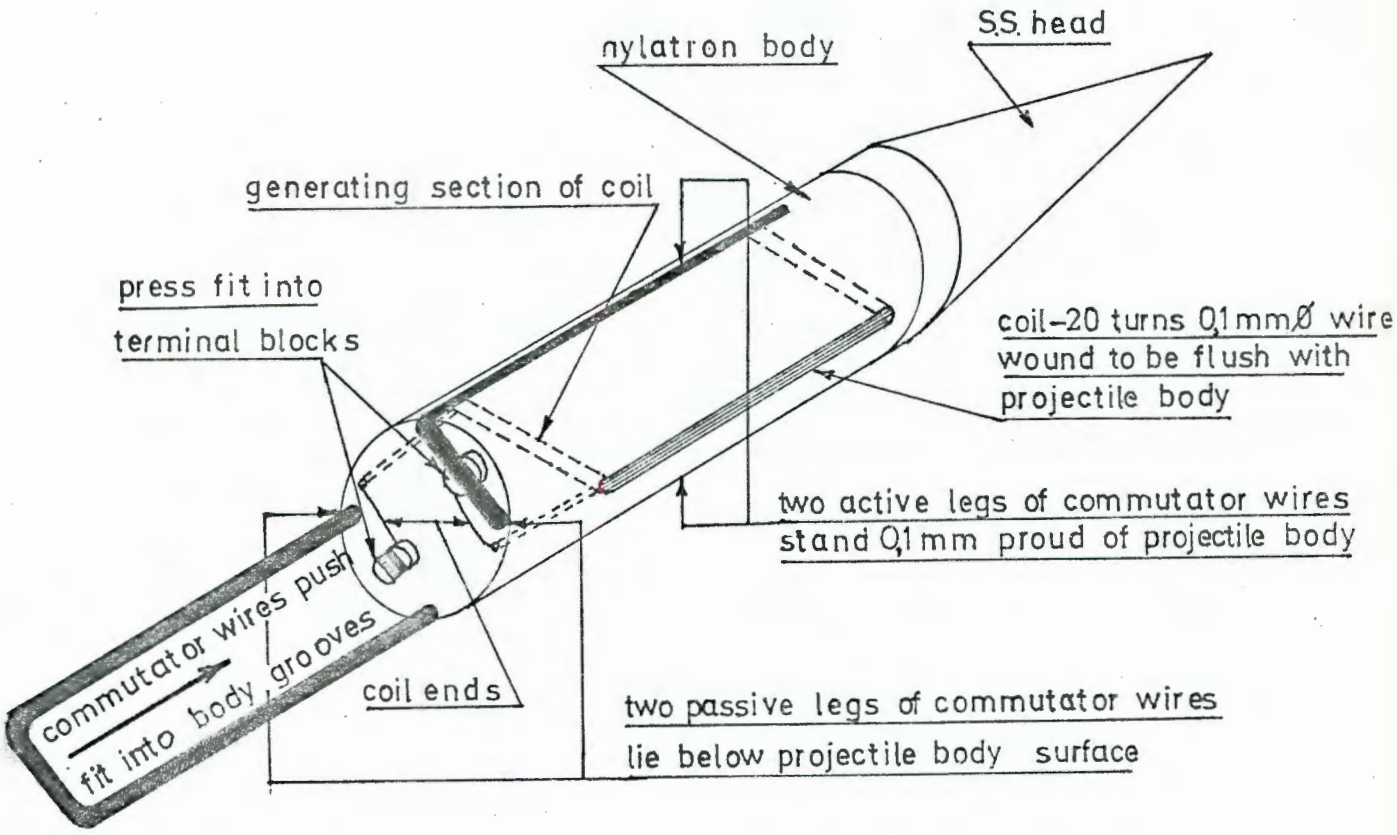

FIG 3.7 PROJECTILE MK II

As with the Mk I projectile, U shaped Aluminium wire commutators were used. This was done to keep the "mass balance" of wire the same on either side of the projectile, as the large decelerations encountered (200,000 m/s^2) would rip an assymetrical configuration apart. The arrangement was also economical on wire, since after each shot the wire U would be turned around to present the unscratched leg as a commutator. Initially, copper wire was used, but later abandoned as its high density to strength ratio caused the wire to fail continually at the high decelaration rates encountered.

The use of a coil of 20 turns of wire increased the output twenty-fold, so that on the average, the present output signal is in the order of one volt. It will be appreciated that additional precautions had to be taken using a coil. Firstly if a coil is passed through a magnetic field the net flux cutting the coil is zero and hence no e.m.f. is generated. If one section of the coil can be effectively shielded from the field, e.m.f. will again be generated. In the Mk II configuration, the forward diametral section of the coil is allowed to leave the uniform magnetic field and passes

through/29.....

through a magnetic shield during the critical part of the penetration measurement. This leaves the rear diametral section of the coil as the sole e.m.f. generator.

By using a coil to generate an e.m.f., added problems of distortion and phase lag due to self inductance were anticipated. The following calculations show however that for the given coil and expected rates of change of voltage, the back e.m.f. induced by the coil are insignificant.

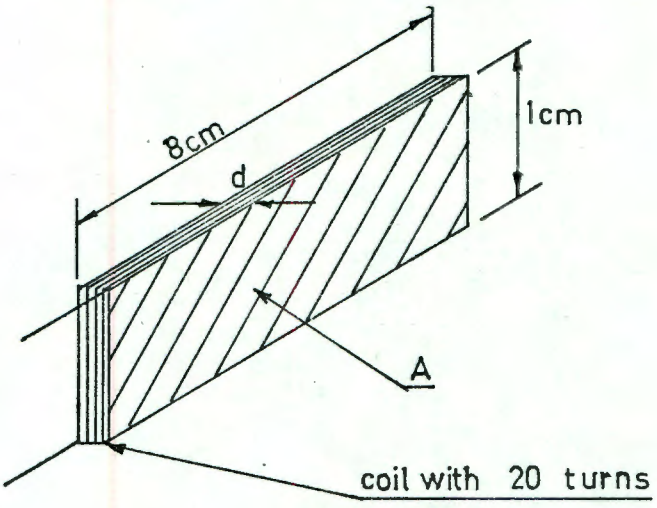

A = area of coil
d = depth of coil = 0,1cm
n = number of turns
$\mu = 4\pi \times 10^{-7}$

FIG 3.8

For a coil the self inductance is given by

$$L = \frac{N^2 \mu A}{d} \quad \text{Henries} \quad \ldots\ldots\ldots\ldots\ldots\ldots\ldots\ldots \quad (3.1)$$

Photo 3.3/30 .....

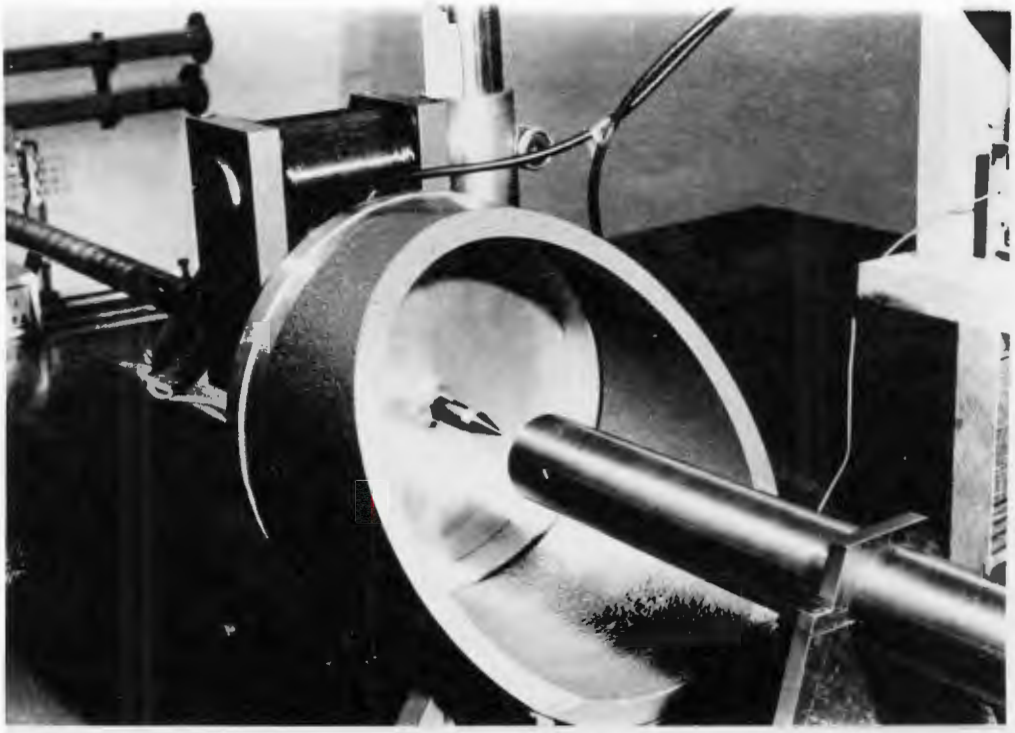

Photo 3.3 Target Holder and Projectile Catcher (Details in Appendix A).

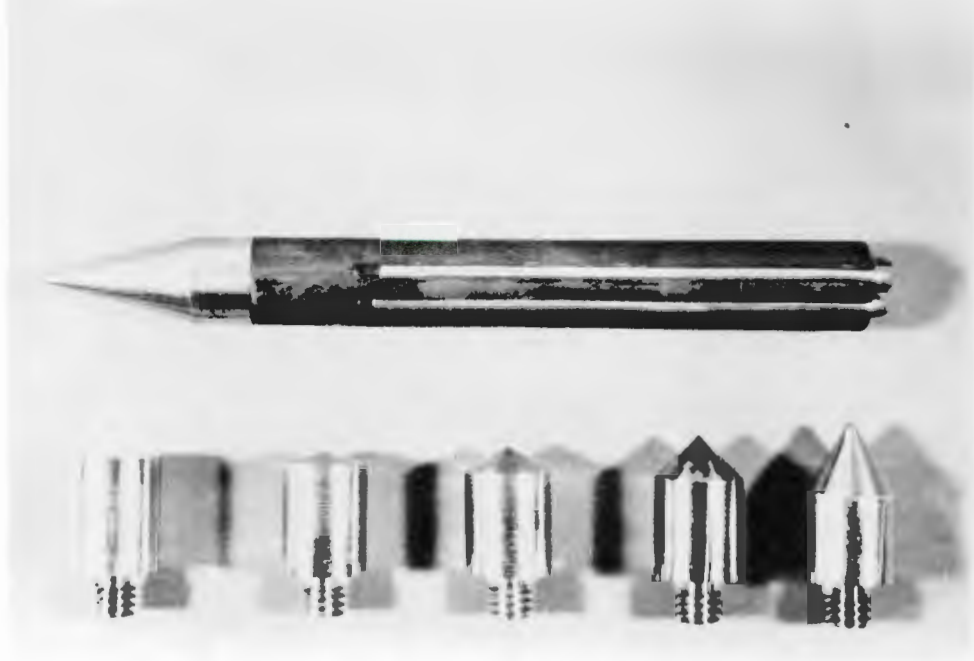

Photo 3.4 The Projectile and Range of Heads.

Substituting/31....

Substituting in 3.1 we get

$$L = \frac{20^2 \times 4\pi \times 10^{-7} \times 8 \times 10^{-4}}{1 \times 10^{-3}} = 4{,}02 \times 10^{-4} \text{ Henry}$$

From a typical voltage-time trace the maximum slope gives: $2{,}5 \times 10^3$ V/S. This signal is fed to the oscilloscope input whichhas a resistance of 1 MΩ giving :

$$\left(\frac{di}{dt}\right)_{max} = \frac{2{,}5 \times 10^3}{10^6} = 2{,}5 \times 10^{-3} \text{ A/S}$$

The back e.m.f. generated in the coil is therefore

$$L\left(\frac{di}{dt}\right)_{max} = \frac{2{,}5 \times 10^{-3} \times 4{,}02 \times 10^{-4}}{1} = 1{,}05 \times 10^{-6} \ V$$

Compared with the primary voltage this is negligably small.

3.4 Approach Velocity Measurement

Rather than rely on the absolute determination of the e.m.f.-velocity relationship from a knowledge of the effective coil length and the magnetic field strength, a device was made to measure the approach velocity of the projectile. Knowing this,the calibration constant K_1 can be found, since the vertical axis of the oscilloscope is calibrated in volts, and the initial part of the velocity time trace,which is horizontal, represents the approach velocity; see Fig. 3.11. Hence

$$E = K_1 V \quad \ldots\ldots\ldots\ldots\ldots\ldots\ldots\ldots\ldots\ldots\ldots\ldots\ldots\ldots\ldots\ldots (3.2)$$

Both deceleration and displacement can be calculated from this initial calibration.

The device itself consists of two light beams across the projectile path and a measured distance D mm apart. The beams are arranged to fall onto two photo-transistors, which are connected to two Schmitt triggers.. These triggers are used to start and stop an electronic digital clock capable of measuring to an accuracy of $\pm$ 1 μs. When the projectile breaks the first beam, the timer is started and when it breaks the second beam the timer is stopped. Knowing the time taken to cover the measured distance D mm, the muzzle or approach velocity can be calculated.

The photo-sensors are mounted on the gun barrel by means of adjustable

collars/32.....

collars (see Fig 3.9 and photo 3.2). To ensure that the projectile is no longer being accelerated by the driver pressure of the gun, four 15 cm long slots are cut in the barrel to vent the driver pressure to atmosphere.

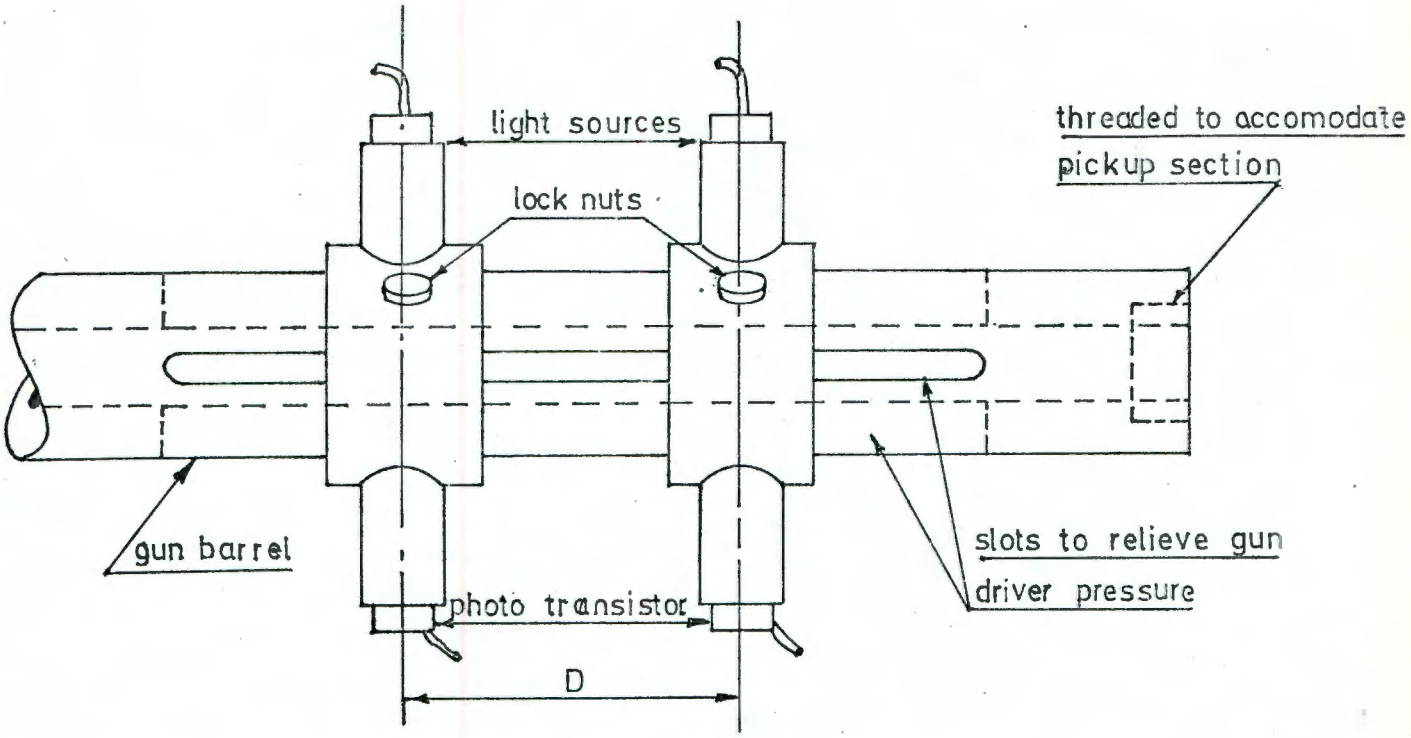

FIG 3.9 APPROACH VELOCITY MEASURING DEVICE

3.5 Electronics

The signal obtained from the projectile is proportional to the instantaneous velocity of its tail, and to derive deceleration-time and displacement-time relations from this, the signal is differentiated and integrated electronically. The three resulting signals are then fed to a four channel Tektronix oscilloscope which has a storage facility. A camera attachment to the oscilloscope is used to obtain a permament record of the penetration data. The general layout of the system is shown in Fig.3.10.

Fig. 3.10/33.....

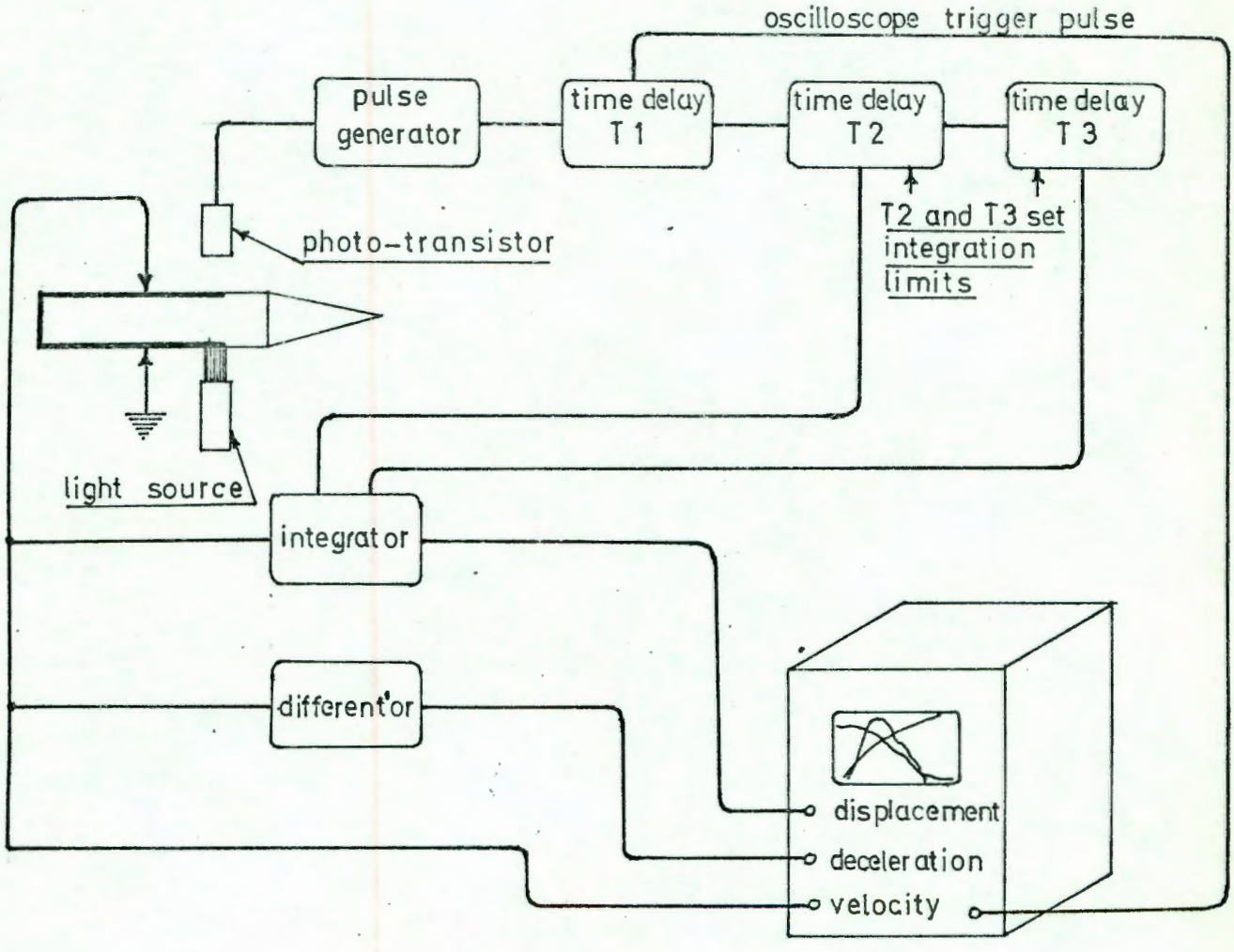

FIG 3.10 SCHEMATIC ELECTRICAL LAYOUT

Details/34.....

Details of the differentiator, integrator and delay circuitry can be found in Appendix C.

Fig. 3.11 illustrates the pulsing sequence necessary to co-ordinate the velocity transducer and the oscilloscope. Whereas the velocity and deceleration channels can be switched on before the impact occurs, the integrator must be started and stopped at the desired limits since it is a summing device. LT 1 and LT 2 can be selected by graduated dials on the integrator control panel.

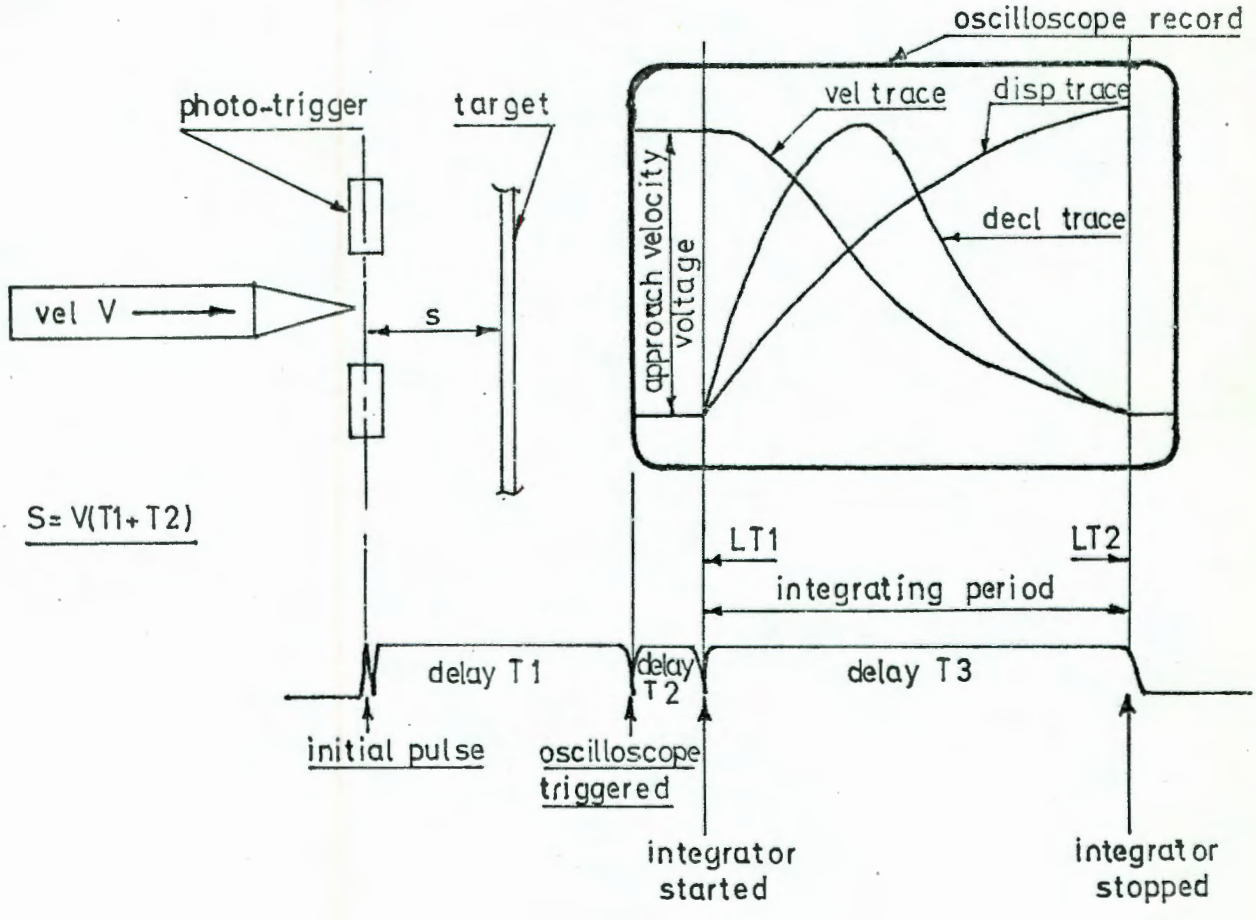

FIG 3.11 PULSING SEQUENCE

CHAPTER IV

Preliminary Tests and Operating Proceedure

4.1 Scratch Contact Characteristics

A perfect commutator and brush should transmit a voltage or current without distortion. The scratch contact concept is open to several disturbances departing from this perfect behaviour.

Firstly, the relative motion between the aluminium commutator and high speed steel brush generates heat, and the contact of two dissimilar metals at an elevated temperature will produce Seebeck and Peltier e.m.f's. Fortunately however, the pickup contains two such thermocouples in opposition (see Fig. 3.17) so the overall effect should be zero.

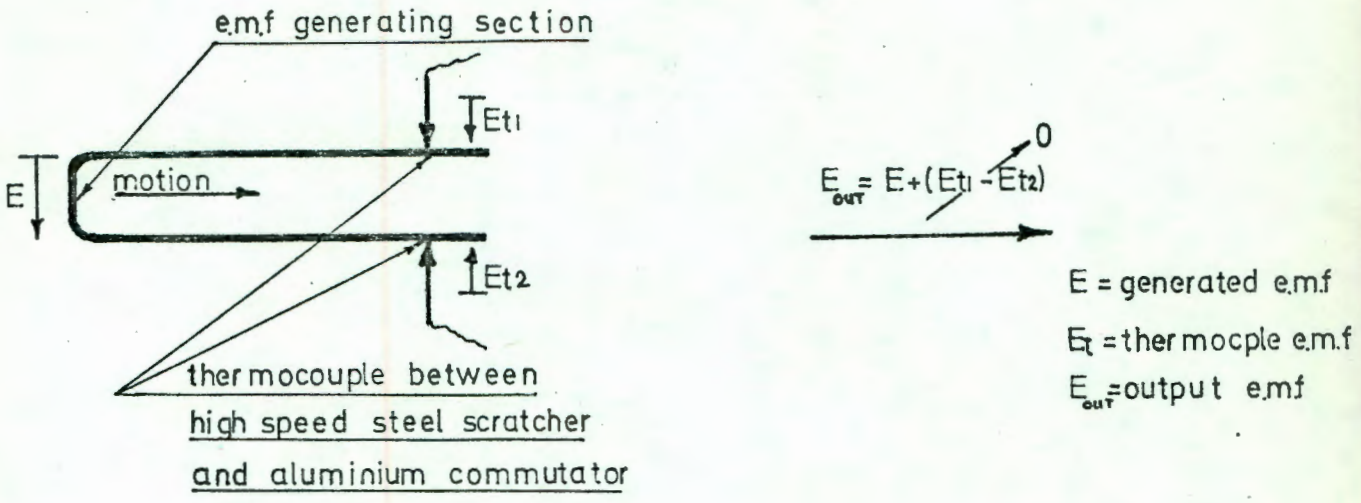

FIG 4.1 THERMOCOUPLE DISTURBANCE

The other effect to disturb the output voltage is variation in contact resistance at the scratch pickups. As the oscilloscope and integrated circuits draw only about one microamp of current from the projectile's generating coil, the scratch pickup can vary from its normal fraction of an ohm resistance to 10 000 ohms before a 1% fluctuation will be noticed in a 1 V signal. This is not too demanding on the pickups.

The above assumptions were substantiated in the following tests:-

Test 1. With the field coil removed, a 20 mV dc signal was applied across the scratch pickups. On firing the projectile between the pickups at a velocity of 74,5 m/s and into a 0,2 mm thick Al target, the 20 mV

signal/36.....

signal was recorded on the storage oscilloscope. Photo 4.1 shows the resulting trace.

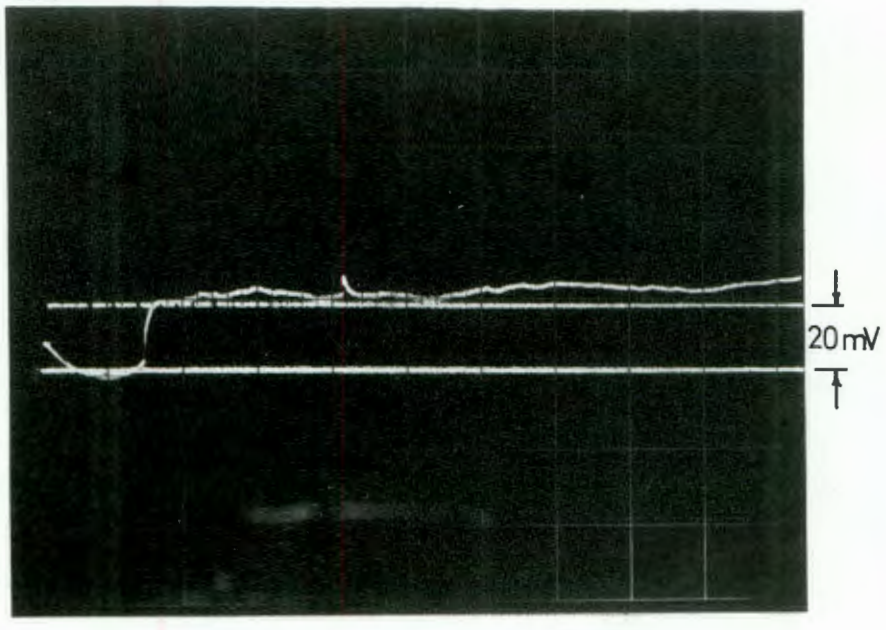

Photo 4.1 Small Signal Commutation.

The resulting fluctuation of approximately $\pm$ 5 mV gives a fluctuation of

$$\frac{5}{1\ 000} = \pm \frac{1}{2}\ \%$$

for a one volt signal.

Test 2. The same layout as in Fig. 4.2 was used except that a signal

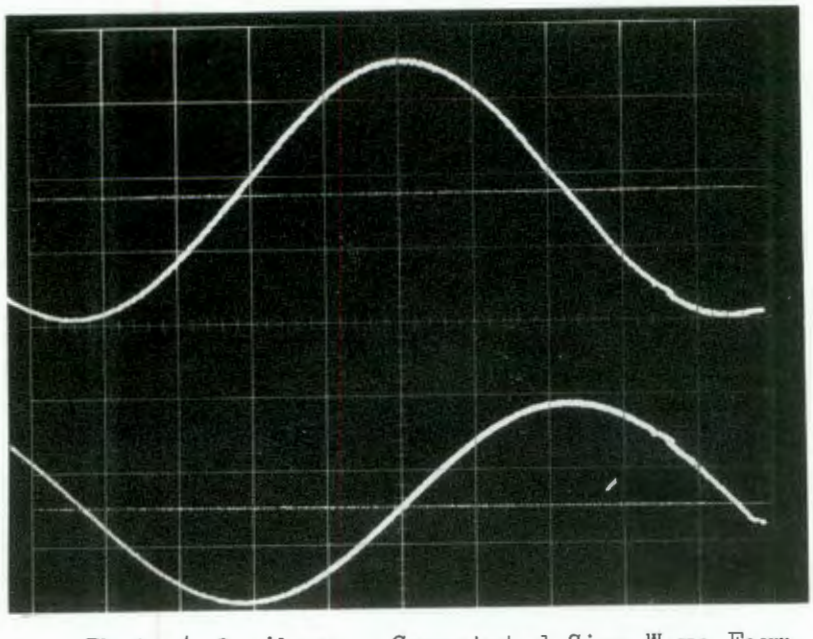

Photo 4.2 Above: Commutated Sine Wave Form.
Below: Differentiated Wave Form.

generator/37 .....

generator was connected instead of the battery, and the differentiator trace was also recorded. The test signal was a sine wave of 2 kH_2 frequency 20 mV amplitude.

4.2 Range and Linearity of Transducer.

This test was designed to investigate the following:-

(1) The loss of velocity and hence of voltage, due to the mechanical resistance of the scratch pickups.
(2) The effectiveness of the magnetic shield described in section 3.3.
(3) The range, i.e. the displacement, over which the velocity transducer remains linear.

The above were tested by firing the projectile through the magnetic field with no target in place, and looking at the velocity time trace produced. Two shots were fired, one with the magnetic shield in place, and the other without the shield. The results are shown in Photos 4.3, and 4.4. The markers on the trace were produced by cutting notches in the commutator strips. From these marks the displacement corresponding to the linear range can be found.

The rise in voltage with time is to be expected in Photo 4.3, as the forward diametral section of the coil which ideally should be magnetically shielded, is travelling through an ever-decreasing magnetic field.

From the trace in Photo 4.4 it can be seen that the linearity between the notches, which are 24,1 mm apart, is good. The slight fall in velocity due to the mechanical resistance of the scratch pickups gives only a 0,8% deviation over the whole linear range.

The method of marking the velocity-time trace by means of notches in the commutator strip was considered as a way of determining the initial projectile velocity. If the notches are placed near the front of the commutator a known distance apart, the breaks in the initial part of the velocity time trace, before the projectile impacts the target, will give a measure of the projectile's velocity. To attain any accuracy however, the method was found to use up too much of the projectile's linear range, and to restrict the traces to the right hand side of the oscilloscope screen. Because of these limitations the method described in Section 3.4 was adopted instead.

Photo 4.3 /38 .....

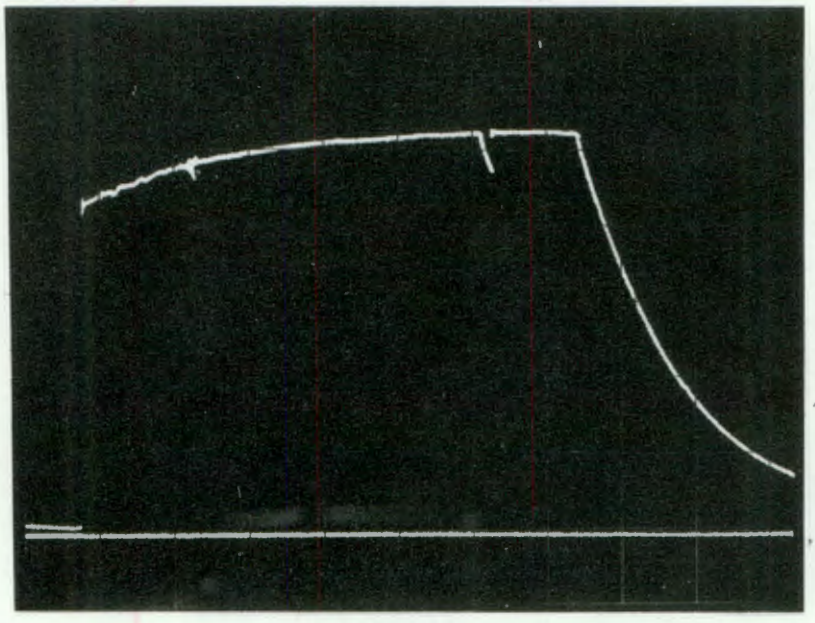

Photo 4.3 Free Velocity Trace with no Shield.

4.3 Operating Proceedure

The following proceedure was followed to obtain displacement velocity and deceleration traces:-

(1) Screw a projectile head to the "Nylatron" body and press-fit the commutator wires into their slots. The wires can be used for up to three shots before renewal is necessary. Making sure the commutator

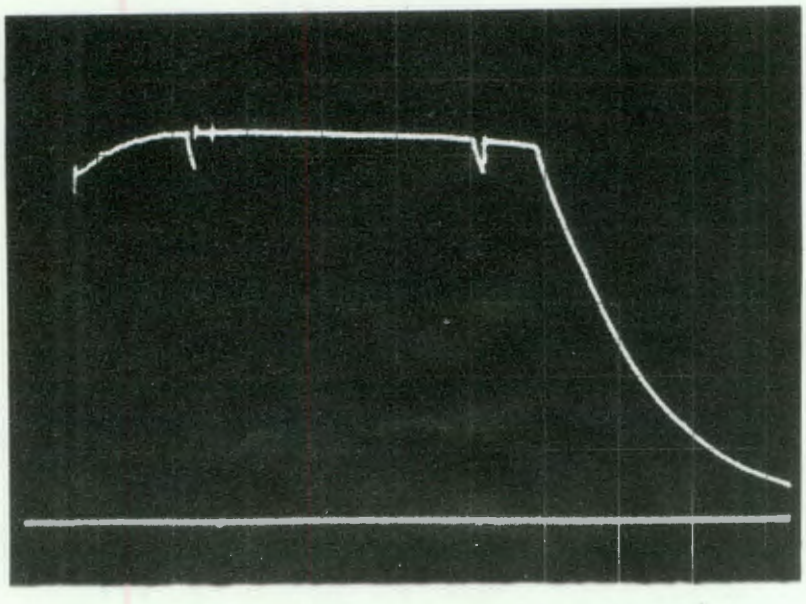

Photo 4.4 Free Velocity Trace with Shield.

strips align with the barrel grooves the projectile may then be pushed into the breach, and is ready for firing.

(2) The /39.....

(2) The "Digital Timer" is switched on as well as the power supply to the light sources of the photo sensors. The Schmitt triggers in the timer are adjusted to maximum sensitivity and the timer read-out is zeroed.

(3) According to preliminary calculations, the three time delays, T1, T2 and T3, are set, and their circuits switched on. Usually several test shots are required to position all three traces on the oscilloscope screens correctly. The differentiator, integrator, photo-trigger and field magnet can now be switched on. Current through the latter is adjusted using a rheostat, according to the output required.

(4) The oscilloscope is housed in an acoustic box, as the electronic valves, etc., used in its circuitry are sensitive to the shock wave produced by the gun. The three shielded cables carrying displacement, velocity and deceleration information, pass through a plugged hole in the side of the box, and are connected to three of the four available channels. A wire also connects the oscilloscope trigger to time delay T1. The amplification required on each channel is selected, and before the lid is place on the acoustic box, the trigger and storage facility are set.

(5) The magnetic shield is clipped onto the field magnet and the target holder with target clamped in place, is brought up against the shield. This ensures that the time delay between the projectile breaking the trigger beam and arriving at the target, can be accurately estimated for each shot. In case the projectile perforates the target, a "catcher" (see Appendix A) is placed centrally behind the target.

(6) Usually several test shots are needed to ascertain the best settings of field strength, amplifier gains, and the various time delays. For this purpose, a small 100 mm diameter target holder is used to economise on target material. On obtaining a good trace, the "Canon" camera attachment is dipped onto the oscilloscope and using "ASA 400 Tri × PAN" film, a permanent record is made.

(7) Data reduction requires that the co-ordinates of the various traces be known. This is done by reading approximately 50 data points from each photographic negative using a travelling microscope. The instrument gives an accuracy of about 2% of the mean ordinate height.

CHAPTER V. /40.....

CHAPTER V

Analysis of Projectile Vibration On Impact.

When two elastic bodies collide, a stress wave travels through each at the acoustic velocity of the medium concerned. On reaching a boundary, the wave will reflect back into the body and thus initiate a vibration.

The only researchers to date, to account for projectile vibration during the penetration process, have been Masket (1) and Bluhm (10). This is because the methods employed by them were sensitive enough to detect the vibration phenomena. Other experimentalists such as Goldsmith (et al) and Wingrove have overlooked the vibration problem. On the theoretical side, models of penetration which were outlined in Chapter I, have been far too crude to consider projectile vibrations (see Fig. 1.2).

In this study, vibrations set up in the projectile had to be considered. The reasons are two-fold. Firstly as the primary data obtained is a deceleration-time trace on an oscilloscope, no data smoothing is possible as was done by Goldsmith (14). His method of deriving a force function from displacement-time data is, in the author's opinion, debatable. The present technique records very pronounced vibrations in the projectile (as predicted by Masket (1)) and the interpretation of these is very important. Secondly the elastic nature of the projectile body (Nylatron GS) tends to amplify the vibration phenomenon.

5.1 Masket's Analysis

On impact a projectile is set into vibration so that all particles in the axial direction are in motion relative to one another. In Masket's work the tail surface of the projectile was photographed and was therefore the station from which measurements were made. His problem was to describe the projectile motion as a whole, when the motion at the tail only was known. To do this Masket made the following assumptions:-

(1) The pointed end of the projectile is short in comparison with its total length, and it may therefore be treated as a cylinder of equivalent mass but calculably shorter length.

(2) In normal impact, transverse vibrations are negligible.

Under these conditions the problem of a projectile impacting a target and executing longitudinal vibrations can be simplified to the problem of an elastic rod moving with velocity V_o which at a time $t_o = 0$

encounters/41.....

encounters a force F(t). (See Fig. 5.1) acting on the leading face and opposing the motion.

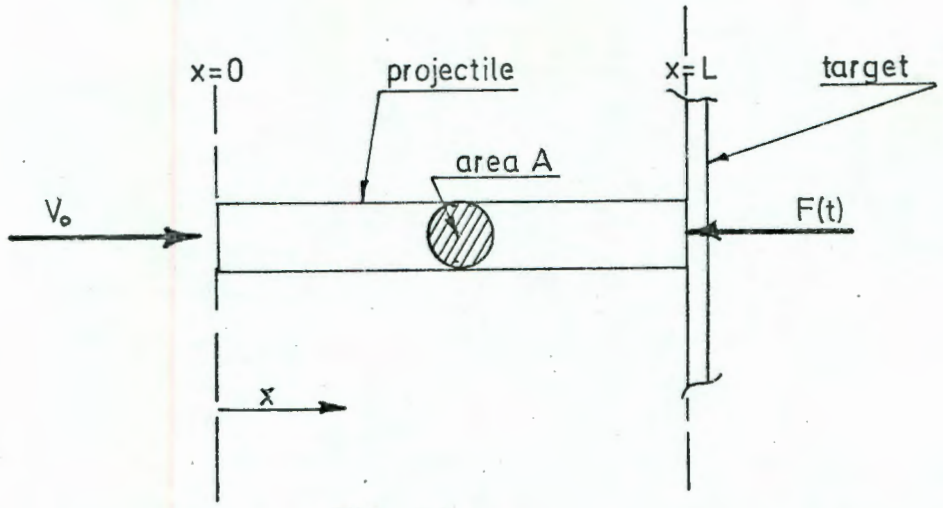

FIG 5.1

For small strains and damping the solution to the differential equation:-

$$\frac{\partial^2 u}{\partial t^2}(x,t) = c^2 \frac{\partial^2 u(x,t)}{\partial x^2} \quad \ldots\ldots\ldots\ldots\ldots\ldots\ldots \quad (5.1)$$

enables the motion of the projectile to be predicted.

Masket's solution to equation 5.1 is presented in Appendix B. From the solution he postulated the following four theorems.

Theorem I The displacement, velocity and deceleration of the centre of mass at any instant t' are respectively equal to the average values of the displacement velocity and deceleration of the projectile base over the time interval

$$(t' - \ell/c,\ t' + \ell/c) \text{ for all } -\infty < t' < \infty$$

Theorem II The velocity at any instant t' is equal to the difference between the displacements of the base at the end points of the time interval $(t' - \ell/c,\ t' + 1/c)$ divided by the magnitude of the interval (the fundamental period of longitudinal vibration $2\ell/c$)

Theorem III The deceleration of the centre of mass at any instant t' is equal to the difference between the velocities of the base at the end points of the time interval $(t' - \ell/c,\ t' + \ell/c)$ divided by the magnitude of the interval $2\ \ell/c$.

Theorem IV/42.....

Theorem IV The displacement, velocity and deceleration of the centre of mass at any instant are respectively equal to the average of the values of displacement, velocity and deceleration distributed throughout the projectile at that instant.

5.2 Generalised Analysis.

In the present study the point at which measurements of the projectile's motion were made is not located in the tail itself but a distance d mm from it. Accordingly an analysis was done to reveal the motion of the centre of mass in terms of the pickup motion. This analysis is presented in Appendix B. The new solution to equation 5.1 prompted the formulation of Theorem V which states that:

Theorem V The displacement velocity and deceleration of the centre of mass at any instant t may be computed from the average of the displacement velocity and deceleration respectively of a point on the projectile a distance d mm from the base by the equation:

$$c/\ell \int_{t-(d+\ell)/c}^{t+(\ell-d)/c} X(d,t)dt = X_{cm}(t) + X_{cm}(t - 2d/c) \quad \ldots\ldots \quad (5.2)$$

Where X = displacement, velocity or deceleration.

Equation 5.2 is a general form of Masket's relationship and the two are identical when d is set to zero.

While penetrating, a projectile can be regarded as executing two superimposed motions. The one is the relatively smooth deceleration experienced by the centre of mass of the projectile and the other an oscillation relative to the centre of mass. Bluhm (10) and Masket (1) used their solutions to the plane wave equation to separate the motion of the centre of mass from the overall motion. Similarly the motion of the head of the projectile can be found once the motion at any other point on the projectile is known.

To date little has been reported on the influence of the vibratory behaviour of projectiles on the impact process. Bluhm (10) mentioned the phenomenon with regards to projectile failure after penetration. Generally however, theories of penetration are too crude for the vibration phenomenon to play a significant role.

CHAPTER VI/43.....

CHAPTER VI

Testing and Use of the Velocity Transducer.

In the following experiment the projectile cone angle was chosen as the independent variable. This was done partly to fill a gap in the current literature on penetration, but mainly because it strongly controls the impulse shape and thus provides a wide spectrum of data on which the accuracy, reliability and limitations of the velocity transducer can be ascertained.

The experiment which was performed primarily to test the transducer, was also used to check certian aspects of penetration reported by other researchers. These include:-

6.2 Description of Impulse Shape.
6.3 Bilaminar Impulses.
6.4 Post-penetration Friction.
6.5 Derived Parameters.

The methods used and results obtained are presented in sections 6.1 - 6.5 followed by a general discussion in section 6.6.

The differentiated output signal from the velocity transducer was used to test the accuracy of the apparatus. The data obtained was processed as described in Chapter 5, to derive the motion of the projectile's centre of mass. Once this is known, as well as the drop in velocity experienced by the projectile, the impulse momentum law can be used to relate the two parameters, viz:

$$\Delta MV = \int_o^t Fdt = \int_o^t Madt$$

where 'a' describes the average deceleration of all the particles in the projectile, and m their total mass. The expression thus simplifies to:-

$$\Delta V = \int_o^t adt \qquad \ldots\ldots\ldots\ldots\ldots\ldots\ldots\ldots\ldots\ldots\ldots\ldots \quad (6.1)$$

6.1 Momentum Balance

To test the transducer over a range of impacts varying in amplitude and duration, a series of conical projectile heads was used. These heads each had the same mass and varied in cone angle from 30° to 150° in 30° intervals (see Photo 6.1).

Two types/ 44 .....

Two types of target were used, monolaminar and bilaminar. Both types were made from ALCAN 2 HS4 aluminium plate, the monolaminar being 1,6 mm thick and the bilaminar 2 x 0,8 mm thick. The targets were circular and clamped circumferentially on a 190 mm diameter by two steel rings (see Appendix A).

For each shot the case of containment, i.e. where the projectile is arrested in the target plate, was approached as closely as possible. To achieve perfect containment is difficult, especially with the blunter projectiles which penetrate by a punching process rather than a petalling one. The reason for this difficulty is discussed in section 6.3. The accuracy of the test is not affected by varying degrees of containment, since the velocity-time trace which is recorded simultaneously on the oscilloscope screen, enables the initial and final velocities to be obtained. This gives an accurate measure of ΔV. Photo 6.1 shows a typical oscilloscope record.

Data obtained from the deceleration-time traces was processed by computer (see Appendix C) to give the motion of the centre of mass of the projectile. This data is presented in the form of a computer plot of the sensor motion with the motion of the centre of mass superimposed. A typical computer output is shown in Appendix D. Graph 6.1 shows the impulses obtained for the five shots.

Results

The results of the impulse-momentum verification are presented in figure 6.1.

Cone Angle	Impulse Area cm^2	Scale Factor 0,45 cm^2 =	$\int adt$	ΔV	% Diff.
30°	80,05	4 m/s	49,62	49,18	0,89%
60°	98,0	4 m/s	60,75	60,12	1,05%
90°	44,7	8 m/s	55,42	55,05	0,67%
120°	122,6	3,2 m/s	61,12	60,02	1,8 %
150°	67,6	3,2 m/s	33,73	33,0	2,14%

Fig. 6.1 Table of Results for Momentum Check

6.2 Analysis of Impulse Shape. Several researchers have tried to describe experimentally derived impulse curves, by means of analytical expressions. The use of such expressions is discussed in section 6.6.2.

Force-Time Plot/45 .....

GRAPH 6.1

FORCE-TIME PLOT FOR PROJECTILES OF EQUAL MASS-DIFFERENT CONIC ANGLE

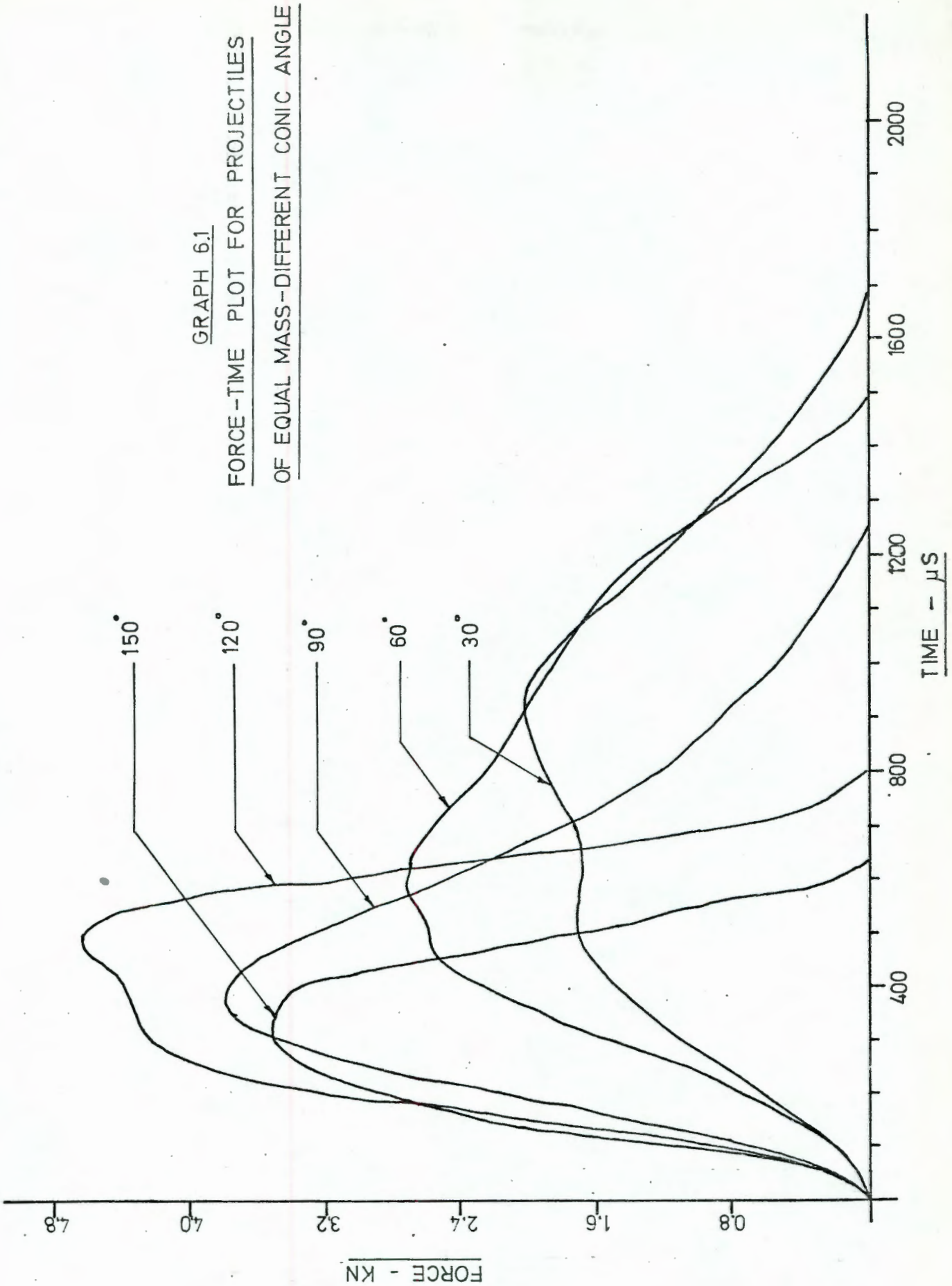

Graph 6.1a/ 46.....

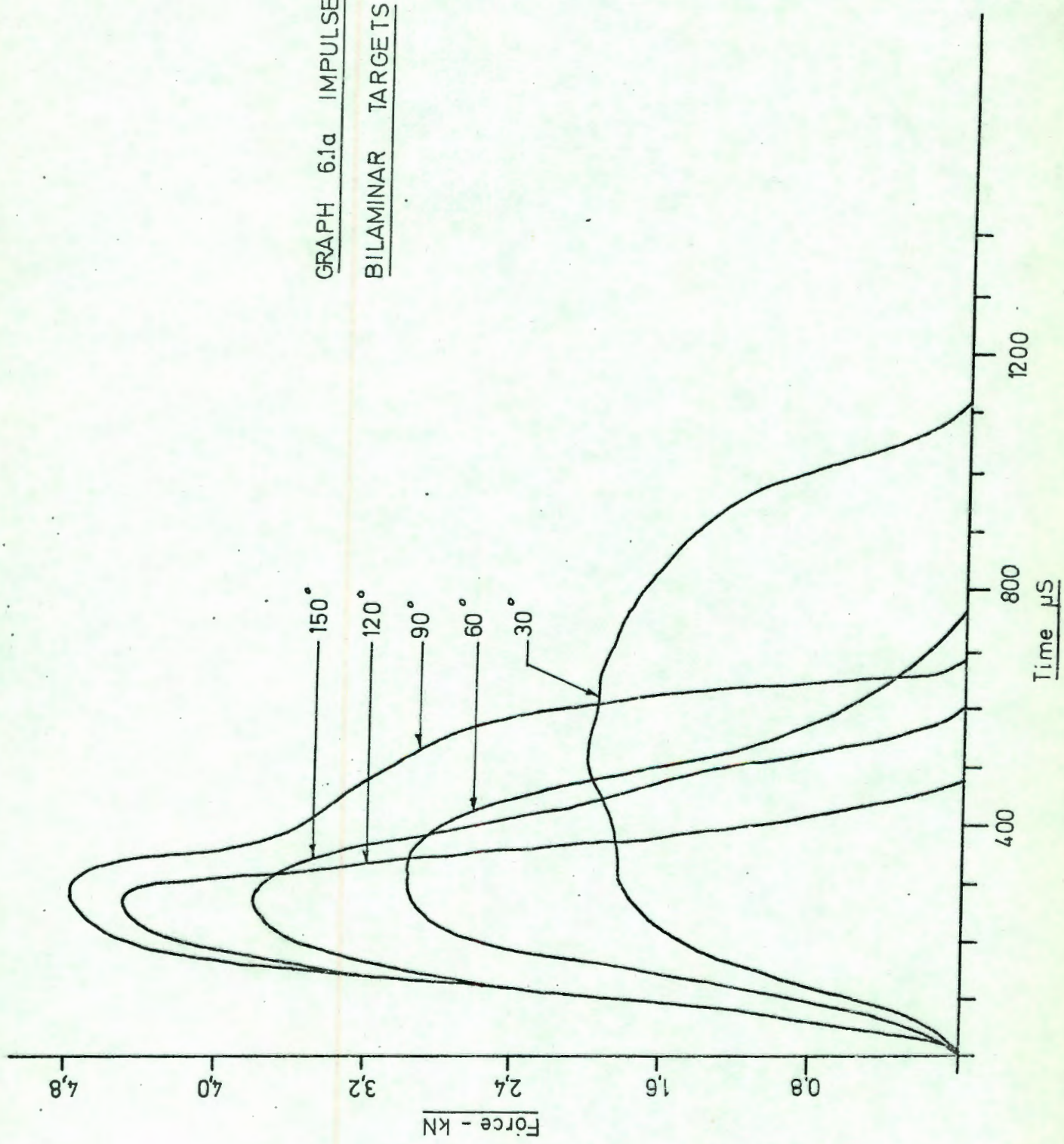
GRAPH 6.1a IMPULSES FOR
BILAMINAR TARGETS
150°
120°
90°
60°
30°
Force - kN
0,8
1,6
2,4
3,2
4,0
4,8
400
800
1200
Time µS

The form/ 47.....

The form suggested by Masket (1) and subsequently used by Bluhm (10) and Goldsmith (14) is generally regarded as a reasonably accurate description of the impulse curve. It takes the form:-

$$F = Kt^2 e^{-\beta t} \qquad \ldots\ldots\ldots\ldots\ldots\ldots\ldots\ldots\ldots\ldots \quad (6.2)$$

Where K and β are constants chosen to fit the expression to the experimental results.

To compare this expression with the results of the present study a more general relation was used:

$$F = kt^n e^{-mt} \qquad \ldots\ldots\ldots\ldots\ldots\ldots\ldots\ldots\ldots\ldots \quad (6.3)$$

Curve fitting was done by a least squares technique. The criteria used were:

(1) The area under the analytical curve is equal to the drop in velocity ΔV experienced by the projectile.

(2) The time t_{max} when the impulse reaches its peak is the same for both the analytical impulse and the experimental one. This condition conveniently gives a relationship between n and m, viz:

$$t_{max} = \frac{n}{m}$$

The least squares fitting procedure was carried out by computer giving the following expressions:

Cone Angle	Analytical Expression
30	$F = 1{,}21\ t^{3{,}36} e^{-0{,}14\ t}$
60	$F = 4{,}72\ t^{2{,}09} e^{-0{,}11t}$
90	$F = 3{,}22\ t^{2{,}40} e^{-0{,}16t}$
120	$F = 0{,}21\ t^{4{,}20} e^{-0{,}14t}$
150	$F = 0{,}33\ t^{4{,}32} e^{-0{,}18t}$

Fig 6.2. Analytical Expressions

6.3 Bilaminar Targets

To investigate how the lamination of target material affects the

impulse/48.....

impulse shape, the procedure described in 6.1 was repeated for bilaminar targets of the same aluminium material and equal thickness. The impulse shapes obtained are presented in Graph 6.1a.

6.4 Post-penetration Friction.

Containment is a loose term used to describe the situation when a projectile manages to penetrate a target but not fully perforate it. Since a projectile has a finite length there exists a band of energy levels which will satisfy this condition.

Fig 6.2 illustrates the various regimes of a penetration.

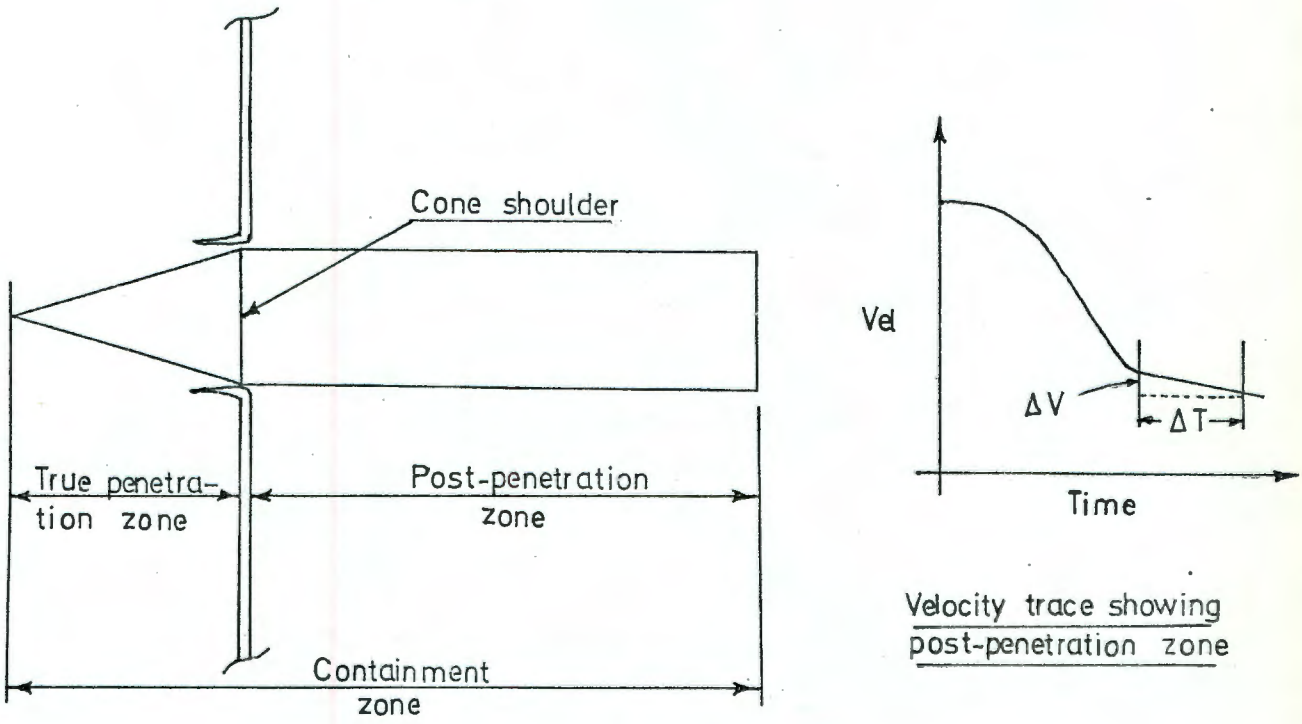

FIG 6.2 PENETRATION ZONES

The true penetration zone is that in which the conical section of the projectile is moving the target material aside until the shoulder of the cone passes through the target and the parallel sides of the projectile start to slide through the hole produced. Ideally containment should end here, but the condition is difficult to produce experimentally. In practice the frictional force between the target and projectile acts to absorb excess energy in the post-penetration zone.

The velocity-transducer method has made the measurement of post-penetration friction possible. The velocity-time trace is seen to have a uniform gradient in the post-penetration zone, and from this slope the

frictional/49 .....

frictional resisting force can be determined from the impulse momentum law, viz:

$$F = \frac{\Delta V}{\Delta t} \quad \ldots\ldots\ldots\ldots\ldots\ldots\ldots\ldots\ldots\ldots \quad (6.3)$$

Where ΔV is the uniform velocity drop in the time increment Δt seconds.

The results are shown in the table of Fig. 6.4

Cone Angle	Post Penetration Friction
30°	157 N
60°	162 N
90°	149 N
120°	155 N
150°	160 N

Fig. 6.4 Post Penetration Friction

6.5 Derived Parameters

Once the motion of a projectile is accurately known (especially the higher derivatives) it is possible to describe the motion by means of derived parameters. This is done graphically as follows:-

(1) Force-displacement (graph 6.2).
(2) Energy-displacement (graph 6.3).
(3) Power-displacement (graph 6.4)

These parameters were calculated from the original motion of the centre of mass by means of a computer programme which worked out:-

$$\text{Displacement } x = \iint \frac{d^2x}{dt^2}\, dt$$

$$\text{Energy} \qquad E = \int F\, ds$$

$$\text{Power} \qquad P = \int F\, dV$$

Finally the two graphs 6.5 and 6.6 are presented with the maximum power and containment energy plotted against cone angle.

Energy-Displacement Plot/50.....

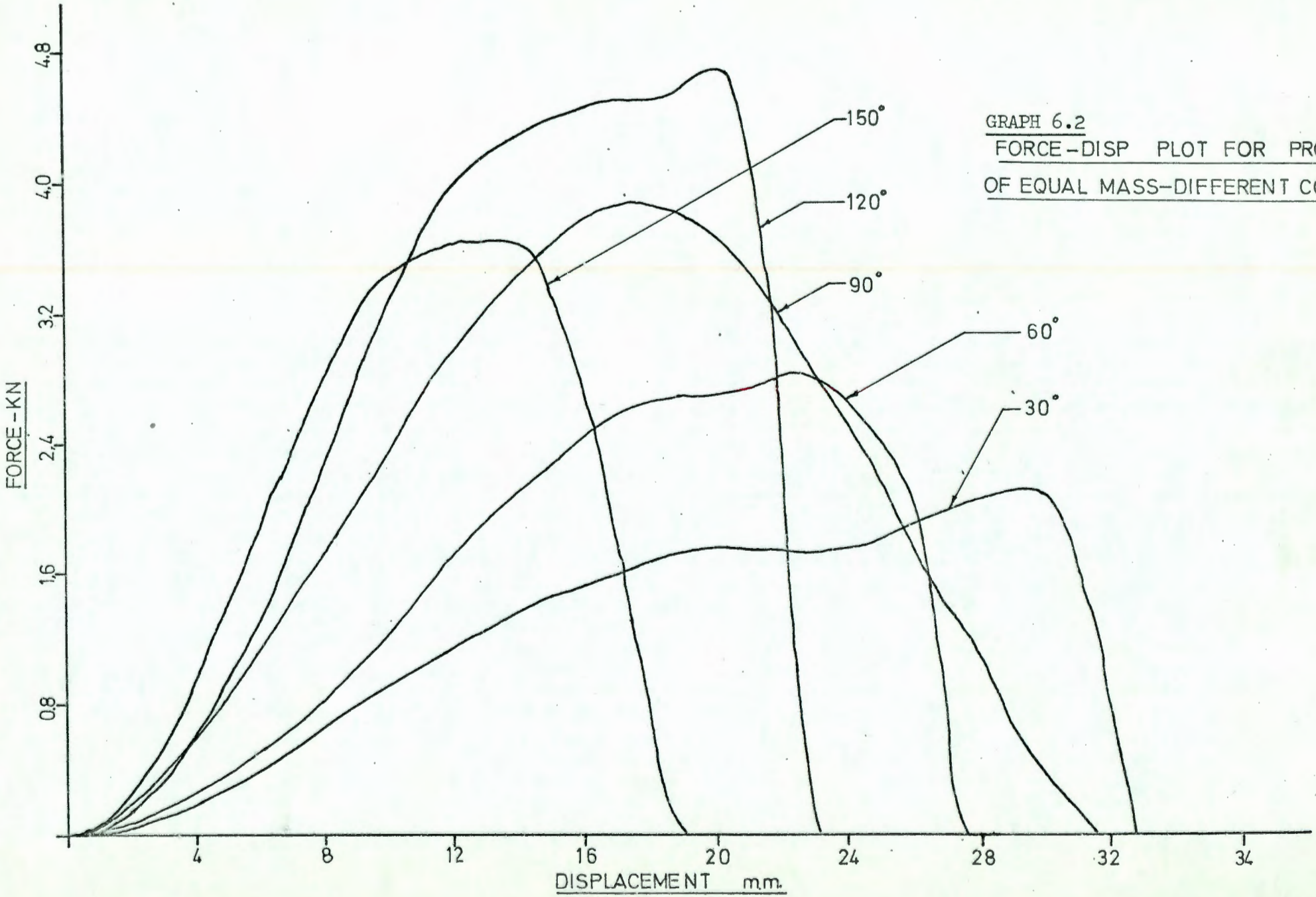

GRAPH 6.2

FORCE-DISP PLOT FOR PROJECTILES OF EQUAL MASS-DIFFERENT CONIC ANGLE

Power-Disp. Plot/51.....

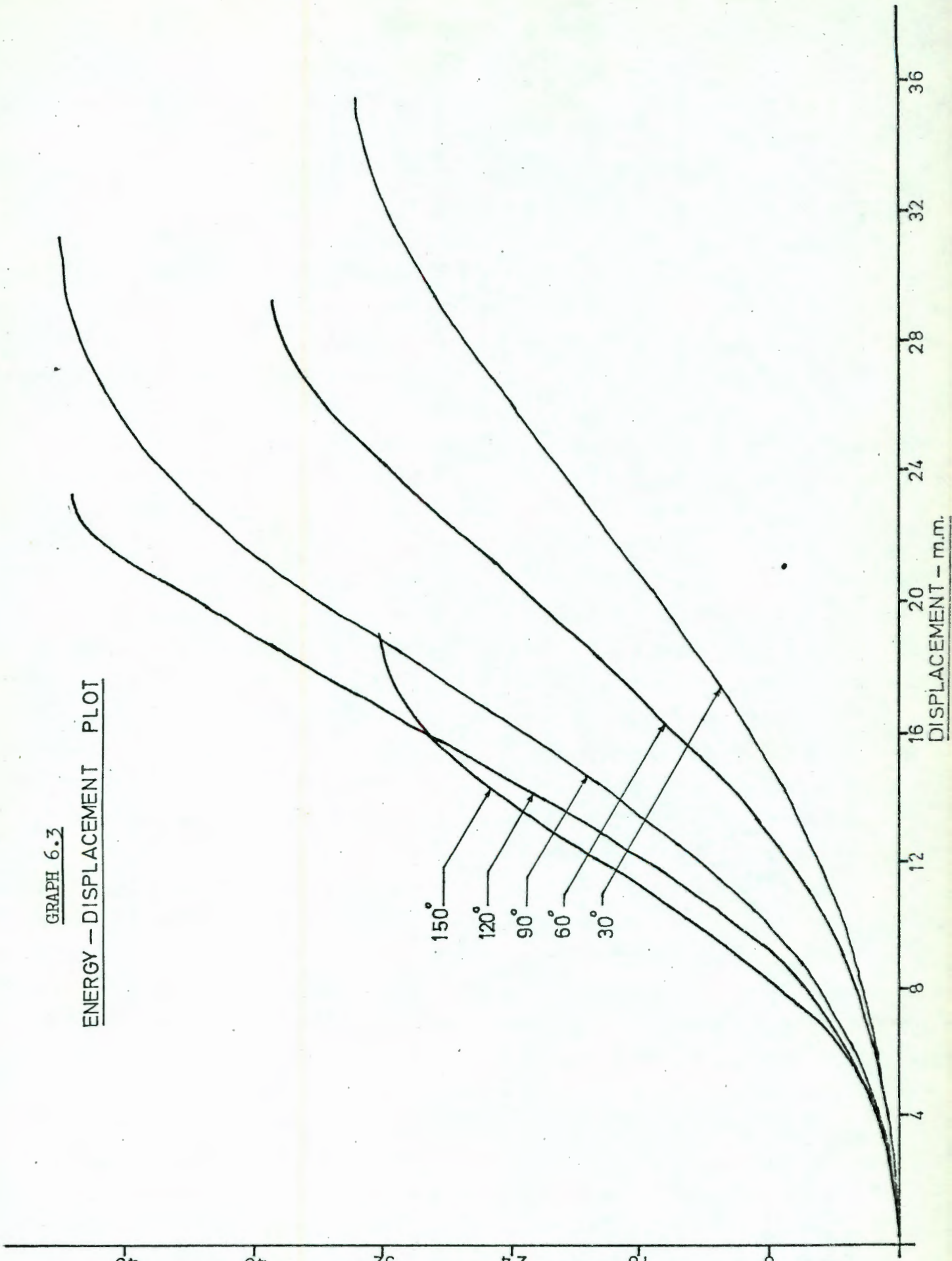

GRAPH 6.3

ENERGY – DISPLACEMENT PLOT

Force-Disp. Plot/52.....

GRAPH 6.4

POWER-DISPLACEMENT PLOT

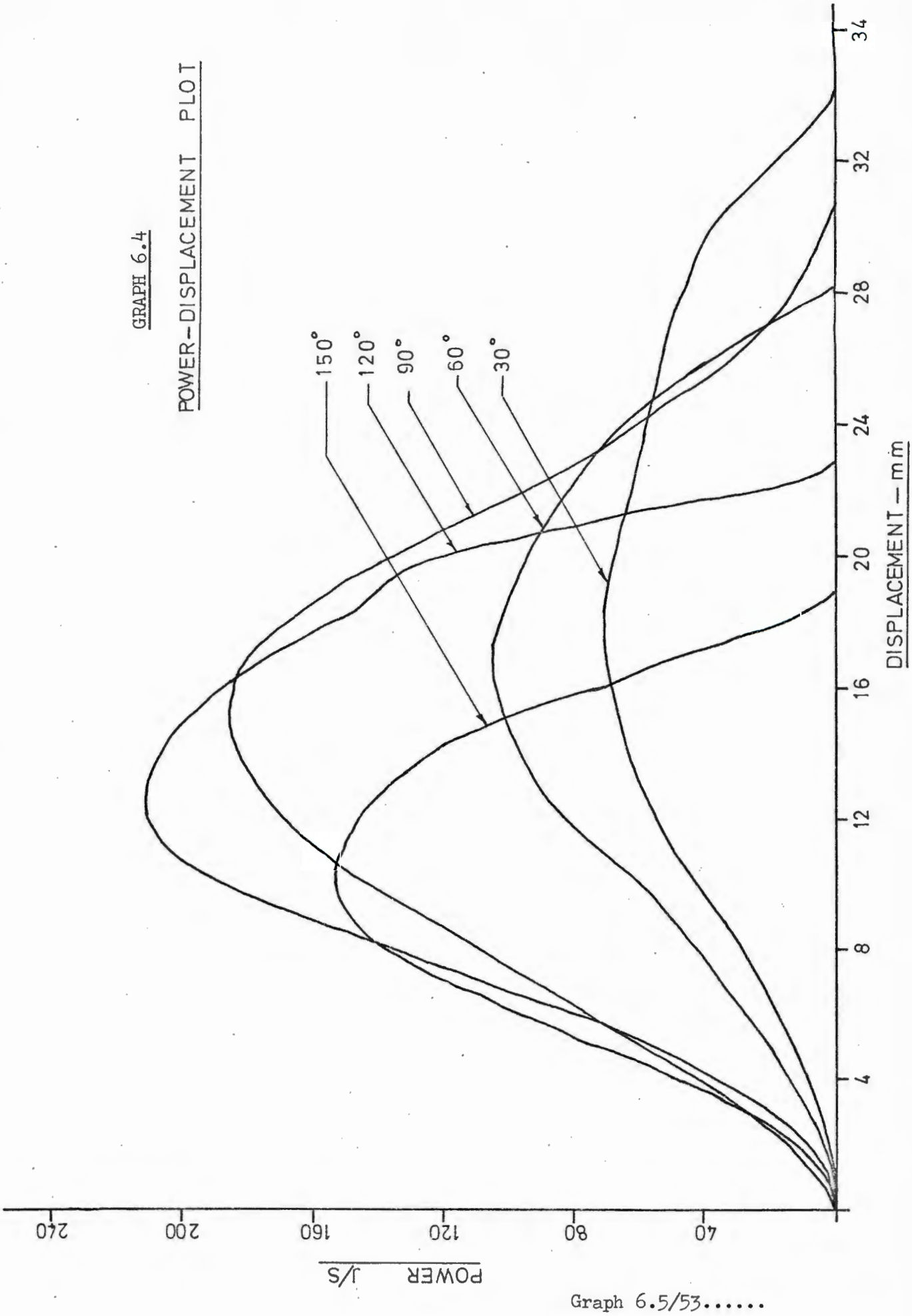

Graph 6.5/53.....

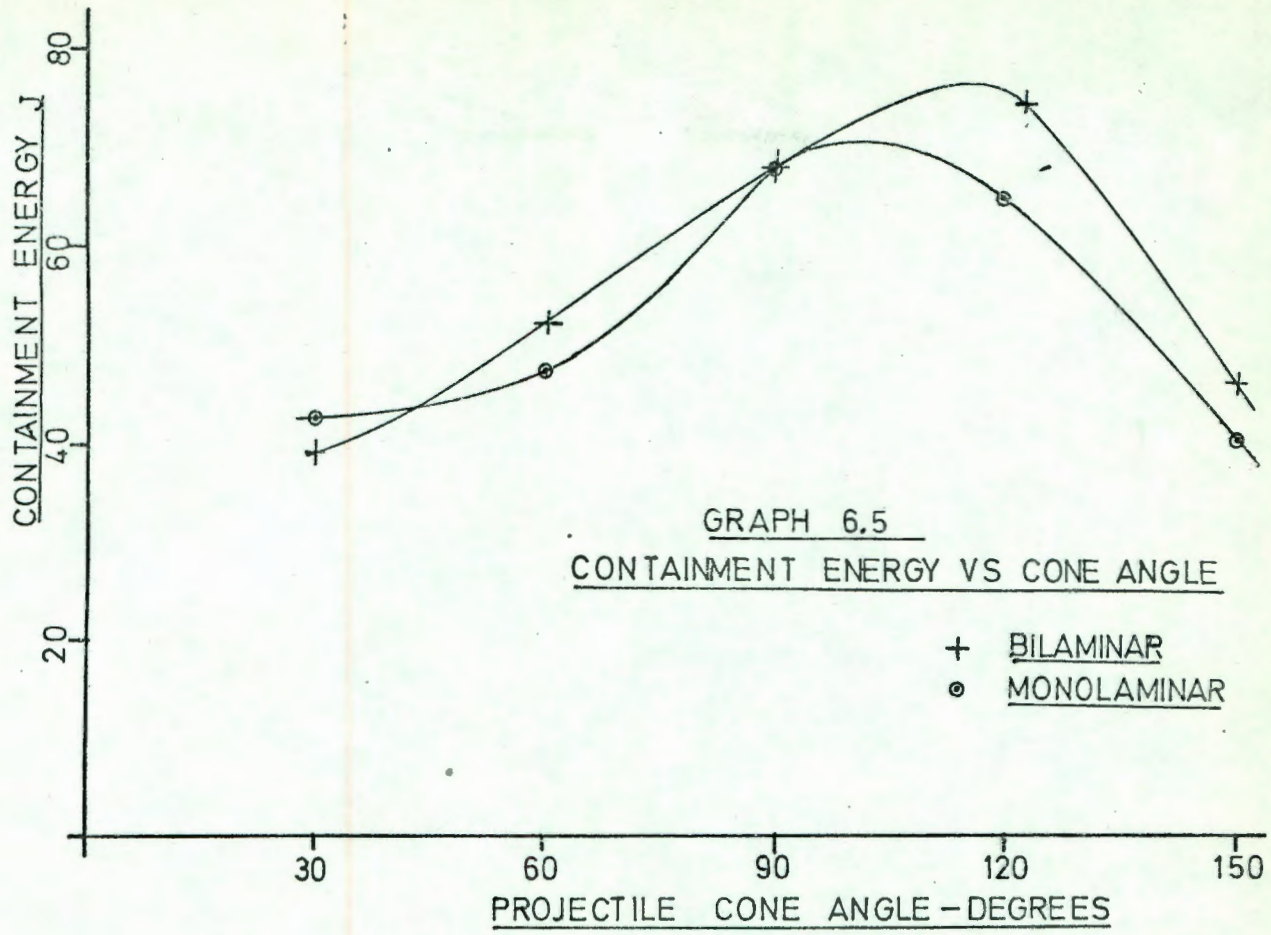

GRAPH 6.5

CONTAINMENT ENERGY VS CONE ANGLE

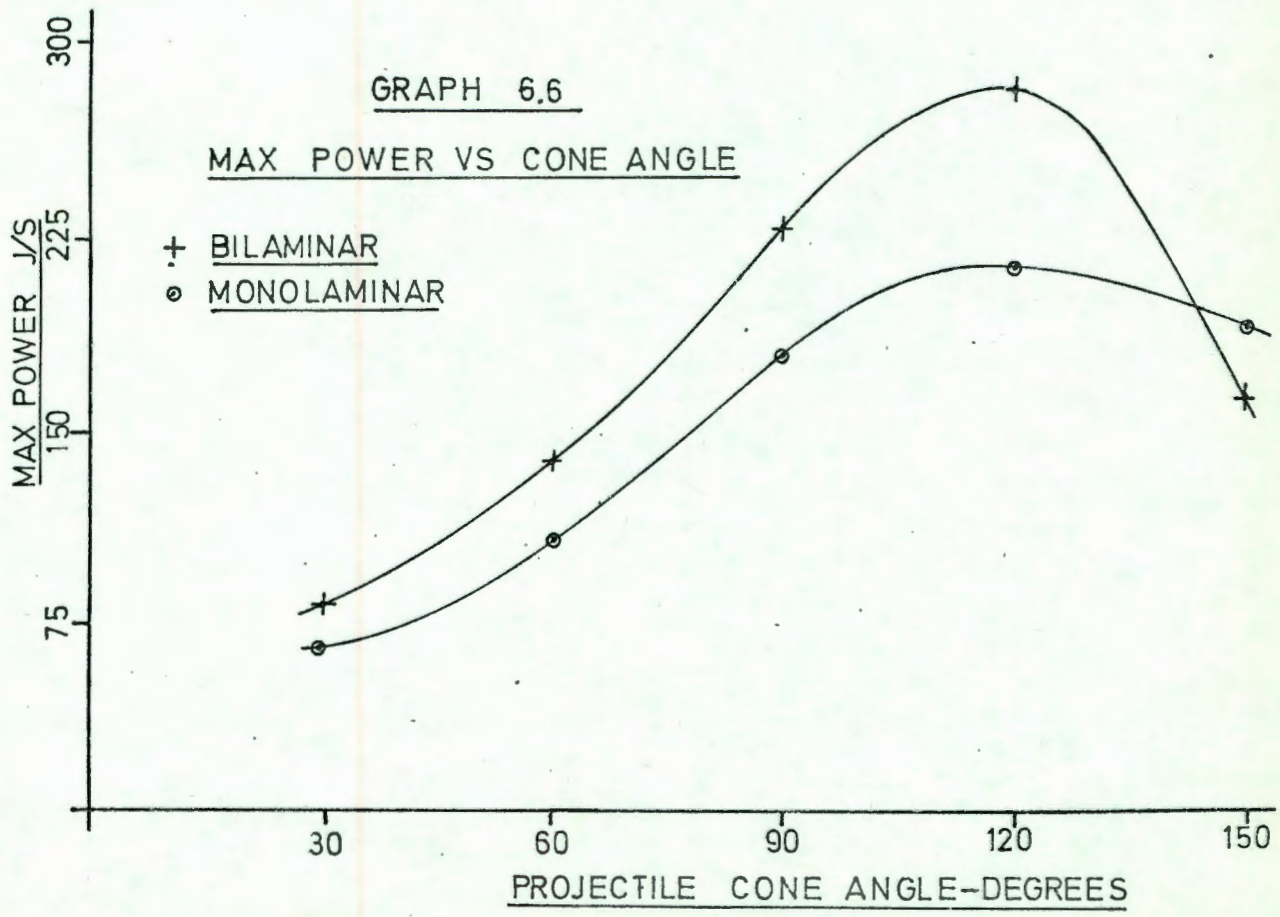

GRAPH 6.6

MAX POWER VS CONE ANGLE

Photo 6.1/54.....

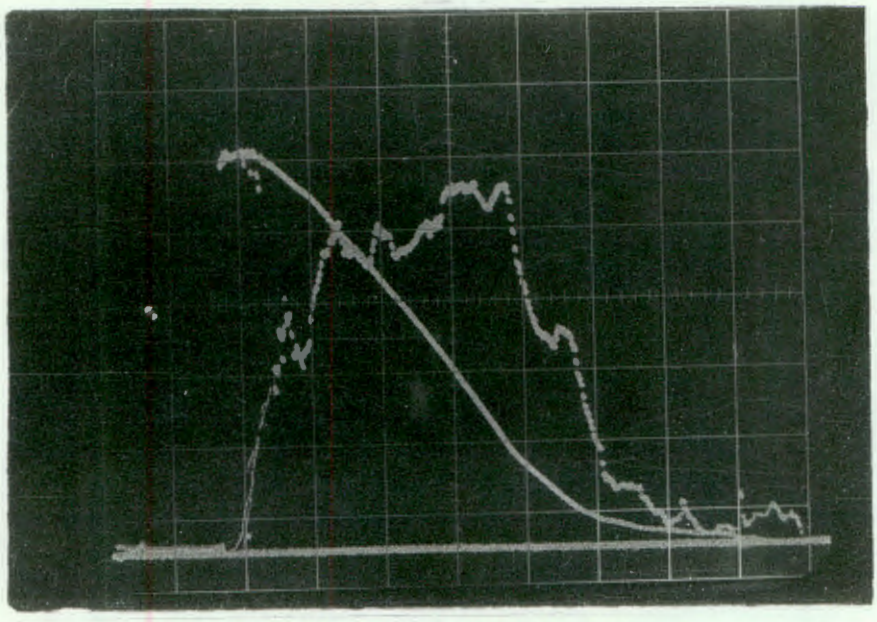

Photo 6.1 Typical Oscilloscope Record Showing Velocity-Time and Deceleration-Time traces. Note: the superimposed vibration on the latter.

6.6 Discussion/55 .....

6.6 Discussion of Results.

6.6.1 Accuracy and Limitations of the Transducer. There are two independent characteristics of the velocity transducer which determine its overall accuracy. Firstly, the area under the impulse trace it produces must relate to the momentum drop of the projectile, and secondly, the force function of the impact, i.e. F = F(t), must have a characteristic shape defined by a rise in the force from zero to a peak, and then a return to zero at the end of the penetration.

The results in the table of fig 6.1 show that the agreement between measured and calculated velocity drops is good, the error increasing with the projectile cone angle to 2.14% for the 150° projectile. The reason for this trend can be found by considering the deceleration time trace in photo 6.1. The trace can be considered to be composed of two motions, the average deceleration of the centre of mass and the superimposed vibration of the projectile. As the shape of the vibratory component is determined to a large extent by parameters which have not been accounted for in the analysis of cahpter 5, such as changing boundary conditions, the less emphasis placed on the shape of this component, the more accurate the final result will be. By considering at least five periods of oscillation, such as the trace in photo 6.1, it is evident that slight vibration deviations will not affect the overall impulse shape significantly.

As the cone angle of the projectile is increased, the severity of the impact is seen to increase, the amplitude becoming greater and the duration shorter. In the case of the 150° projectile the duration approaches the natural period of oscillation of the projectile and thus raises the uncertainty in the final result.

The form of the impulse function, i.e. F = F(t),cannot be checked as readily as the impulse-momentum balance. Since there are no realistic theoretical predictions for F(t),the only way in which the experimentally derived impulses could be checked is by comparison with results obtained from a completely independent experimental method.

Intuitively, however, the trend in the shape of the impulse curves is correct. The 30° projectile shows a slow rise to a small peak followed by a gradual decrease to zero. As the cone angle of the projectile becomes more obtuse the impulses become shorter in duration with an increase in amplitude.

The limitations of the transducer lie mainly in the construction of the projectile. As the projectile body is made from a nylon compound, the

amplitude/ 56.....

amplitude of measured impulses is limited to about 10 kN. The projectiles natural period is of the order of 150 μs and to obtain reliable impulse curve shape, at least five periods should be included in the penetration period. Photo 6.1 is a good example of this. The apparatus is therefore ideally suited to impacts lasting about 750 μs and amplitudes not exceeding 10 kN.

The scratch pickups have been tested to velocities of up to 150 m/s with no change in their commutating efficiency. It is only in the upper ballistic range that scratch pickups may prove to be a limitation.

6.6.2 Analytical Description of Impulse Curve Shape.

Correlation between the analytical expression 6.3 and the experimentally derived impulse curves is generally poor, the only curve to show slight correlation being that for the 90^{o} projectile. From the table in figure 6.2 it can be seen that 'n', the power to which t is raised, varies from 2,04 to 4,32. Even with this greater flexibility over Masket's equation (equation 6.2) the fit of the experimental data is poor.

The use of such analytical expressions is clearly demonstrated in work done by Goldsmith and Calder (14). To circumvent the problem of doubly differentiating photographic displacement-time data to derive deceleration-time data, an analytical expression such as equation 6.2 is assumed to describe the projectile deceleration. This expression is analytically differentiated twice and the experimental data fitted to the resulting displacement-time expression. This yields the necessary constants for the analytical deceleration expression.

The strength of the method lies entirely in the assumed deceleration-time expression. The present study has indicated that a wide range of impulse curve shapes are generated depending on the projectile cone angle and that it is unlikely that one simple analytical expression could be used to describe them all.

6.6.3 Bilaminar Targets

Several researchers have investigated the effect of laminating targets (10). Zaid (22) found that bilaminar targets required more energy to effect penetration than did their monolaminar equivalents. His study however was mainly qualitative and only energy differences were presented.

The bilaminar impulses in Graph 6.1 differ from their monolaminar equivalents in that the bilaminar penetration is shorter in duration and has a faster rise time and greater amplitude. The projectile in the

bilaminar/ 57.....

bilaminar case, behaves as though the cone angle of the head were more obtuse than it is in reality. This is to be expected since after penetrating the first lamina, the petals of that layer are forced through the second lamina to effect total penetration. It is for this reason that the largest impulse occurs for the 120° projectile in the monolaminar case and for the 90° projectile in the bilaminar case. The trends in the graphs 6.5 and 6.6 can be seen to be the same for monolaminar and bilaminar penetration.

6.6.4 Post-Penetration Friction.

Amongst other researchers, Goldsmith and Zaid (14) have speculated about post-penetration friction and Zaid attributed the spread in containment energies to this factor. The table of results in Fig 6.4 indicates that post-penetration friction is of the order of 150 N in the present study, and independent of projectile cone angle. This being the case, the energy absorbed per mm of post penetration displacement is 0,15 J/mm or on the average about 4%/mm of the total containment energy. These results confirm Zaid's assumption that post-penetration friction can account for a significant part of the containment energy.

6.6.5 Derived Parameters.

Derived parameters are useful to enable the penetration process to be described in a number of different ways, each one highlighting a different aspect of the penetration.

Whereas the area under an impulse can be related to the drop in momentum experienced by a projectile, the area under the force-displacement curve is a measure of the energy absorbed by the penetration process. This instantaneous energy is plotted in the graph 6.3 and against projectile displacement and gives an idea of how the projectile's energy is absorbed and distributed throughout the penetration process.

The series of power-displacement curves represent the rate at which the target material is absorbing the projectiles energy. This parameter which has not appeared in published work to date, could be important in the formulation of a theory of penetration since strain rate effects and material flow are related to the rate of energy absorbtion.

The Graphs 6.5 and 6.6 show the effect of projectile cone angle on the containment energy and maximum power absorbtion. The curves have a pronounced maxima around 120°. The reason for this is not self-evident, but a study of the target plates indicate that there are two distinct processes of plate failure and the transition occurs around this angle.

For the/58 .....

For the more pointed projectiles (30°, 60°, 90°) the plate failure is by a petalling process. The target material in the impact zone, splits into a number of petals (between 3 and 6) and the projectile pushes these aside to effect penetration. As the projectile's cone becomes more obtuse (120°) the petalling process becomes more difficult to initiate and penetration is accompanied by severe plastic deformation around the central impact zone.

For cone angles above 120° the penetration is accomplished not be petalling, but by a punching process which shears out a disc of target material. This process requires less energy than the extreme petalling one and explains the downward trend in the parameters of graphs 6.5 and 6.6 above cone angles of 120°.

6.7 Conclusions and Potential Uses of the Transducer.

The apparatus developed for the project operates reliably, economically and with a high degree of accuracy. In its present form the velocity transducer is limited to moderate impacts in the lower ballistic range, where impact durations are longer than 750 μs and amplitudes less than 10 kN. This is by no means an intrinsic limitation to the method as a differently designed projectile could monitor much more severe impacts.

There are several applications for which the velocity transducer is ideally suited.

In the empirical design of laminated armour plate, impulse modifications due to various laminate configurations can be studied. The impulse shape can be adjusted, depending on the criterion of the armour plate design, to give maximum energy absorbtion or momentum absorbtion. The simultaneous production of the projectiles deceleration-time trace with the impact, makes the method quick and simple.

To develop a theory of penetration the present study has indicated that a knowledge of projectile motion is insufficient in itself. As can be seen from Fig. 6.5 the target can be divided into two zones, the central impact zone and the outer plastic zone. By monitoring the motion of the boundary of the damage done (x_1) with a tubular velocity transducer mounted on the target itself, as well as the overall motion (x) with the projectile velocity transducer, an insight could be gained into the separate dishing and petalling processes which occur during penetration.

Fig 6.5 /59.....

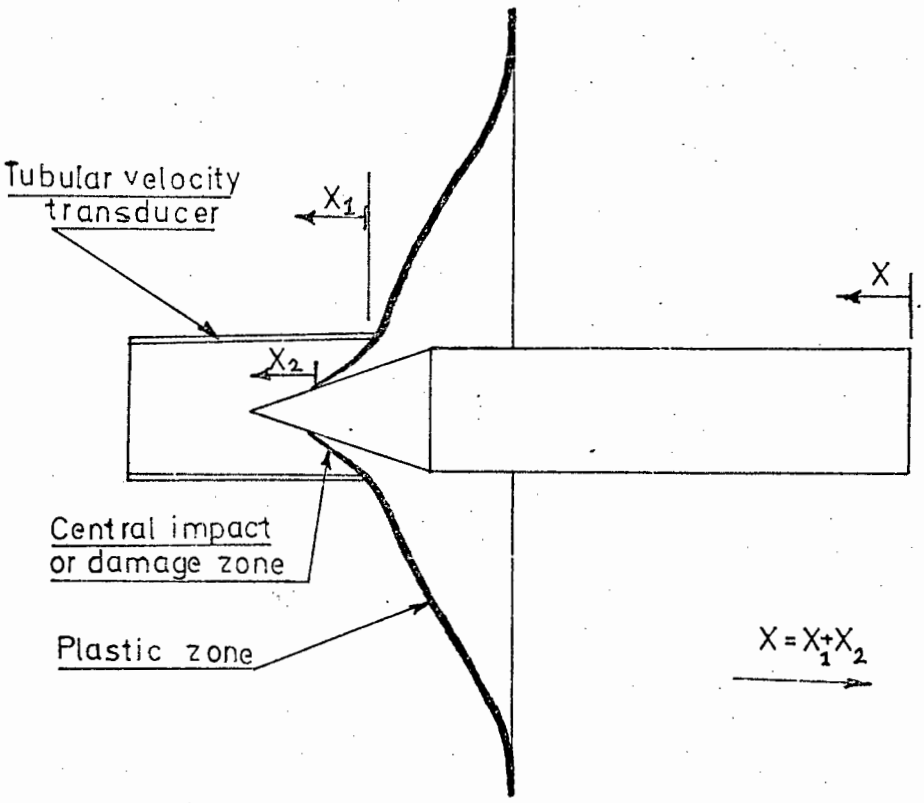

FIG 6.5 PROPOSED LAYOUT FOR PENETRATION THEORY APPARATUS

APPENDIX A

Gas Gun Design and Performance

7.1 The Gas Gun

The general layout of the gas gun and mounting is shown in Figure A1. To give a rigid and massive foundation, the gun is mounted on a 300 mm x 100 mm rolled steel joist which itself stands on legs of 50 mm square steel tubing. The upper flange of the rolled steel joist is covered with a 100 mm x 8 mm thick bright mild steel strip and provides a test bed, facilitating the alignment of the field magnet, target holder and projectile catcher with the gun barrel.

A console at the breech end of the gun is used to house the pressure regulating valves, the monostable circuit for the sonenoid valve and the Schmitt triggers for the approach velocity measuring apparatus. The gas bottle lies conveniently under the test bed and its weight helps to stabilise the rig. The general layout can be seen from the frontispiece and Fig. A.1.

7.2 Principle of Gas Gun Valve

The gas gun was designed specifically to launch the special projectile described in section 3 to 4. To penetrate 3 mm thick aluminium sheet, a projectile velocity of around 100 m/s is required although the gun is capable of delivering velocities of up to 200 m/s.

The desirable characteristics of a gas gun are ease of loading and firing and economy in the usage of compressed air. A comprehensive literature survey was carried out on the subject but no suitable designs were found. The following design by the author and Mr. A.W. Miles was finally used (20).

The gas gun incorporates a snap action pneumatic valve the function of which is to provide rapid admission of compressed air from the driver chamber to the barrel for propulsion of the projectile and a rapid closure to prevent excessive loss of pressure in the driver, once the projectile has been expelled from the barrel. A schematic of the valve assembly is shown in Fig. A2. The valve is actuated by compressed air from a secondary pressure reservoir, the pressure of which acts on the valve actuating piston in opposition to the driver chamber pressure to ensure valve closure. A three-way solenoid valve coupled into the valve pressurizing line is used to either admit pressure to the valve chamber

Fig.A1. /61.....

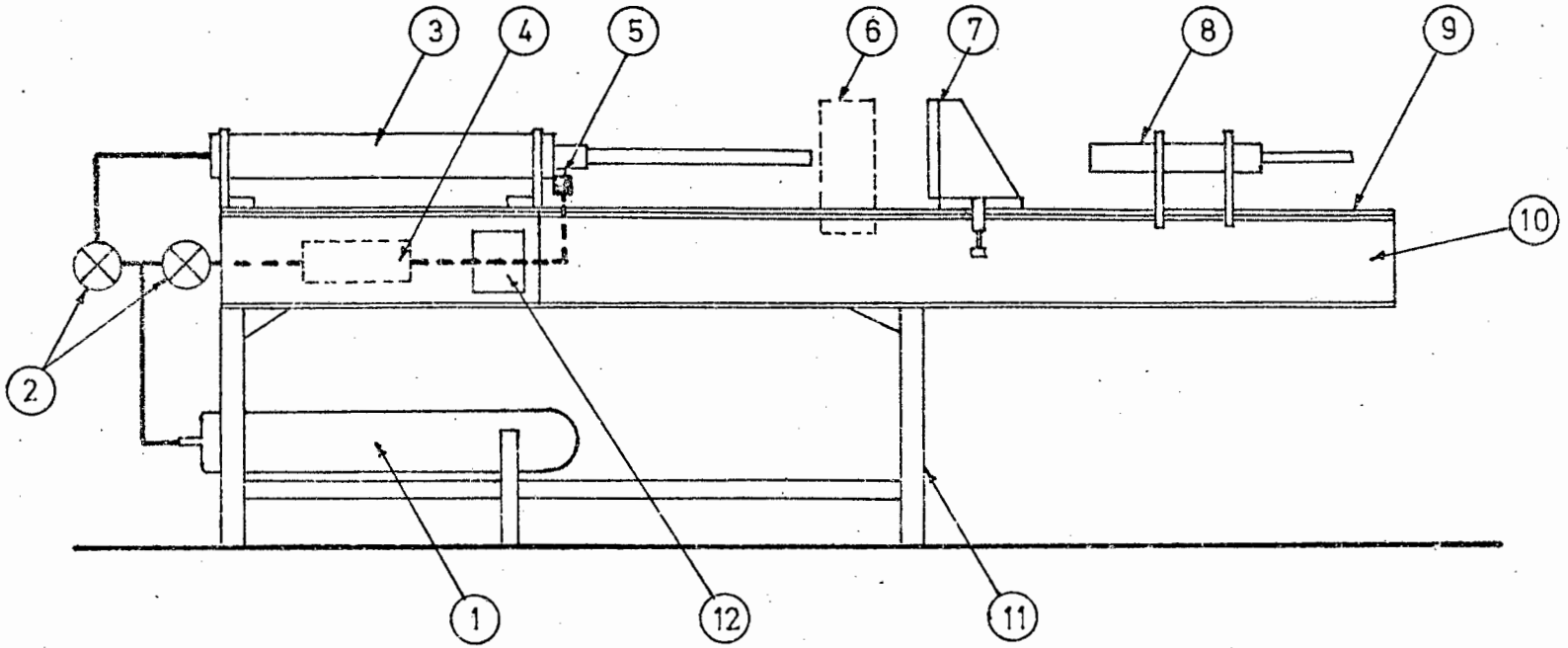

1	compressed air cylinder (150 bar)
2	pressure regulating valves
3	driver chamber
4	valve pressure reservoir
5	solenoid valve
6	position of velocity transducer

7	target holder
8	projectile catcher
9	bright mild steel bed
10	300 X 125 R.S.J.
11	sq steel tubular legs
12	control panel

0 1
metre

FIG A1 GENERAL LAYOUT OF GUN AND ANCILLARIES

for valve/ 62.....

for valve closure, or to vent the pressure in the valve chamber to effect rapid opening of the piston-valve. The solenoid valve is operated by a monostable circuit which de-energises the solenoid valve, to pressurise the valve chamber, after a pre-selected delay. The delay of the monostable can be selected to coincide with the time of passage of the projectile through the barrel, thereby reducing the pressure loss in the driver chamber and minimising the make-up pressure required to restore the chamber pressure.

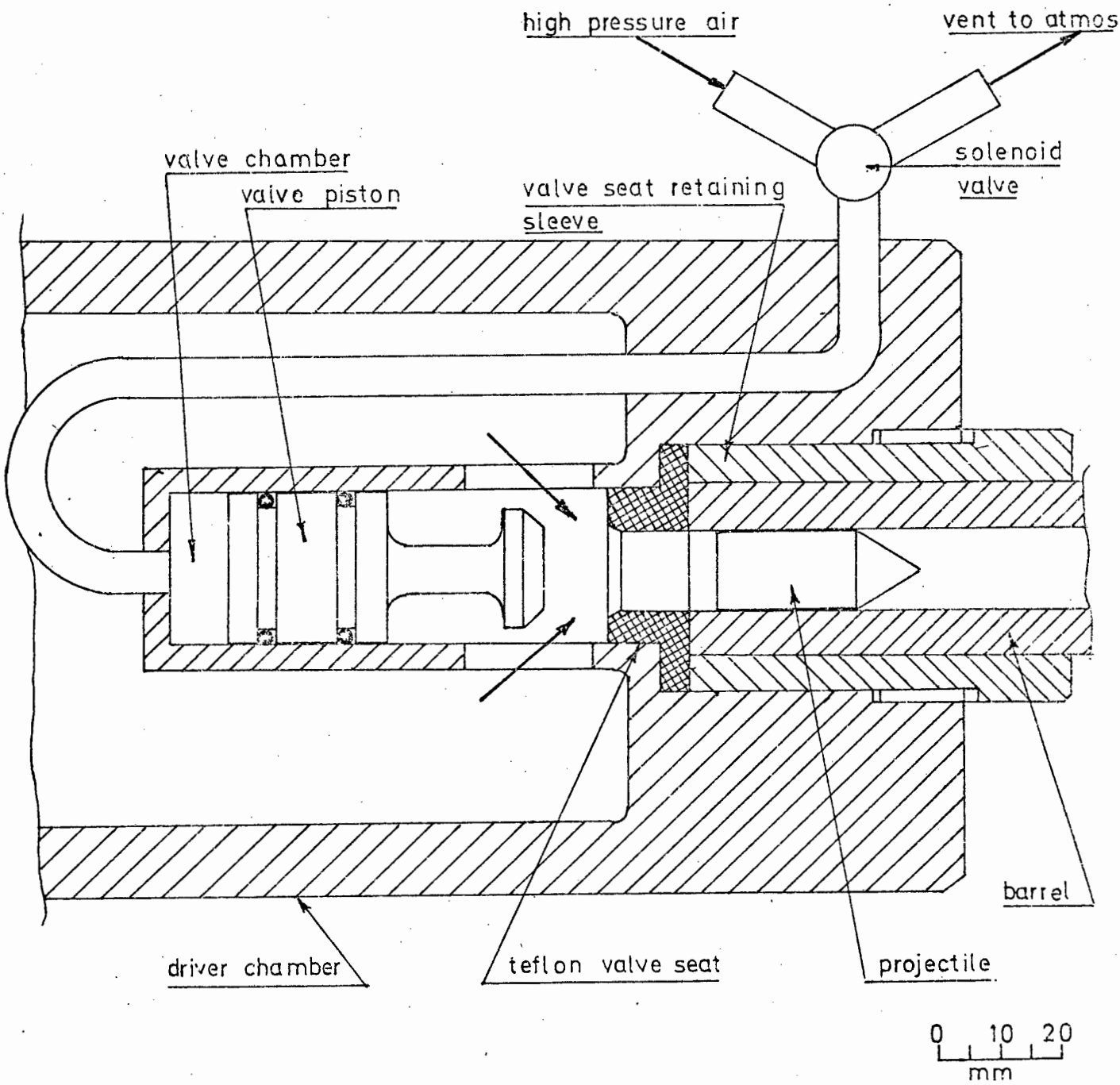

FIG.A2 SCHEMATIC OF GUN VALVE

The valve head/63.....

The valve head, stem and actuating piston are made from aluminium to reduce the mass of the working parts of the valve and so minimise the inertia effects on the valve opening and closing times. To ensure rapid venting and pressurising of the valve chamber, the chamber volume is small and the length of the pressurising line between the chamber and the solenoid valve is as short as possible. A solenoid valve with a large orifice size is used to ensure that rapid venting and pressurising can be achieved even when the solenoid valve is only partially open. The valve seat is made from "Teflon" and can easily be replaced.

Both the driver chamber and secondary pressure reservoir are connected via pressure regulating valves to a compressed air bottle so that manual pressure make up adjustments between shots are obviated.

7.3 Target Clamp.

To permit cross checking of results with other experimenters in the field, a standard method of clamping is adopted. The present design is similar to that used by Goldsmith (14, 15, 18).

The arrangement consists of two steel rings 190 mm in diameter (internally) between which the target is clamped by means of eight 8 mm Allen screws. One of the rings is threaded to enable the arrangement to be screwed onto the holder which slides along the test bed. This layout is very rigid and setting up of the target and removal is rapid.

Fig. A3./64.....

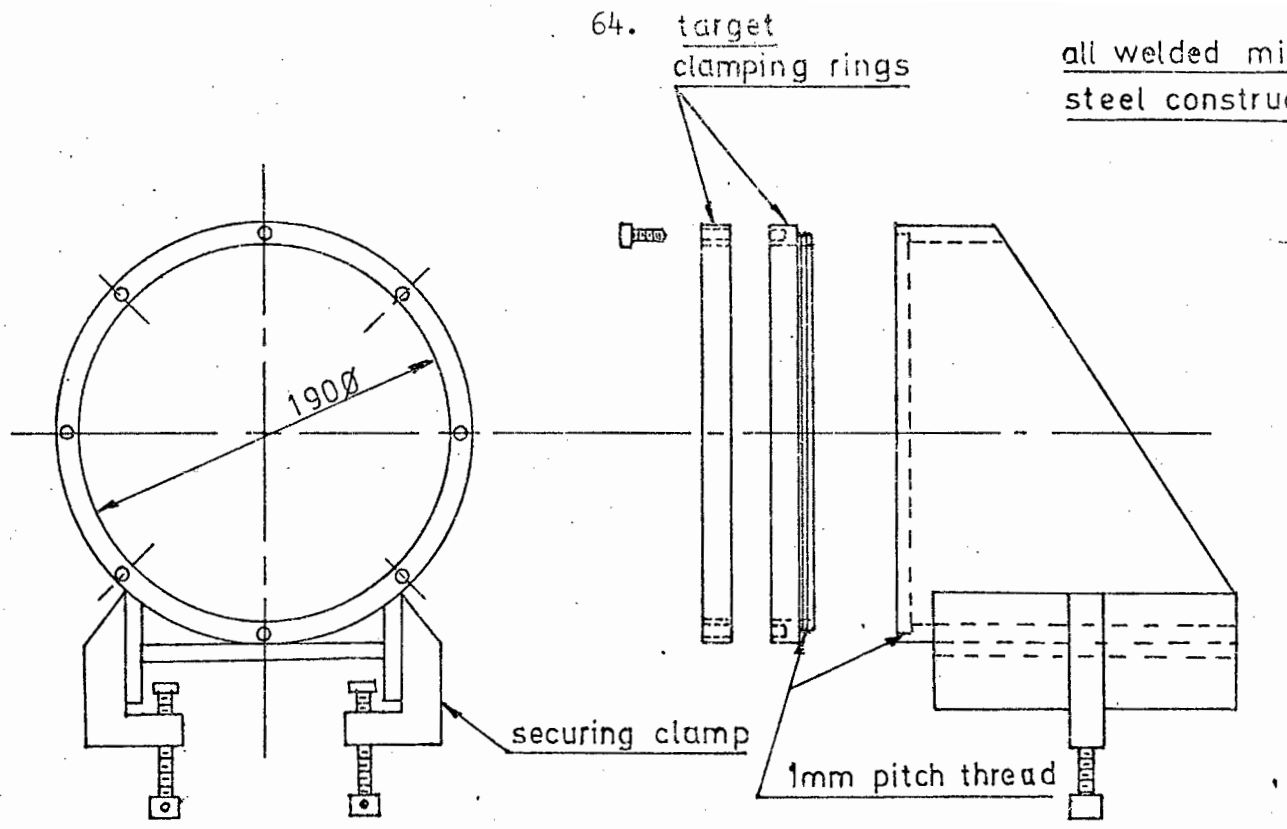

FIG.A3 TARGET CLAMP

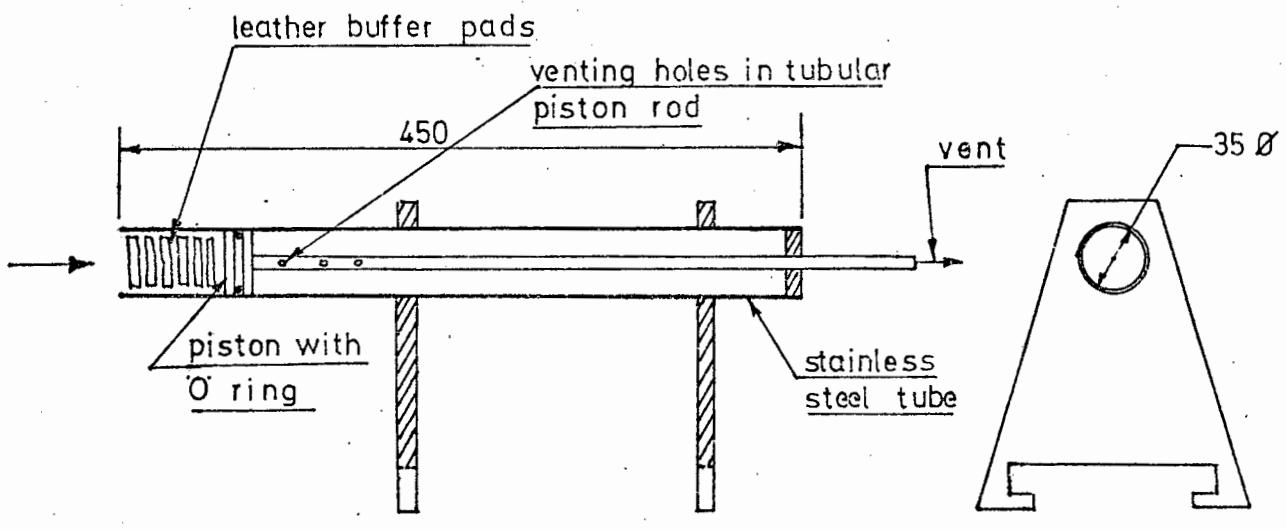

FIG.A4 PROJECTILE CATCHER

all dimensions in mm

7.4 Projectile Catcher

For free flight shots when no target is placed in the projectile's path, and when perforations are being studied, it is necessary to absorb the projectile's residual energy. The pneumatic projectile catcher shown in Fig. A4 is used for this purpose. Air trapped behind the piston is allowed to bleed to atmosphere through an adjustable vent. This adjustment allows the resistance of the catcher to be varied. The leather pads serve to soften the impact with the catcher piston and to hold the projectile and thus prevent rebound.

7.5 Monostable Circuit

The Monostable provides a pulse for a pre-determined length of time. This pulse is fed to the gate of a triac which controls the A.C. supply to the solenoid valve. In its normal state the high pressure air supply is directed via the solenoid valve to effect the closure of the gun valve. On depressing the trigger switch the pulse from the monostable switches the solenoid valve to vent the valve closing pressure to atmosphere. After the predetermined time the monostable reverts to its initial state, the solenoid is switched off and the high pressure air re-admitted to effect closure of the gun valve. An additional switch sw2 is placed in the solenoid circuit as a safety measure to isolate the latter as a precaution against random triggering due to electrical noise.

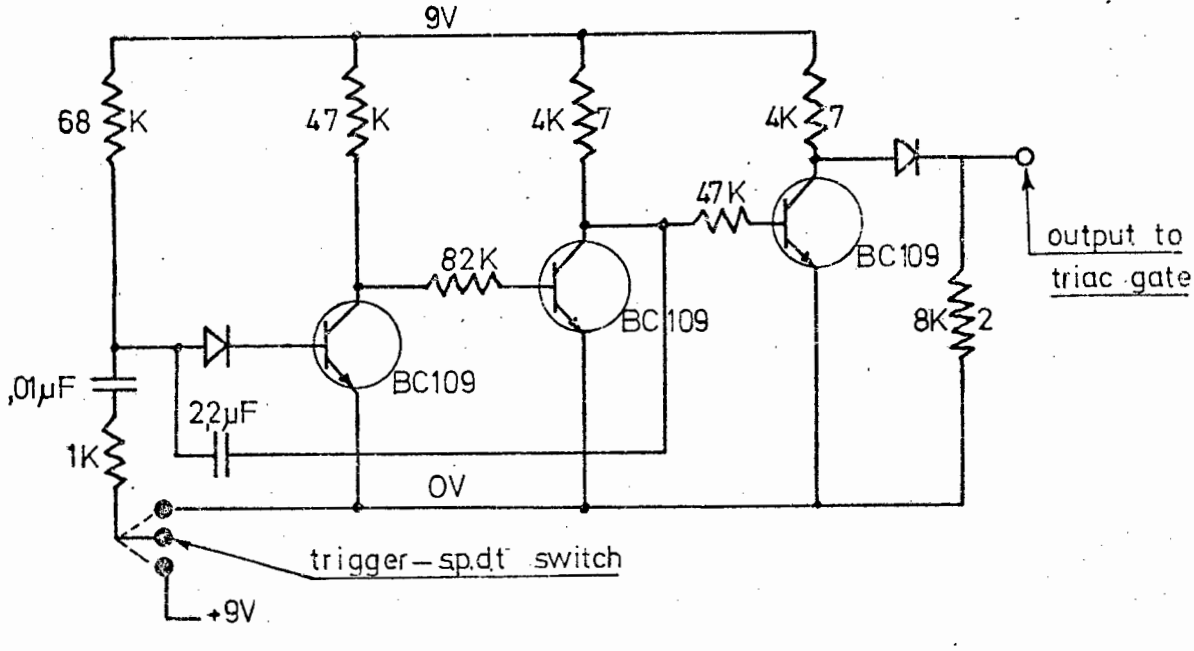

FIG. A5 MONOSTABLE CIRCUIT

7.6 Gun/66.....

7.6 Gun Performance

For a gun barrel length of L metres and a constant driver pressure of P Pascals, the velocity V_o attained by a projectile of mass M kg, cross sectional area A m^2, on leaving the barrel can be calculated from energy considerations; viz:

$$PAL = \frac{1}{2} MV_o^2$$

$$\text{or} \quad V_o = \sqrt{\frac{2PAL}{M}}$$

For an actual gun however there will be deviations from this ideal behaviour due mainly to friction and windage losses experienced by the projectile and the fact that the driver pressure P is not constant but falls as the projectile moves down the barrel. Since the valve has a finite opening and closing time, the assumed square pulse shape of the pressure pulse will also be ideal - the actual shape having a finite rise and fall time. These deviations all act in a way to reduce the ideal muzzle velocity. This is exactly the trend that was found in practice. The results are shown in Graph A6.

Graph A6/67.....

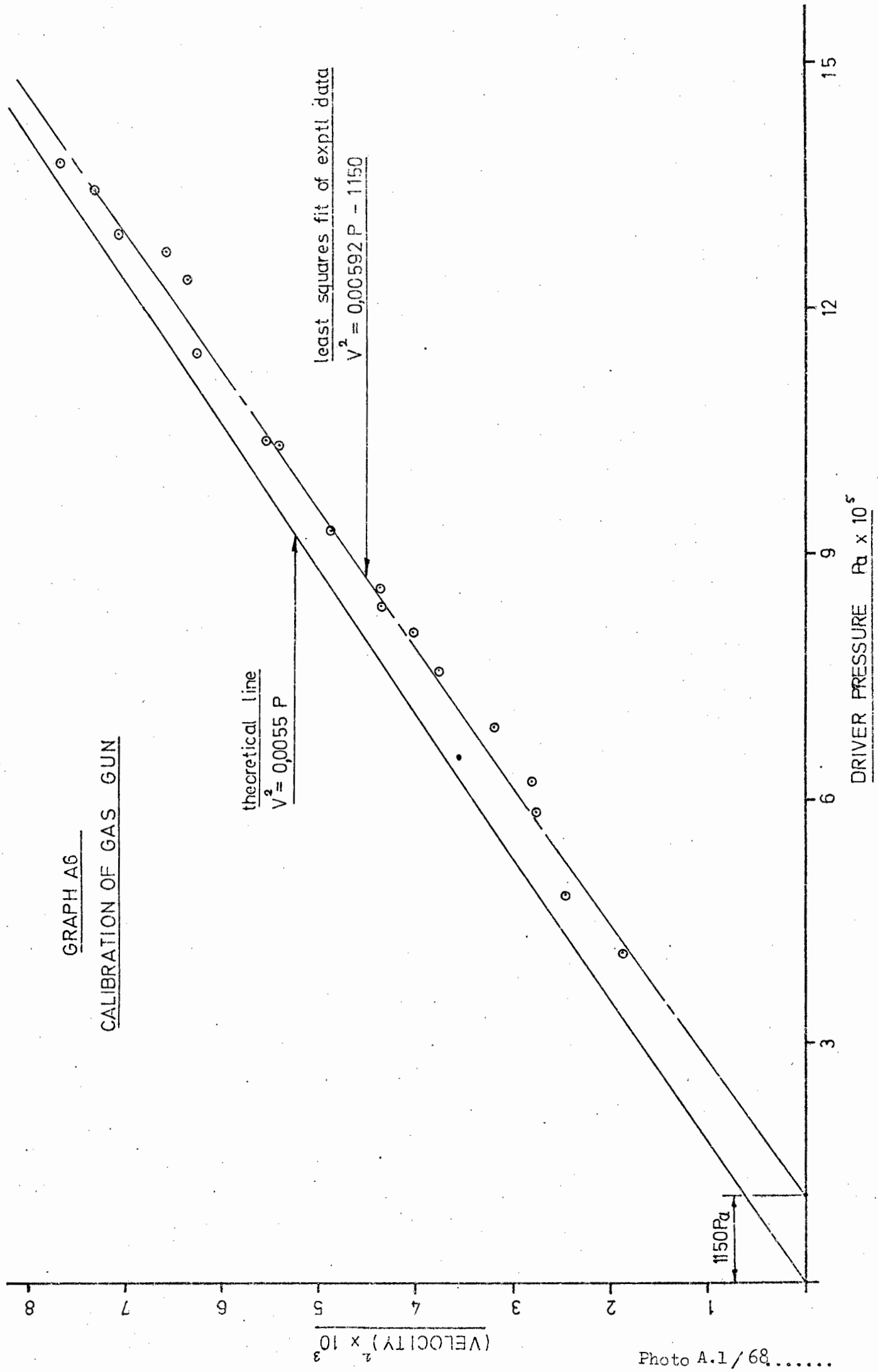
GRAPH A6
CALIBRATION OF GAS GUN
theoretical line
$V^2 = 0{,}0055\ P$
least squares fit of exptl data
$V^2 = 0{,}00592\ P - 1150$
1150Pa
(VELOCITY)$^2 \times 10^3$
DRIVER PRESSURE Pa x 10^5
1
2
3
4
5
6
7
8
3
6
9
12
15

Photo A.1/68.....

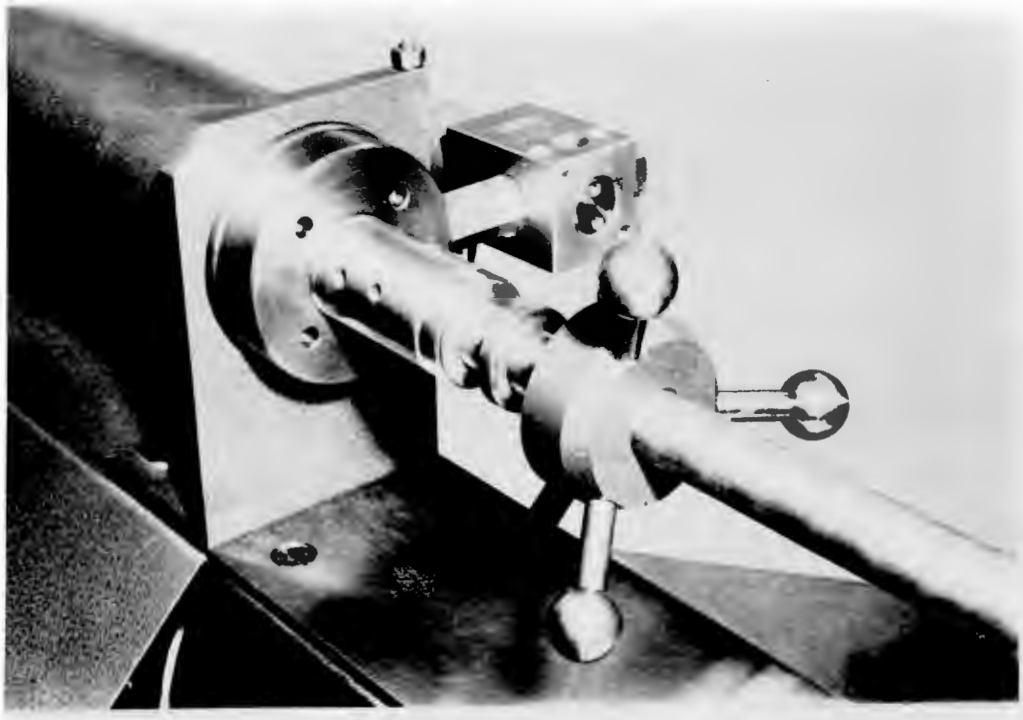

Photo A 1. Breach of Gas-Gun Showing Triggering Solenoid.

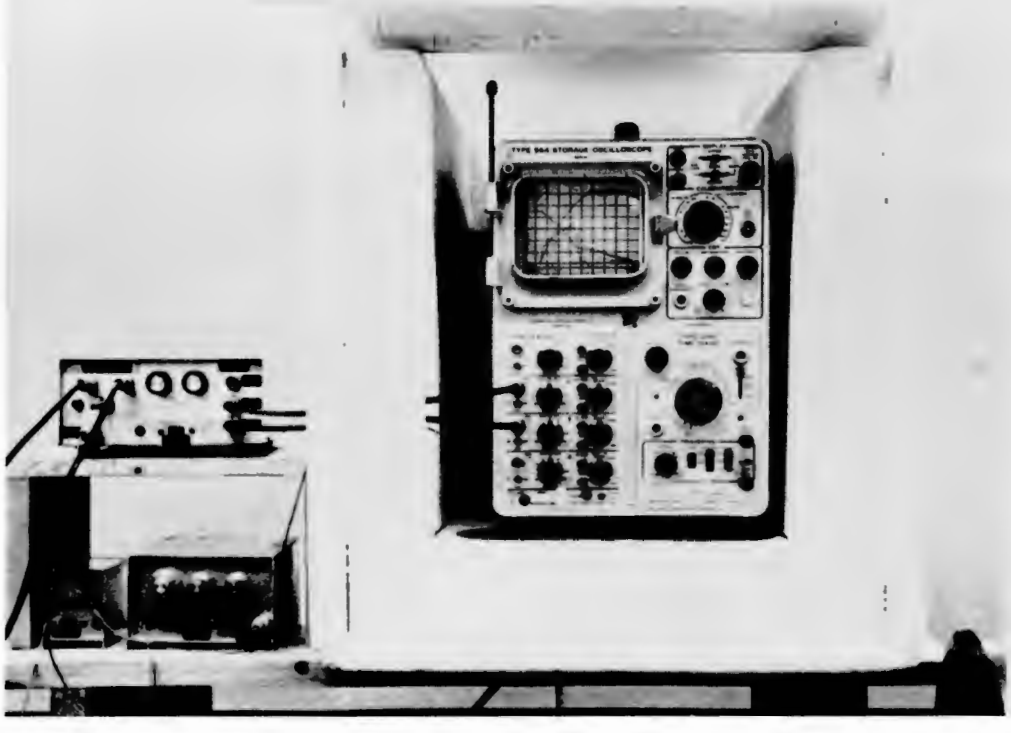

Photo A 2. The Oscilloscope and Processing Electronics. Note Acoustic Housing to Prevent Radiophonic Interference from the Gas-Gun.

APPENDIX B/69 .....

APPENDIX B

Processing Electronics

The processing electronics can be summarised as follows:-

(1) Differentiator.
(2) Integrator.
(3) Triggering and Co-ordinating Circuitry.

8.1 Differentiator.

An ideal electronic differentiator should sense the slope of an input signal (which is varying in time) and produce an output voltage proportional to it. The circuit shown in Fig.B1 which uses a high speed operational amplifier (LM 318H) will approximate this.

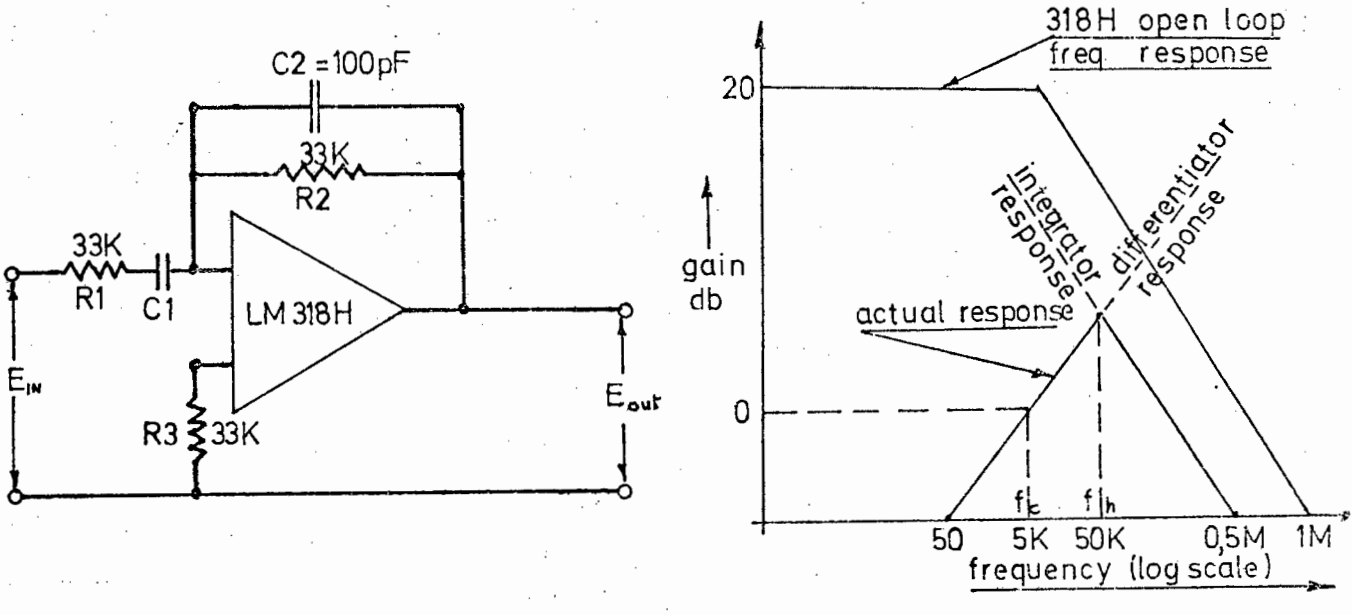

FIG. B1 DIFFERENTIATOR

In practice, a perfect differentiator is undesirable since any input will contain a degree of noise and the differentiator will sense the sharp slope of the noise and produce a corresponding output which will distort the main signal or even swamp it. The circuit shown in Fig B1 has a built-in break point so that for input signals above f_h = 20 kHz the operational amplifier will in conjunction with C_2, act as an integrator and thereby filter out the effects of noise. F_h was chosen as a compromise between the actual requirements and the frequency limitations of the special high-speed operational amplifier. The actual response of the differentiator is presented in Graph B 5.

8.2 Integrator/70.....

8.2 Integrator

The function of an electronic integrator is to sum an input voltage E_{in} in the time domain over a given period of time, and provide an output voltage E_{out} proportional to the instantaneous value of the sum. By its very nature, the integrator is a more stable device than a differentiator and if noise is present in the input signal, it is automatically filtered by the integrating process.

The main problem encountered with integrators is the fact that definite limits must be set to the integrating process. In the present system, limits LT 1 and LT 2 (see Fig. 3.11) are set by means of the adjustable time delays T2 and T3. The output from T3 is a 9 V pulse of T3 seconds duration corresponding to the period over which the integration will be carried out.

The inverting and switching circuit (see Fig B2) is controlled by the pulse from T3. The output from the inverter is normally at +9 V potential and for the duration of the pulse T3, the output falls to -9 V. This output is connected to the gate of the field effect transistors (F.E.T's) in the feedback loop of the integrator. These F.E.T.'s are used as switching devices to either ground the output of the integrator, or allow it to operate.

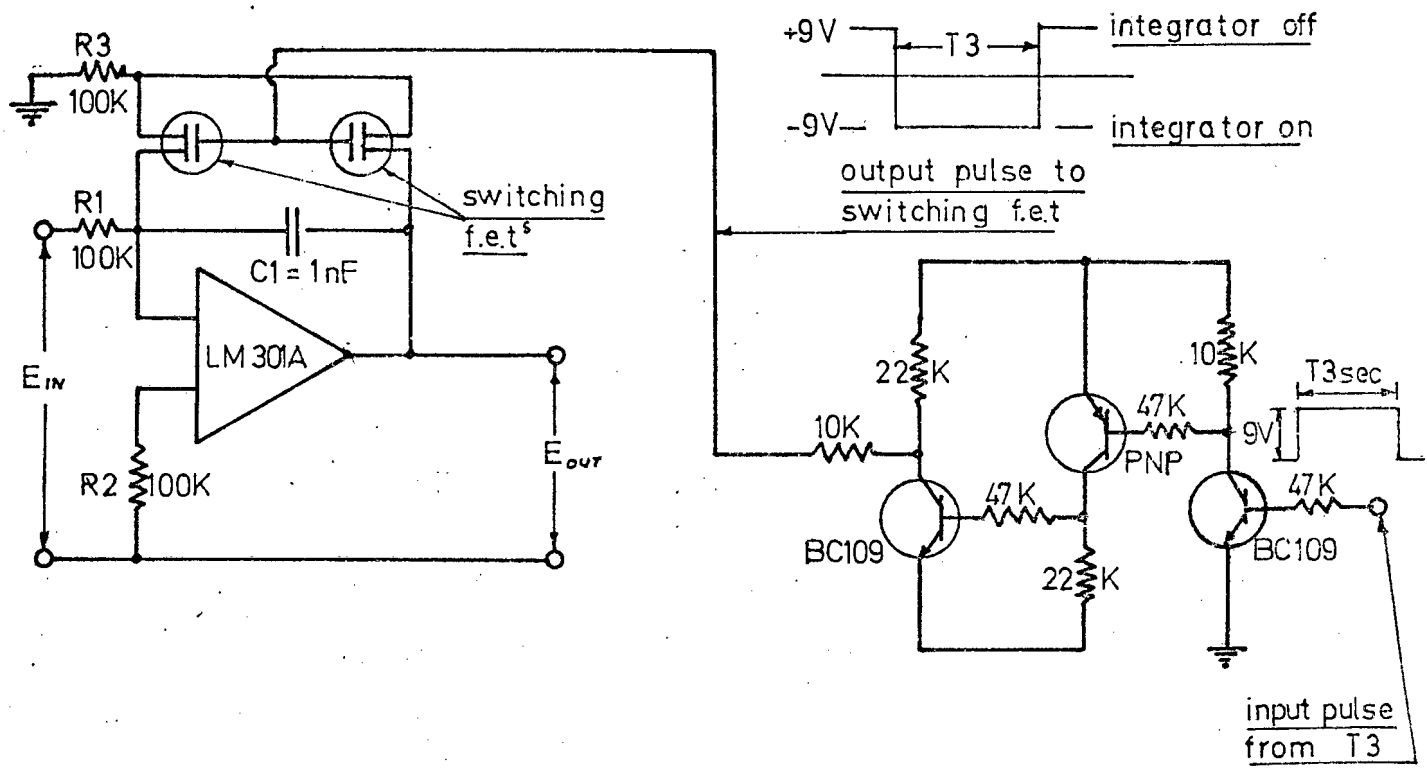

FIG. B2 INTEGRATOR AND SWITCHING CIRCUIT

8.3/ 71.....

8.3 Triggering And Co-ordinating Circuitry.

To co-ordinate the integrator and the recording oscilloscope with the impact of the projectile, the following circuitry is necessary.

8.3.1 Photo-Trigger. The circuit for this device is shown in Fig B3. A light beam situated in the pickup section next to the scratch pickups falls onto the base of a photo-transistor and effectively holds the output terminal at ground potential. When the projectile breaks the light beam, an output pulse of about 18 V is generated. This pulse marks the projectile's motion in time and space.

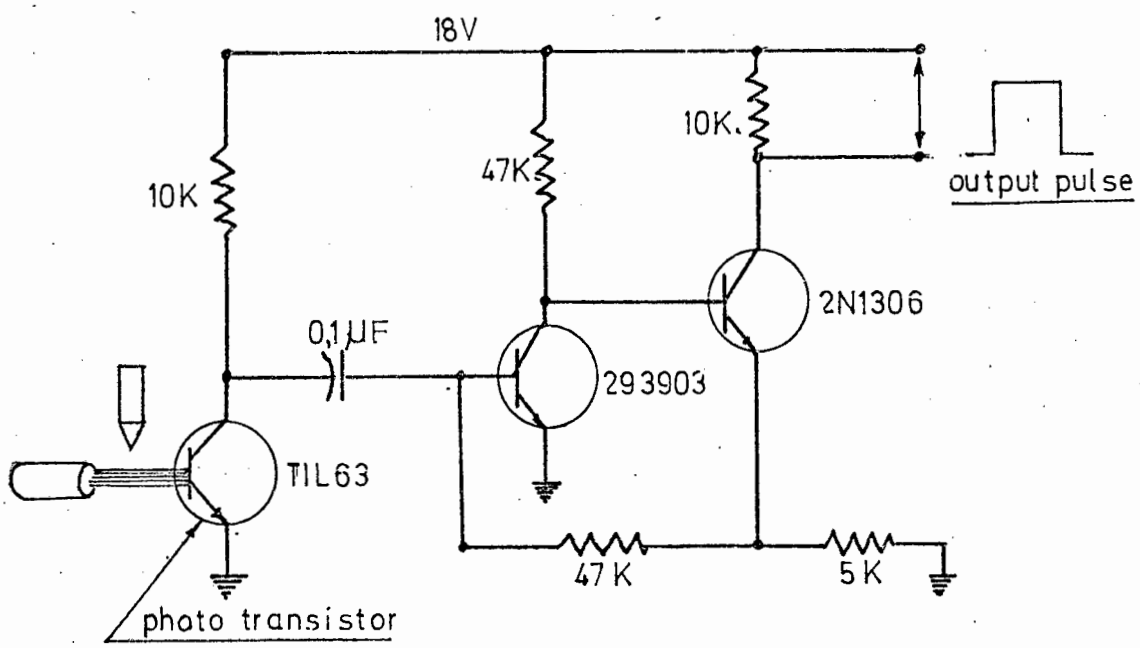

FIG.B3 PHOTO PULSE GENERATOR

8.3.2. Sequencing Circuitry With an initial pulse to give a reference point, co-ordination of the electronics with the impact is accomplished by a series of delay circuits which are started by the initial pulse. The pulsing sequence is explained in Fig. 3.11.

The delay circuits T1, T2, T3 are all built around the signetic SE 555 integrated circuit. The desired time delay is set by means of the capacitor C and resistance R. (See Fig B4) according to the relationship:

$T = RC$ where T is the delay time in seconds.

All the delays are adjustable by means of a variable resistance. To give an even greater range of delays, T1 also has a selection of capacitors

Fig.B 4./72.....

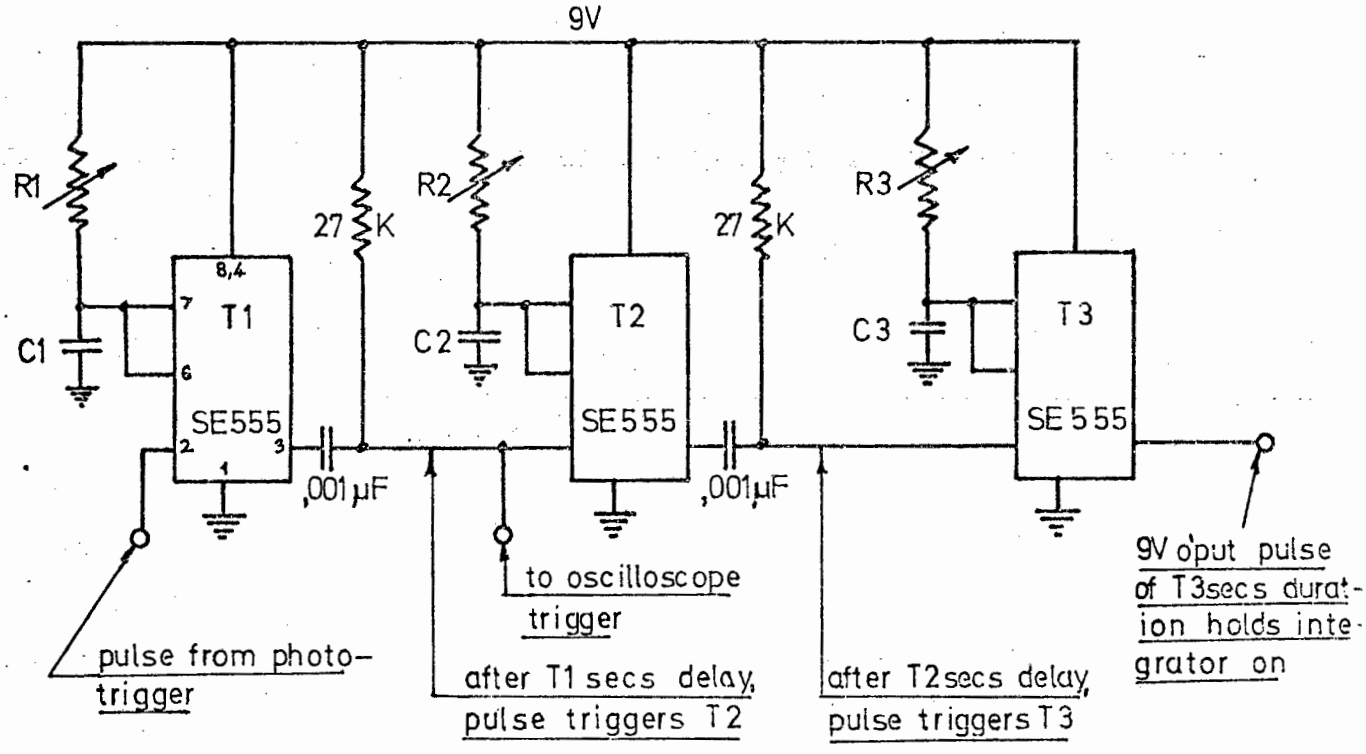

FIG.B4 DELAY CIRCUITRY

to vary/73....

to vary.

The delay times used are:

T1 from 5 μs to 5 000 μs

T2 from 100 μs to 300 μs

T3 from 200 μs to 1 500 μs

8.4.1. Calibration of Differentiator. The ideal differentiating process can be represented as:-

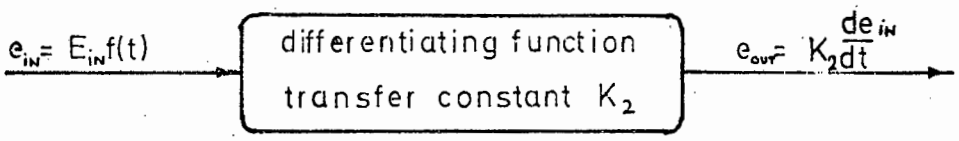

In practice an electronic differentiator will have a transfer function K2 which depends on the components used (see Fig B1). This can be calculated from

$$K_2 = RC$$

Instead of relying on an absolute determination of K_2 from a knowledge of the exact values of the resistance and capacitance used, the constant was determined experimentally.

Using a sine wave generator as the input signal, the differentiator was tested over a range of frequencies.

If the input to the differentiator is:

$$e_{in} = E_{in} \text{ Sin } \omega t$$

Then ideally, $e_{out} = \omega E_{in} \text{ Cos } \omega t$

Since in practice $e_{out} = K_2 \frac{de_{in}}{dt}$

We get/ 74.....

We get $K_2 = \frac{E_{out}}{\omega E_{in}} = 3,45 \times 10^{-4}$ for the differentiator used.

Thus for each input frequency, K_2 can be calculated from a knowledge of the amplitudes E_{in} and E_{out} and the circular frequency ω. Ideally the phase shift between the input and output signals should be 90°. In practice this is approximated only, the approximation deteriorating towards the designed breakpoint of the circuit when the phase shift approaches 180°. The results of the calibration are presented graphically in Graph B.5.

8.4.2. Calibration of Integrator. The same procedure was adopted for the integrator as was used for the differentiator.

In this case we have:

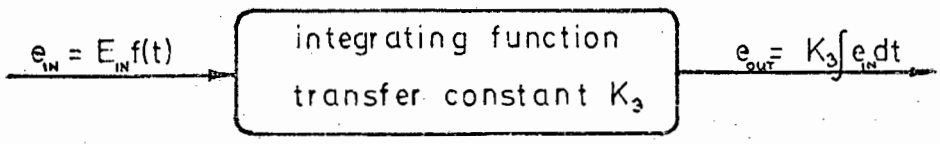

Theoretically $K_3 = \frac{1}{RC}$ (see Fig. B2.). A calibration was carried out using the sine wave generator as the input signal, and using the same reasoning as for the differentiator we get:

$$K_3 = \frac{\omega E_{out}}{E_{in}} = 8,18 \times 10^{3} \text{ for the integrator used.}$$

The results are presented graphically in Graph B.5.

Graph B.5./ 75.....

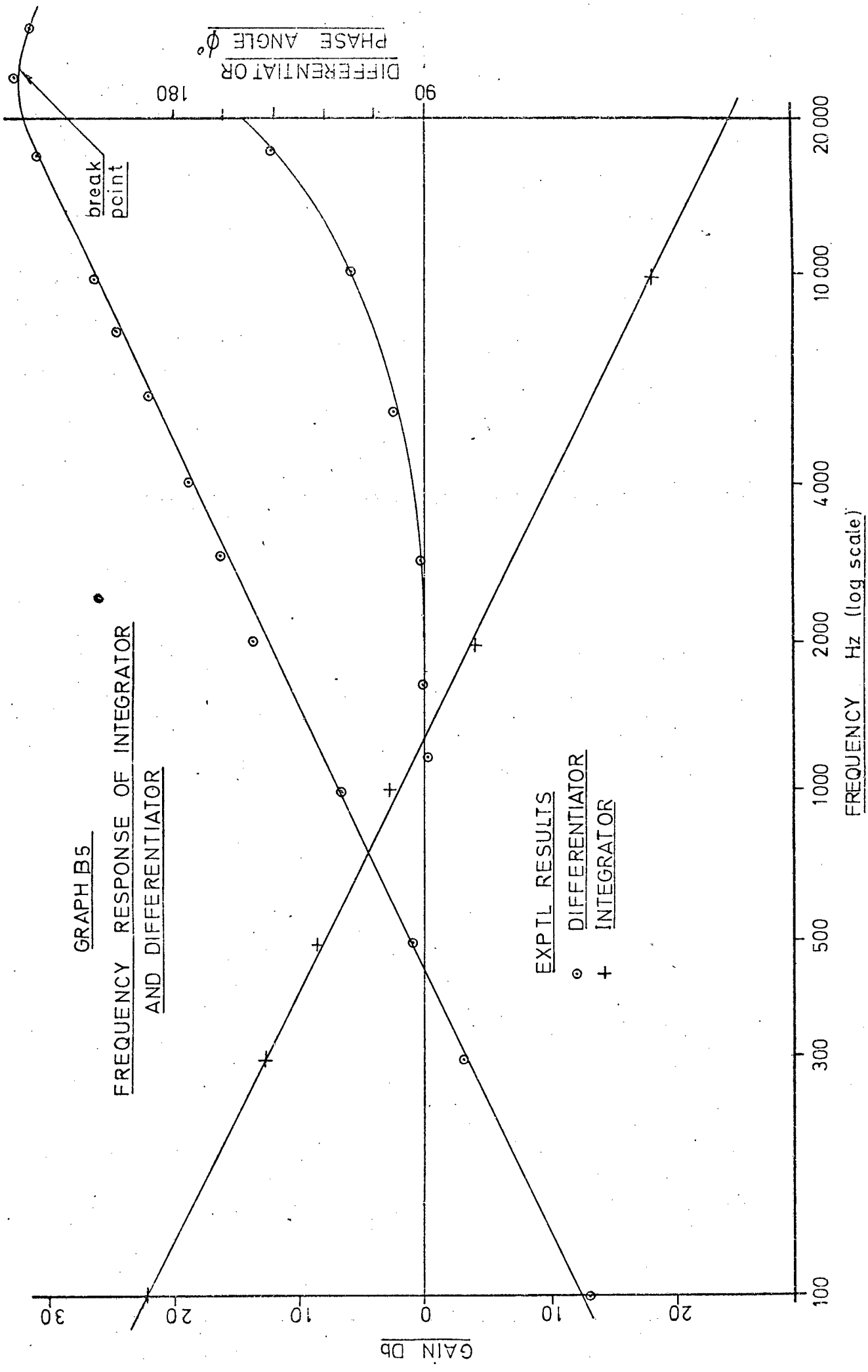

APPENDIX C/76....

APPENDIX C

Analysis of Projectile Vibration

9.1. General

Due to the projectile's elastic nature, acoustic waves are initiated by the impact and travel up and down the length of the projectile during the penetration process. This gives rise to relative motion within the projectile itself and in order that Newton's second law of motion can be applied to the projectile as a whole, i.e.

$$P = Ma$$

the average motion of the whole of the projectile must be found before a resisting force P can be calculated.

To analyse the motion of the particles in the projectile which are subject to an acoustic wave travelling to and fro, requires a solution to the plane wave equation:

$$\frac{\partial^2 u}{\partial t^2}(x,t) = c^2 \frac{\partial^2 u(x,t)}{\partial x^2} \quad \ldots\ldots\ldots\ldots\ldots\ldots (9.1)$$

This is a partial differential equation in two variables, x - the position from the projectile tail and t - time. In Masket's solution the point of interest on the projectile was the tail surface, i.e. at x = 0. In the present study the point at which measurements are made is a distance d mm from this surface. Because of this, a separate analysis was carried out and gives a generalised form of Masket's equation.

9.2 Masket's Solution.

For small strains and damping the equation to be solved is:-

$$\frac{\partial^2 u}{\partial t^2}(x,t) = c^2 \frac{\partial^2 u(x,t)}{\partial x^2} \quad \ldots\ldots\ldots\ldots\ldots\ldots (9.1)$$

Where $c^2 = E/\rho$
and $u = u(x,t)$ is the displacement of position x at time t, relative to laboratory co-ordinates.

The solution to 9.1 will be subject to the following boundary conditions:-

at time/ 77.....

at time $t = 0$, $u = 0$ and $\left.\frac{\partial u}{\partial t}\right|_{t=o} = V_o$

at position $x = 0$, $\left.\frac{\partial u}{\partial x}\right|_{x=o} = 0$

at position $x = \ell$, $\left.\frac{\partial u}{\partial x}\right|_{x=\ell} = \frac{F(t)}{AE}$

Taking the Laplace Transform $U = \mathcal{L}(u)$ of equation 9.1 we get:-

$$\lambda^2 U - \lambda U(x,0) - \left.\frac{\partial U}{\partial t}\right|_{x,o} = c^2 \frac{d^2U}{dx^2}.$$

$$\frac{d^2U}{dx^2} = \frac{\lambda^2}{c^2} U - \frac{V_o}{c^2}$$ Where λ is a complex variable

..... (9.2)

The standard solution for 9.2 is:-

$$U = a\ \mathrm{Cosh}\left(\frac{\lambda}{c}x\right) + b\ \mathrm{Sinh}\left(\frac{\lambda}{c}x\right) + \frac{V_o}{\lambda^2} \quad \ldots\ldots\ldots\ldots (9.3)$$

Differentiating W.R.T. x, 9.3 yields:-

$$\frac{dU}{dx} = \frac{\lambda a}{c}\ \mathrm{Sinh}\left(\frac{\lambda}{c}x\right) + \frac{\lambda b}{c}\ \mathrm{Cosh}\left(\frac{\lambda}{c}x\right) \quad \ldots\ldots\ldots\ldots\ldots (9.4)$$

The boundary conditions at the tail are :-

$$\left.\frac{dU}{dx}\right|_{x=o} = \mathcal{L}\left(\left.\frac{\partial u}{\partial x}\right|_{x=o}\right) = 0$$

$\therefore\ b = 0$

The boundary conditions at the nose are:-

$$\left.\frac{dU}{dx}\right|_{x=\ell} = \frac{\overline{F}(\lambda)}{AE} \quad \text{where } \overline{F}(\lambda) \equiv \mathcal{L}(F(t) \equiv \int_o^\infty e^{-\lambda t} F(t)dt$$

$$\therefore\ \frac{\overline{F}(\lambda)}{AE} = \frac{\lambda a}{c}\ \mathrm{Sinh}\left(\frac{\lambda \ell}{c}\right)$$

or a = / 78.....

$$\text{or } a = \frac{c}{AE} \cdot \frac{\bar{F}(\lambda)}{\text{Sinh}(\lambda \ell/c)}$$

Substituting the values of a and b back into 9.2 yields:-

$$U = \frac{c}{AE} \cdot F(\lambda) \frac{\text{Cosh}(\lambda x/c)}{\lambda \ \text{Sinh}(\lambda \ell/c)} + \frac{V_o}{\lambda^2}$$

Taking the inverse transform gives:-

$$u(x,t) = \frac{1}{2\pi i} \int_{\gamma-i\infty}^{\gamma+i\infty} e^{\lambda t} \left[\frac{V_o}{\lambda^2} + \frac{c}{AE} \bar{F}(\lambda) \frac{\text{Cosh}\ (\lambda x/c)}{\lambda \ \text{Sinh}(\lambda \ell/c)} \right] d\lambda \quad ..(9.5a)$$

At the base of the projectile which is the point of interest, i.e. x = o we have the following three expressions for displacement velocity and deceleration:-

Displacement: $$u(o,t) = \frac{1}{2\pi i} \int_{\gamma-i\infty}^{\gamma+i\infty} e^{\lambda t} \left[\frac{V_o}{\lambda^2} + \frac{c}{AE} \frac{\bar{F}(\lambda)}{\lambda \ \text{Sinh}(\lambda \ell/c)} \right] d\lambda \quad .. \quad (9.5)$$

Velocity: $$\frac{\partial u(o,t)}{\partial t} = \frac{1}{2\pi i} \int_{\gamma-i\infty}^{\gamma+i\infty} e^{\lambda t} \left[\frac{V_o}{\lambda} + \frac{c}{AE} \frac{\bar{F}(\lambda)}{\text{Sinh}(\lambda \ell/c)} \right] d\lambda \quad .... \quad (9.6)$$

Deceleration: $$\frac{\partial^2 (o,t)}{\partial t^2} = \frac{1}{2\pi i} \int_{\gamma-i\infty}^{\gamma+i\infty} e^{\lambda t} \left[V_o + \frac{c}{AE} \frac{\lambda \bar{F}(\lambda)}{\text{Sinh}(\lambda \ell/c)} \right] d\lambda \quad .... \quad (9.7)$$

These solutions were used by Masket to prove his four theorems stated in Section 5. They are also used in the following general analysis:-

9.3 Generalised Solution

Generalised Theorem: The displacement, velocity and deceleration of the centre of mass at any instant t may be computed from the average of the displacement, velocity and deceleration respectively, of a point on the projectile a distance d from the base, by the equation:-

$$\frac{c}{\ell} \int_{t-(\ell+d)/c}^{t+(\ell-d)/c} X(d,t)dt = X_{cm}(t) + X_{cm}(t - \frac{2d}{c}) \quad \ldots\ldots\ldots\ldots \quad (9.8)$$

Where X = displacement, velocity or deceleration.

The proof/ 79.....

The proof of 9.8 is as follows:-

$$\text{Let } U^{*} = c/\ell \int_{t'-\ell/c}^{t'+\ell/c} u(d,t)dt$$

Now the solution for $u(x,t)$ was found in 9.5a. Substituting this solution into the above relationship and setting $x = d$ $\Rightarrow$

$$U^{*} = \frac{1}{2\pi i}\frac{c}{\ell}\int_{\gamma-i\infty}^{\gamma+i\infty}\int_{t'-\ell/c}^{t'+\ell/c} e^{\lambda t}dt\left[\frac{V_o}{\lambda^2} + \frac{c}{AE}\,\bar{F}(\lambda)\frac{\text{Cosh}\,(\lambda d/c)}{\lambda\ \text{Sinh}(\lambda\ell/c)}\right]d\lambda$$

evaluating the inner integral $\Rightarrow$

$$U^{*} = \frac{1}{2\pi i}\,\frac{c}{\ell}\int_{\gamma-i\infty}^{\gamma+i\infty} e^{\lambda t'}\frac{(e^{\lambda\ell/c} - e^{-\lambda\ell/c})}{\lambda}\left[\frac{V_o}{\lambda^2} + \frac{c}{AE}\,\frac{\bar{F}(\lambda)\ \text{Cosh}\,(\lambda d/c)}{\lambda\ \text{Sinh}(\lambda\ell/c)}\right]d\lambda$$

$$\Rightarrow U^{*} = \frac{1}{2\pi i}\int_{\gamma-i\infty}^{\gamma+i\infty}\left[\frac{c}{\ell}\cdot\frac{e^{\lambda t'}}{\lambda^3}\cdot 2\,\text{Sinh}\left(\frac{\lambda\ell}{c}\right)V_o + \frac{e^{\lambda t'}c^2}{AE\ell}\,\bar{F}(\lambda).\frac{2\text{Cosh}(\lambda d/c)}{\lambda^2}\right]d\lambda$$

A B

Now A can be simplified by Cauchy's 2nd Integral Formula

$$\text{since } \frac{1}{2\pi i}\int_{\gamma-i\infty}^{\gamma+i\infty}\frac{e^{\lambda t'}}{\lambda^3}\,\text{Sinh}\left(\frac{\lambda\ell}{c}\right)V_o\,d\lambda = V_o\ t'\ell/c$$

B can be rewritten as follows, by expanding Cosh $\lambda d/c$

$$B = \frac{1}{2\pi i}\int_{\gamma-i\infty}^{\gamma+i\infty}\frac{2}{M}\,F(\lambda)\left[\frac{e^{\lambda(t'+d/c)} + e^{\lambda(t'-d/c)}}{2\lambda^2}\right]d\lambda$$

$$\text{Where } \frac{c^2}{AE\ell} = \frac{1}{M}$$

By writing $T = t + d/c$ the exponential part of the integral can be rewritten as:-

$$\int_{-\infty}^{T}$$

/80.....

$$\int_{-\infty}^{T}\int_{-\infty}^{T} e^{\lambda t}dtdT + \int_{-\infty}^{T-2d/c}\int_{-\infty}^{T} e^{\lambda t}dtdT$$

Recombining $U^* = A + B \Rightarrow$

$$U^* = 2V_o t' + \frac{1}{2\pi i}\int_{-\infty}^{T}\int_{-\infty}^{T}\int_{\gamma-i\infty}^{\gamma+i\infty}\frac{1}{M}\bar{F}(\lambda)e^{\lambda t}d\lambda dtdT +$$

$$\frac{1}{2\pi i}\int_{(-\infty)}^{(T-2d/c)}\int_{(-\infty)}^{(T)}\int_{(\gamma-i\infty)}^{(\gamma+i\infty)}\frac{1}{M}\bar{F}(\lambda)e^{\lambda t}d\lambda dtdT$$

or $$U^* = 2V_o t' + \frac{1}{M}\underbrace{\int_{-\infty}^{T}\int_{-\infty}^{T}F(t)dtdT}_{C} + \frac{1}{M}\underbrace{\int_{-\infty}^{T-2d/c}\int_{-\infty}^{T}F(t)dtdT}_{D} \quad \ldots\ldots (9.9)$$

To put C and D into recognisable form we resort to the impulse momentum law, viz:-

$$F(t) = Ma_{cm}(t)$$

$$\therefore \int_{-\infty}^{T} a_{cm}(t)\,dt = V_{cm}(T) - \cancel{V_{cm}(-\infty)}^{V_o} = \frac{1}{M}\int_{-\infty}^{T}F(t)dt$$

$$\text{and } V_{cm}(T) = V_o + \frac{1}{M}\int_{-\infty}^{T}F(t)dt \quad \ldots\ldots\ldots\ldots\ldots\ldots (9.10)$$

integrating 9.10 $\Rightarrow$

$$\int_{-\infty}^{T} V_{cm}(T)dT = \int_{-\infty}^{T} V_o dT + \frac{1}{M}\int_{-\infty}^{T}\int_{-\infty}^{T}F(t)dtdT$$

evaluating the integral gives the displacement relationship $\Rightarrow$

$$u_{cm}(t) = V_o t + \frac{1}{M}\int_{-\infty}^{T}\int_{-\infty}^{T}F(t)dtdT \quad \ldots\ldots\ldots\ldots\ldots\ldots (9.11)$$

9.11/ 81.....

9.11 gives an expression for term C in expression 9.9. Also from 9.10 =>

$$\frac{1}{M}\int_{-\infty}^{T} F(t)dt = \frac{\partial u_{cm}(T)}{\partial t} - V_o$$

$$\therefore \frac{1}{M}\int_{-\infty}^{T-2d/c}\int_{-\infty}^{T} F(t)dtdT = \int_{-\infty}^{T-2d/c} \frac{\partial u_{cm}(T)dt}{\partial t} - \int_{-\infty}^{T-2d/c} V_o$$

Which gives for term D in 9.9 =>

$$u_{cm}(T-2d/c) - V_o(T-2d/c) - V_o(-\infty)^{o}$$

Rewriting 9.9 using the above substitutions gives:-

$$U^* = 2V_o(T-d/c) + [u_{cm}(T)-V_o(T)]+[u_{cm}(T-2d/c)-V_o(T-2d/c)]$$

simplifying => $U^* = u_{cm}(T) + u_{cm}(T-2d/c)$

As defined, $U^* = c/\ell\int_{T-\frac{(\ell+d)}{c}}^{T+(\ell-d)/c} u(d,t)dt = u_{cm}(T) + u_{cm}(T-\frac{2d}{c})$

Q.E.D.

The above can be verified for velocity and deceleration.

9.4 Data Processing

Expression 9.8 is used to derive the motion of the centre of mass, knowing the motion of the velocity senser placed a distance d from the projectile tail. Two simplifying assumptions were used in the actual data reduction. Firstly, the limits of the integration were initially calculated as shown in Fig. C1 for an equivalent uniform projectile made of "nylatron". After studying several traces, however, it was discovered that the frequency of the projectile vibration was not constant and changed throughout the penetration. Computed values of the natural period agree with the experimentally found value to within 10% and a mean value of the experimental value was used in subsequent data reduction.

The second/82.....

The second simplifying assumption made was to assume the term $X_{cm}(t - 2d/c) \simeq X_{cm}(t)$. This is a fair assumption since d is small. The resulting relation becomes:-

$$X_{cm}(t) = \frac{c}{2\ell} \int_{t-(\ell+d)/c}^{t+(\ell-d)/c} X(d,t)dt \quad \ldots\ldots\ldots\ldots\ldots\ldots\ldots\ldots \quad (9.12)$$

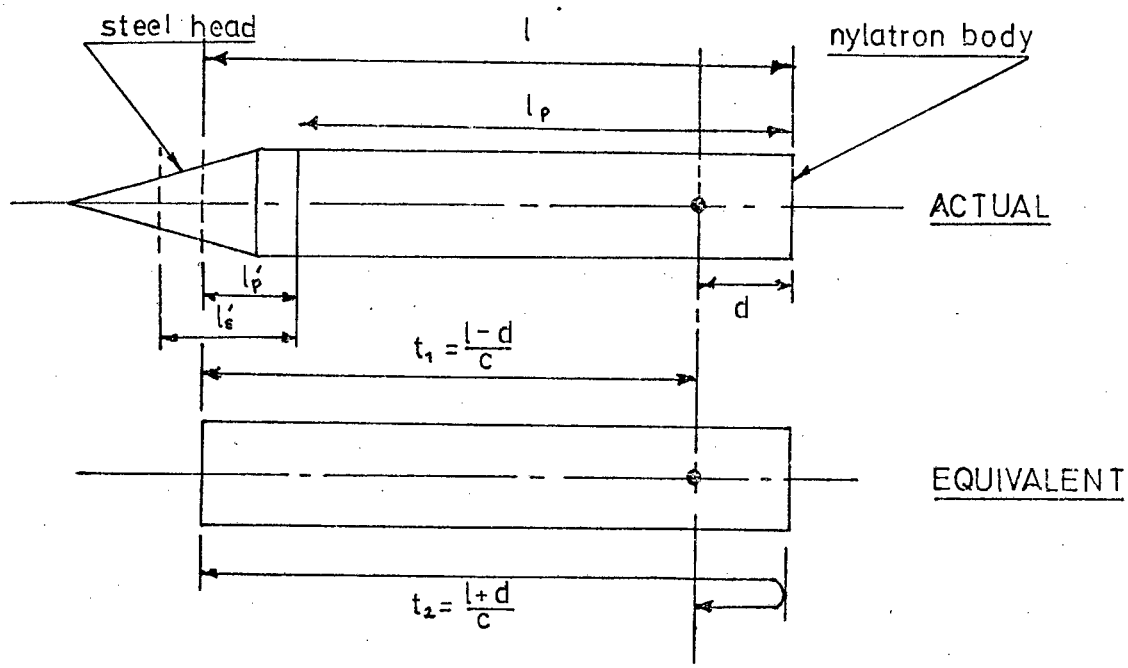

FIG. C1

Note:
$\ell = \ell_p + \ell'_s(c_p/c_s)$

The mechanism of equation 9.12 is clearly shown in Fig.C2. To compute the ordinate $X_{cm}(t)$ at a time t, the area A under the deceleration-time trace is computed between the limits $t + (\ell-d)/c$ and $t-(\ell+d)/c$. This value is then divided by the mean period time of the projectile's natural vibration $(c/2\ell)$ to give the mean ordinate $X_{cm}(t)$.

Fig C2/ 83.....

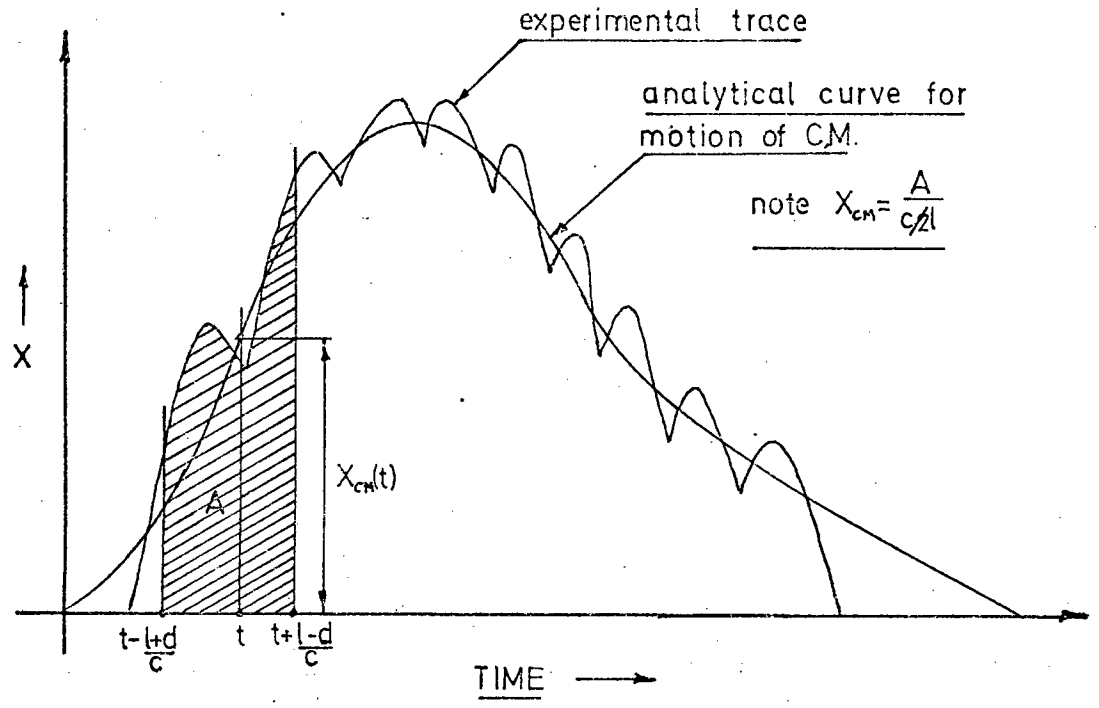

FIG. C2 MECHANISIM OF ANALYSIS

About 60 data points measured from a 35 mm photographic negative of the deceleration-time trace was used as input data for a computor programme. The flow chart for the latter is shown in Fig. C3.

Fig. C3./ 84.....

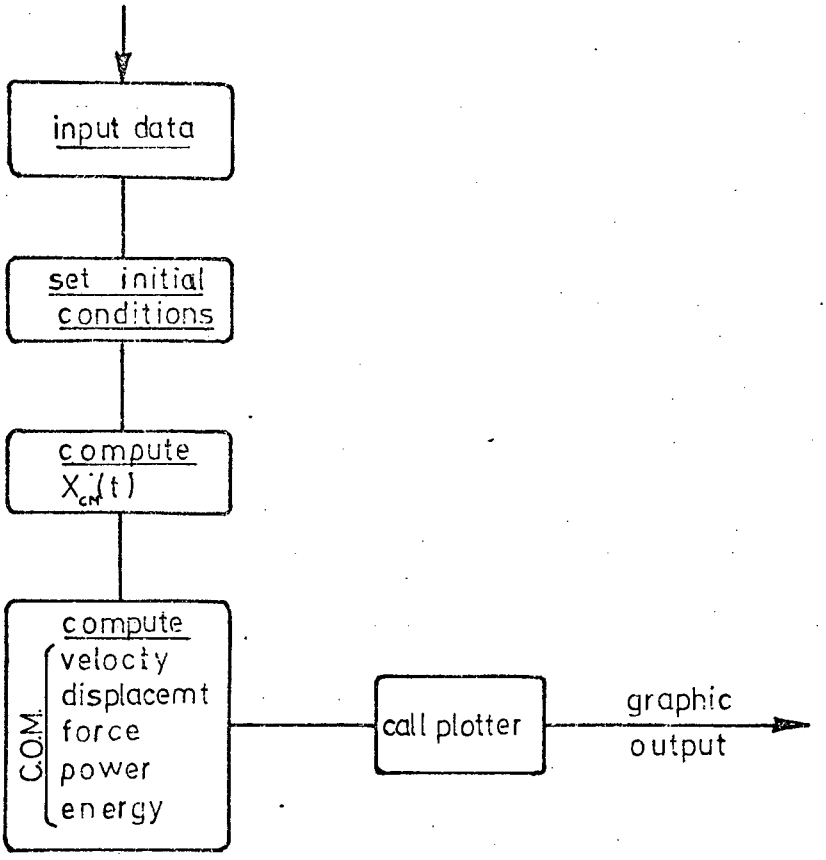

FIG C3 COMPUTER FLOW DIAGRAM

List of References/85....

APPENDIX D

Computer Output Samples

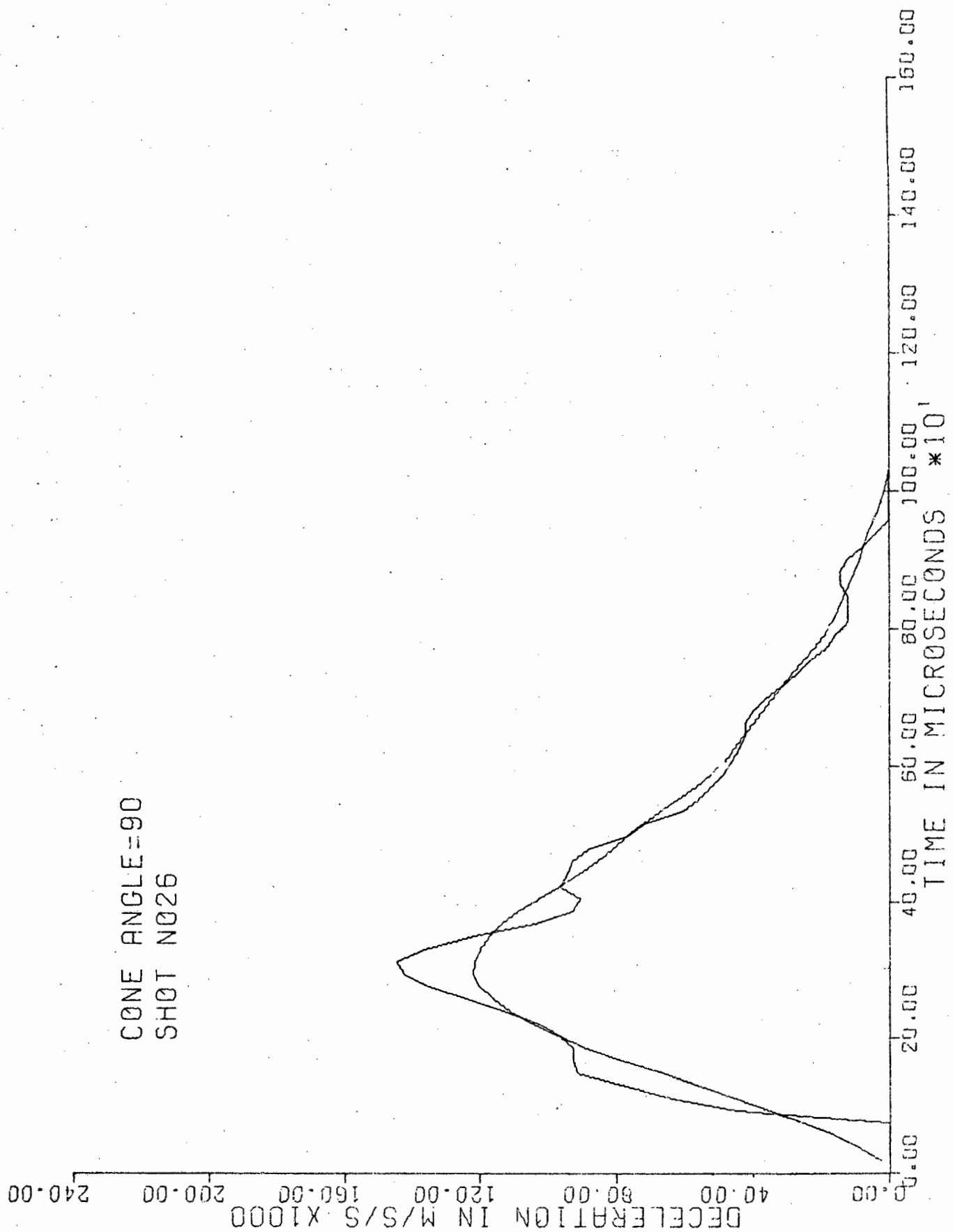

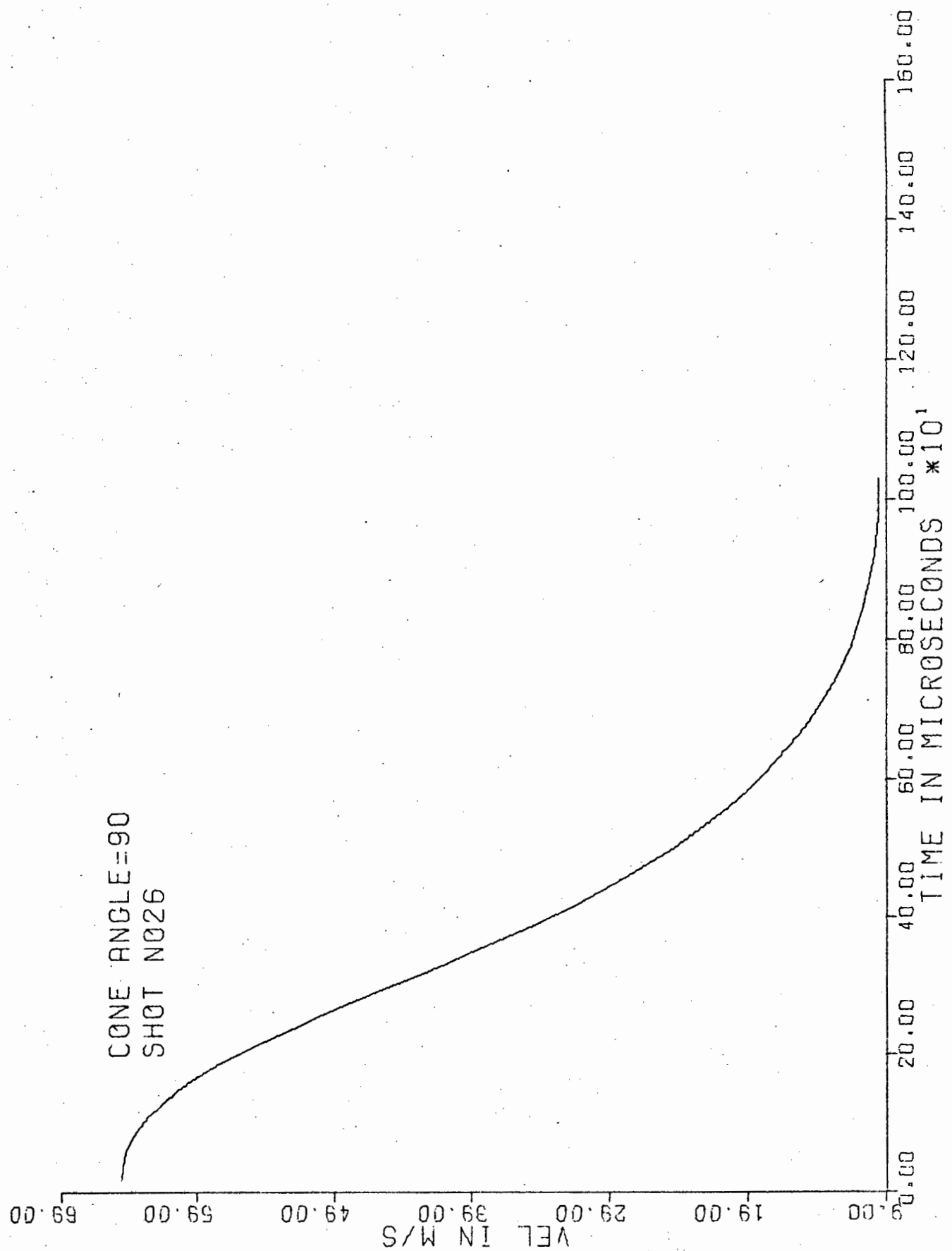
CONE ANGLE=90
SHOT N026
VEL IN M/S
9.00
19.00
29.00
39.00
49.00
59.00
69.00
TIME IN MICROSECONDS *10¹
0.00
20.00
40.00
60.00
80.00
100.00
120.00
140.00
160.00

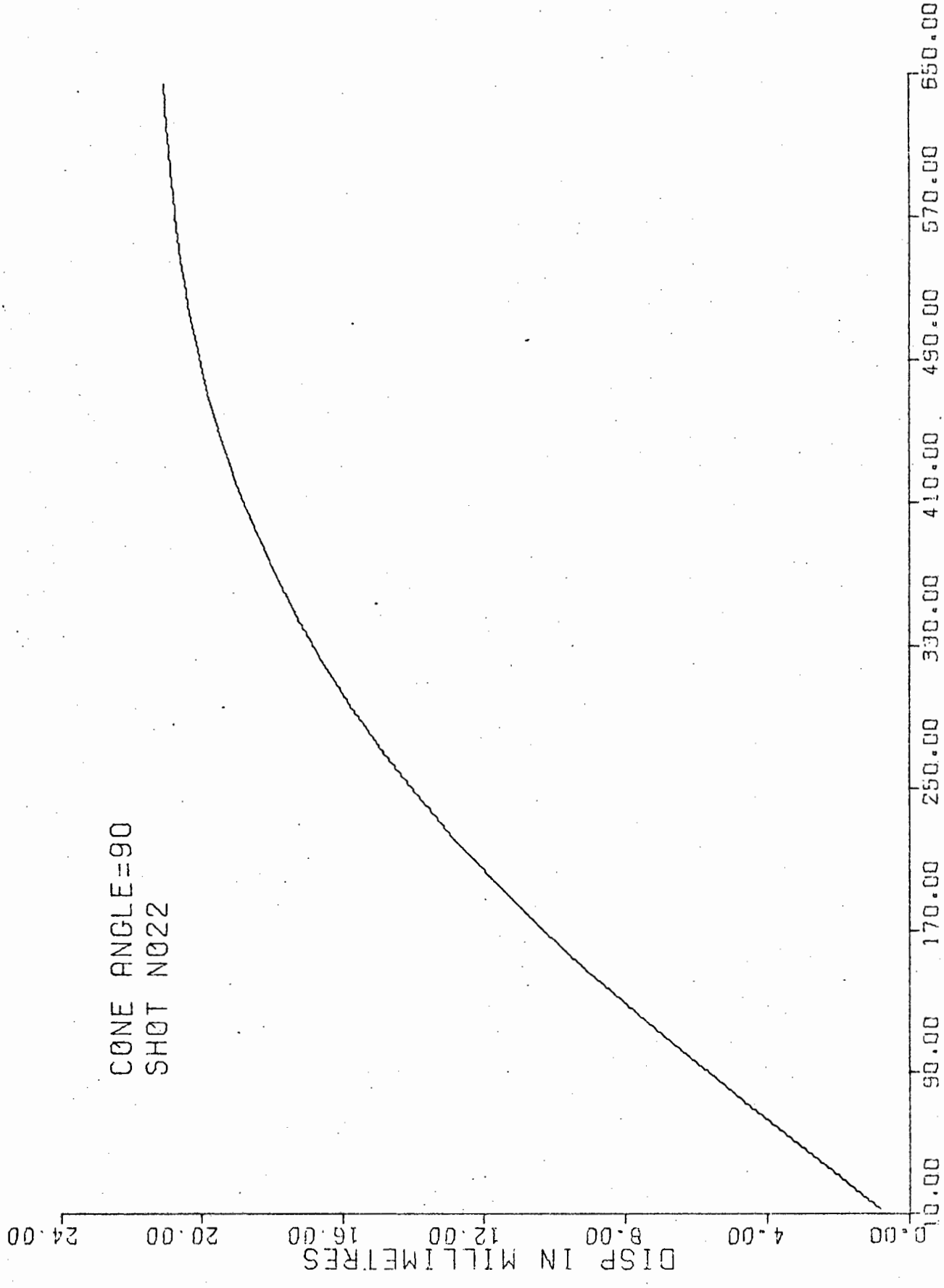
CONE ANGLE=90
SHOT N022
DISP IN MILLIMETRES
0.00
4.00
8.00
12.00
16.00
20.00
24.00
TIME IN MICROSECONDS
10.00
90.00
170.00
250.00
330.00
410.00
490.00
570.00
650.00

LIST OF REFERENCES

1. Masket, A.V. "A measurement of forces resisting armour penetration", Journal of Applied Physics, Vol 20, 1949.

2. Wingrove, A.L. "The forces for projectile penetration of aluminium", Journal of Applied Physics, Vol 5, 1972.

3. Brown, A. "A quasi-dynamic theory of containment", International Journal of Mech. Science, Vol 6, 1964.

4. Huth, J.H. "Some new data on high speed impact phenomena", Journal of Applied Mechanics, 1956.

5. Euler, L. "Neue Grundsätze Der Artillerie". Berlin, 1745.

6. Poncelet, J.V." Cours de Mechanige Industrielle", Brusselles, 1829.

7. Bashforth, F. "Motion of Projectiles" Asher London (1873).

8. Bethe, H.A. "Attempt of A Theory of Armour Penetration" RARDE Report No. R52/1203/3 May, 1941.

9. Taylor, G.I. "Journal of Applied Mechanics".

10. Bluhm, Proc. Society Exp. Stress Analysis, Vol 13, 1956

11. Thompson, W.T. Jnl. Appl. Physics, Vol 26, 1955.

12. Zaid and Paul Jnl. Franklin Inst. Vol 264, 1957.

13. Recht and Ipson Jnl. Applied Mechanics. Vol 30, 1963.

14. Goldsmith and Calder Int. J. Solid Structures, Vol 7, 1971.

15. Goldsmith and Finnegan Int. Jnl. Mech. Science, Vol 13, 1971.

16. Nishiwake Jnl. Physical Soc. of Japan. Vol 6, 1951.

17. Krafft, J. Jnl. of Applied Physics, Vol 26, (1955).

Goldsmith/89 .....

18. Goldsmith and Chulay "Exptl. Mechanics", Vol 5, 1965.

19. Doebelin "Measurement Systems", McGraw Hill.

20. Pearson and Miles "Review of Scientific Instruments", Vol 45, 1974.

21. Tohey, Graeme and Huelsman "Operational Amplifiers - Design and Application", McGraw Hill.

22. Zaid, A. Int. Jnl Science, Vol 15, 1973.

23. Chou, P.C. Proc. 7th Mech. Conf. Vol 1, 1961.

24. Bashian, F.A. Inst. Mech. Acad. Sci., USSR, Appl. Math. Mech. Vol XII, 1948.

25. Thompson, R.G. N.A.S.A. Report No. TR-R211, 1965.

26. Stutterlin Mem. Artill. France 96, 18 (1939).